Multirate Signal Processing Concepts in Digital Communications

Thesis by

Bojan Vrcelj

In Partial Fulfillment of the Requirements

for the Degree of

Doctor of Philosophy

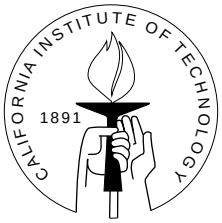

California Institute of Technology

Pasadena, California

2003

(Submitted June 2, 2003)

Acknowledgments

First of all, I would like to express my profound gratitude to my advisor, Professor P.P. Vaidyanathan, for his outstanding guidance and support during my stay at Caltech. P.P. is a fascinating teacher and a thoughtful mentor, always ready to share his expertise with the students. He is also a thorough, brilliant researcher and I benefited greatly from working under his guidance. His encouragement and friendship have been invaluable throughout my studies at Caltech. His academic excellence continues to be a source of inspiration, but beyond that I am especially grateful for his limitless patience and fatherly support during trying times.

I would like to thank the members of my defense and candidacy examining committees for their interest: Prof.Robert McEliece, Prof.Babak Hassibi, Prof.Emmanuel Candes, Dr.Murat Meşe, Dr.Dariush Divsalar and Prof.Pietro Perona. I would also like to thank the professors at the school of Electrical Engineering, University of Belgrade, for providing me with solid foundations which have proved helpful throughout my studies. I should single out my diploma thesis adviser, Prof.Miodrag Popović. My thanks also go to my high school physics teacher, Ms.Nataša Čaluković, who sparked my interest in the field of electrical engineering.

I would like to thank my present and past lab-mates, Andre Tkacenko, Murat Meşe, Sony Akkarakaran, Sriram Murali, and Byung-Jun Yoon, who helped create a very enjoyable and productive environment in the DSP lab. Sony and Murat were mid-way through their doctorate studies when I joined the group. I feel indebted to them for their friendship, support, patience and collegial help, which was so essential during my first year at Caltech. Andre has been my office-mate and a good friend for four years now. I deeply value our academic and personal discussions as well as our daily shots of caffeine. Byung-Jun and Sriram joined our lab two years ago and made the atmosphere even more friendly and enjoyable.

I am grateful to many other people, some affiliated with Caltech, and the others whom I have known long before I joined, for their friendship, company, and entertainment, that helped make my life outside the office very pleasant. I also feel that my Caltech experience was greatly enriched by the institute-wide groups, clubs and organized events. In this capacity I would like to thank the people of the Caltech Y, International Student Program and the water polo crowd.

Finally, I would like to thank my parents for their constant love and support and for providing me with the opportunity and the encouragement to pursue my goals.

Abstract

Multirate systems are building blocks commonly used in digital signal processing (DSP). Their function is to alter the rate of the discrete-time signals, which is achieved by adding or deleting a portion of the signal samples. Multirate systems play a central role in many areas of signal processing, such as filter bank theory and multiresolution theory. They are essential in various standard signal processing techniques such as signal analysis, denoising, compression and so forth. During the last decade, however, they have increasingly found applications in new and emerging areas of signal processing, as well as in several neighboring disciplines such as digital communications.

The main contribution of this thesis is aimed towards better understanding of multirate systems and their use in modern communication systems. To this end, we first study a property of linear systems appearing in certain multirate structures. This property is called **biorthogonal partnership** and represents a terminology introduced recently to address a need for a descriptive term for such class of filters. In the thesis we especially focus on the extensions of this simple idea to the case of vector signals (MIMO biorthogonal partners) and to accommodate for nonintegral decimation ratios (fractional biorthogonal partners).

Some of the main results developed here pertain to a better understanding of the biorthogonal partner relationship. These include the conditions for the existence of stable and of finite impulse response (FIR) biorthogonal partners. A major result that we establish states that under some generally mild conditions, MIMO and fractional biorthogonal partners exist. Moreover, when they exist, FIR solutions are not unique. We develop the parameterization of FIR solutions, which makes the search for the best partner in a given application analytically tractable. This proves very useful in the central application of biorthogonal partners, namely, channel equalization in digital communications with signal oversampling at the receiver. Sampling the received signal at a rate higher than that defined by the transmitter provides some flexibility in the design of the equalizer. A good channel equalizer in this context is one that helps neutralize the distortion on the signal introduced by the channel propagation but not at the expense of amplifying the channel noise. This presents the rationale behind the partner design problem which is formulated and solved. The performance of such equalizers is then compared to several other equalization methods by computer simulations. These findings point to the conclusion that the communication system performance can be improved at the expense of an increased implementational cost of the receiver.

While the multirate DSP in the aforementioned communication systems serves to provide additional degrees of freedom in the design of the receiver, another important class of multirate structures is used at the transmitter side in order to introduce the redundancy in the data stream. This redundancy generally serves to facilitate the equalization process by forcing certain structure on the transmitted signal. If the channel is unknown, this procedure helps to identify it; if the channel is ill-conditioned, additional redundancy helps

avoid severe noise amplification at the receiver, and so forth. In the second part of the thesis, we focus on this second group of multirate systems, derive some of their properties and introduce certain improvements of the communication systems in question.

We first consider the transmission systems that introduce the redundancy in the form of a cyclic prefix. The examples of such systems include the discrete multitone (DMT) and the orthogonal frequency division multiplexing (OFDM) systems. The cyclic prefix insertion helps to effectively divide the channel in a certain number of nonoverlaping frequency bands. We study the problem of signal precoding in such systems that serves to adjust the signal properties in order to fully take advantage of the channel and noise properties across different bands. Our ultimate goal is to improve the overall system performance by minimizing the noise power at the receiver. The special case of our general solution corresponds to the white channel noise and the best precoder under these circumstances simply performs the optimal power allocation.

Finally, we study a different class of communication systems with induced signal redundancy, namely, the multiuser systems based on code division multiple access (CDMA). We specifically focus on the special class of CDMA systems called 'a mutually orthogonal usercode receiver' (AMOUR). These systems use the transmission redundancy to facilitate the user separation at the receiver regardless of the (different) communication channels. While the method also guarantees the existence of the zero-forcing equalizers irrespective of the channel zero locations, the performance of these equalizers can be further improved by exploiting the inherent flexibility in their design. We show how to find the best equalizer from the class of zero-forcing solutions and then increase the size of this class by employing alternative sampling strategies at the receiver. Our method retains the separability properties of AMOUR systems while improving their robustness in the noisy environment.

Contents

List of Figures

Chapter 1 Introduction

The theory of multirate digital signal processing (DSP) has traditionally been applied to the contexts of filter banks [61], [13], [50] and wavelets [31], [72]. These play a very important role in signal decomposition, analysis, modeling and reconstruction. Many areas of signal processing would be hard to envision without the use of digital filter banks. This is especially true for audio, video and image compression, digital audio processing, signal denoising, adaptive and statistical signal processing. However, multirate DSP has recently found increasing application in digital communications as well. Multirate building blocks are the crucial ingredient in many modern communication systems, for example, the discrete multitone (DMT), digital subscriber line (DSL) and the orthogonal frequency division multiplexing (OFDM) systems as well as general filter bank precoders, just to name a few. The interested reader is referred to numerous references on these subjects, such as [7]–[9], [17]–[18], [27], [30], [49], [64], [89], etc.

This thesis presents a contribution to further understanding of multirate systems and their significance in digital communications. To that end, we introduce some new signal processing concepts and investigate their properties. We also consider some important problems in communications especially those that can be formulated using the multirate methodology. In this introductory chapter, we give a brief overview of the multirate systems and introduce some identities, notations and terminology that will prove useful in the rest of the thesis. Every attempt is made to make the present text as self-contained as possible and the introduction is meant to primarily serve this purpose. While some parts of the thesis, especially those that cover the theory of biorthogonal partners and their extensions provide a rather extensive treatment of the concepts, the material regarding the applications of the multirate theory in communication systems should be viewed as a contribution to a better understanding and by no means the exhaustive treatment of such systems. For a more comprehensive coverage the reader is referred to a range of extensive texts on the subject, for example, [71], [18], [19], [39], [38], [53], etc.

1.1 Multirate systems

1.1.1 Basic building blocks

The signals of interest in digital signal processing are *discrete* sequences of real or complex numbers denoted by $x(n)$, $y(n)$, etc. The sequence $x(n)$ is often obtained by sampling a continuous-time signal $x_c(t)$. The majority of natural signals (like the audio signal reaching our ears or the optical signal reaching our eyes) are continuous-time. However, in order to facilitate their processing using DSP techniques, they need to be sampled and converted to digital signals. This conversion also includes signal *quantization*, i.e.,discretization in amplitude, however in practice it is safe to assume that the amplitude of $x(n)$ can be any real or complex

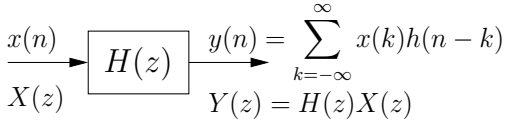

Figure 1.1: Filtering operation: linear time invariant system.

number. Signal processing analysis is often simplified by considering the frequency domain representation of signals and systems. Commonly used alternative representations of $x(n)$ are its z-transform $X(z)$ and the discrete-time Fourier transform $X(e^{j\omega})$. The z-transform is defined as $X(z) = \sum_{n=-\infty}^{\infty} x(n)z^{-n}$, and $X(e^{j\omega})$ is nothing but $X(z)$ evaluated on the unit circle $z = e^{j\omega}$.

Multirate DSP systems are usually composed of three basic building blocks, operating on a discrete-time signal $x(n)$. Those are the linear time invariant (LTI) filter, the decimator and the expander. An LTI filter, like the one shown in Fig.1.1, is characterized by its impulse response $h(n)$, or equivalently by its z-transform (also called the transfer function) $H(z)$. Examples of the M-fold decimator and expander for $M = 2$ are shown in Fig.1.2. The rate of the signal at the output of an expander is M times higher than the rate at its input, while the converse is true for decimators. That is why the systems containing expanders and decimators are called 'multirate' systems. Fig.1.2 demonstrates the behavior of the decimator and the expander in both the time and the frequency domains. In the z-domain this is described by

$$X_E(z) = [X(z)]_{\uparrow M} = X(z^M) \qquad \text{for } M\text{-fold expander, and} \tag{1.1}$$

$$X_D(z) = [X(z)]_{\downarrow M} = \frac{1}{M}\sum_{k=0}^{M-1} X(z^{\frac{1}{M}} e^{-\frac{j2\pi k}{M}}) \qquad \text{for } M\text{-fold decimator.} \tag{1.2}$$

The systems shown in Figs.1.1 and 1.2 operate on scalar signals and thus are called single input—single output (SISO) systems. The extensions to the case of vector signals are rather straightforward: the decimation and the expansion are performed on each element separately. The corresponding vector sequence decimators/expanders are denoted within square boxes in block diagrams. In Fig.1.3 this is demonstrated for vector expanders. The LTI systems operating on vector signals are called multiple input—multiple output (MIMO) systems and they are characterized by a (possibly rectangular) matrix transfer function $\mathbf{H}(z)$.

1.1.2 Some multirate definitions and identities

The vector signals are sometimes obtained from the corresponding scalar signals by *blocking*. Conversely, the scalar signals can be recovered from the vector signals by *unblocking*. The blocking/unblocking operations can be defined using the delay or the advance chains [61], thus leading to two similar definitions. One way of defining these operations is shown in Fig.1.4, while the other is obtained trivially by switching the delay and the advance operators. Instead of drawing the complete delay/advance chain structure, we often use the simplified block notation as in Fig.1.4. It is usually clear from the context which of the two definitions

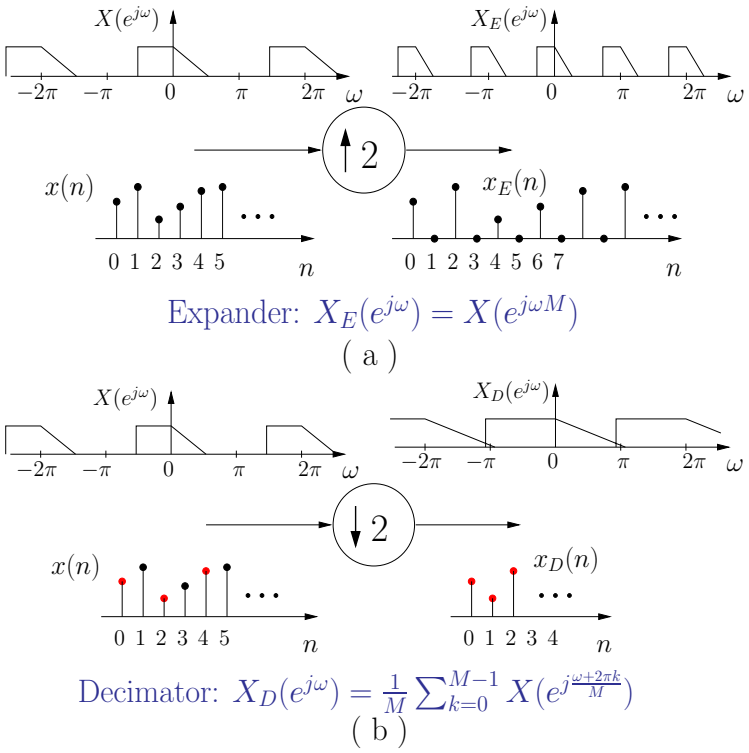

Figure 1.2: Multirate building blocks: (a) 2-fold expander and (b) decimator.

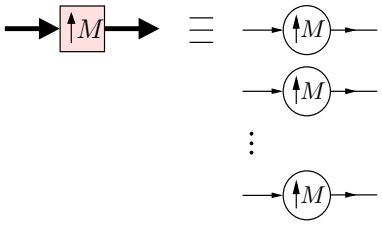

Figure 1.3: The definition and the notation of the vector signal expander.

of the unblocking and blocking operations is employed.

A very useful tool in multirate signal processing is the so-called *polyphase representation* of signals and systems. It facilitates considerable simplifications of theoretical results as well as efficient implementation of multirate systems. Since polyphase representation will play an important role in the rest of the thesis, here we take a moment to formally define it. Consider an LTI system with a transfer function $H(z) = \sum_{n=-\infty}^{\infty} h(n)z^{-n}$ and suppose we are given an integer M. We can decompose $H(z)$ as

$$H(z) = \sum_{m=0}^{M-1} z^{-m} \sum_{n=-\infty}^{\infty} h(nM+m)z^{-nM} = \sum_{m=0}^{M-1} z^{-m} H_m(z^M) \quad \text{(Type 1 decomposition)}. \tag{1.3}$$

Note that this is equivalent to dividing the impulse response $h(n)$ into M nonoverlaping groups of samples

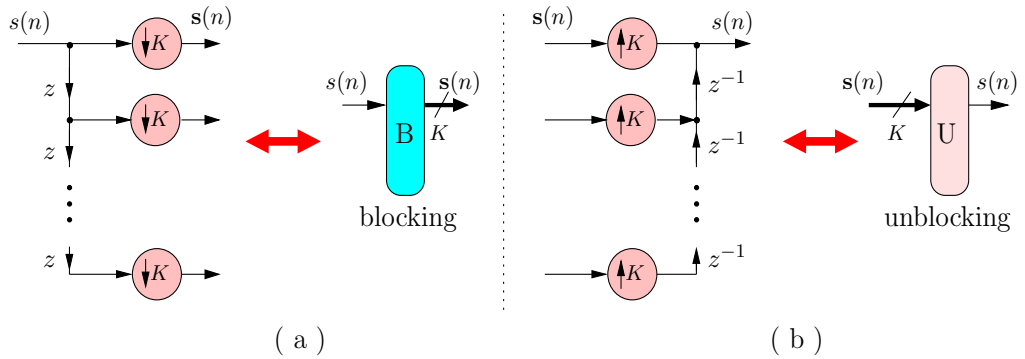

Figure 1.4: Notations: blocking (a) and unblocking (b) operations.

$h_m(n)$, obtained from $h(n)$ by M-fold decimation starting from sample m. In other words, $h(n)$ can be obtained by combining sequences $h_m(n)$ through the unblocking structure shown in Fig.1.4(b). Subsequences $h_m(n)$ and the corresponding z-transforms defined in (1.3) are called the Type 1 polyphase components of $H(z)$ with respect to M. A variation of (1.3) is obtained if we decimate $h(n)$ starting from sample $-m$, for $0 \leq m \leq M-1$. This gives rise to Type 2 polyphase components $\bar{H}_m(z)$:

$$H(z) = \sum_{m=0}^{M-1} z^m \bar{H}_m(z^M) \quad \text{(Type 2 decomposition)}. \tag{1.4}$$

The polyphase notation will be used again very soon in Section 1.3.2 when we discuss the use of filter bank precoders in modern digital communications. However, it is also an important tool in the rest of the thesis. The reader will therefore often be referred to the results from this section. In the following we first describe the notion that plays the central role in Chapters 2 and 3, namely, the concept of *biorthogonal partners*.

1.2 Biorthogonal partners

1.2.1 Generalized inverse

Consider the system shown in the first part of Fig.1.5(a), namely, the system for generating $y(n)$ from $x(n)$. Traditionally, this structure has been called the system for digital interpolation since the rate of $y(n)$ is M times higher than that of $x(n)$. Filter $H(z)$ is usually referred to as the interpolation filter [61]. Suppose the goal is to recover the signal $x(n)$ from $y(n)$. Conceptually the simplest way to achieve this is shown in Fig.1.5(a). Namely, $y(n)$ is first passed through the inverse of the interpolation filter $1/H(z)$. This recovers the signal at the input of the M-fold expander. The M-fold decimator that follows simply discards the zeros inserted by the expander and the recovery of $x(n)$ is complete. Notice, however, that this is not the only way to reconstruct $x(n)$, simply because the inverse filter forces the discarded samples to be zero, while they can take arbitrary values. Indeed, any filter $F(z)$ with the property that its output preserves the desired samples of $x(n)$ in the appropriate locations, with arbitrary values in between [see Fig.1.5(b)] yields a valid

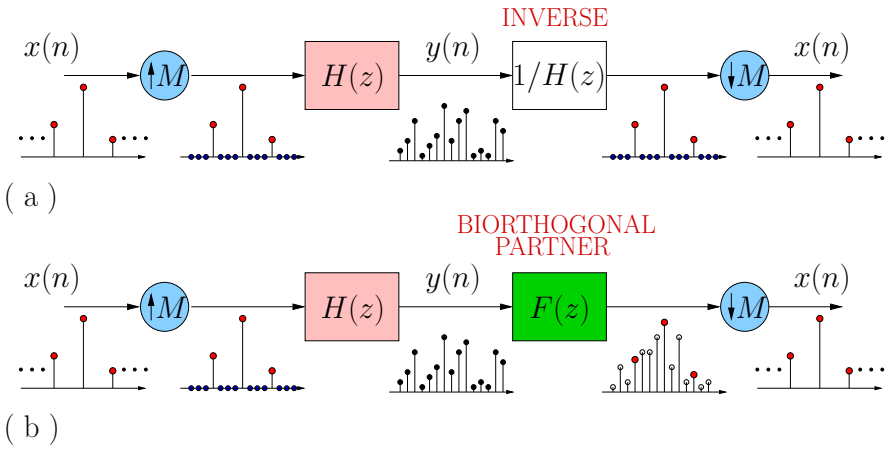

Figure 1.5: Signal recovery after interpolation: (a) using filter inverses, and (b) using 'generalized inverses.'

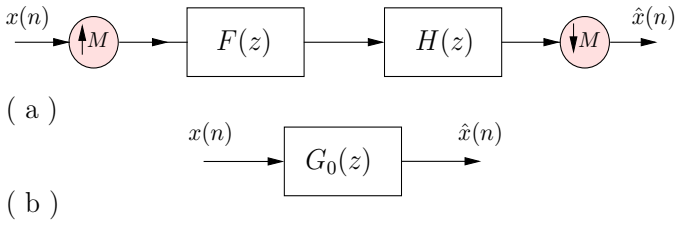

Figure 1.6: Biorthogonal partners: (a) definition and (b) equivalent LTI system.

reconstruction scheme. Filters $F(z)$ with the described property are called *biorthogonal partners* of $H(z)$ and were first introduced in [65]. Notice that the inverse filter is a valid biorthogonal partner. Therefore biorthogonal partners can be thought of as generalized inverses.

Before we provide the formal definition of biorthogonal partners let us answer a potential question: why would we even bother to use the more general reconstruction structure from Fig.1.5(b) if the one in Fig.1.5(a) already works fine? In most practical applications where the interpolation structure arises (e.g.,[59], [74], [65]) filter $H(z)$ has finite impulse response (FIR). Therefore the solution in Fig.1.5(a) involves IIR (infinite impulse response) filtering which is often times unstable or noncausal. In contrast to this, biorthogonal partners often display many desirable properties. Under some mild conditions on $H(z)$ and M there exist *stable* and even *FIR* biorthogonal partners [65]. Moreover, whenever FIR solutions exist they are not unique. This property will be of special importance in the study of multiple input—multiple output (MIMO) and fractional biorthogonal partners in Chapters 2 and 3, respectively, where we use this non-uniqueness to find the optimal biorthogonal partner for the application at hand.

1.2.2 Definition and relation to filter banks

Consider the system in Fig.1.6(a). We say [65] that the filters $F(z)$ and $H(z)$ are biorthogonal partners with respect to an integer M if an arbitrary input $x(n)$ to the system produces $\widehat{x}(n) = x(n)$ as the output;

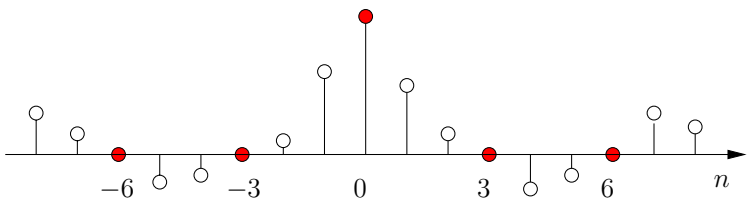

Figure 1.7: Nyquist(M) property demonstrated for $M = 3$.

in other words if the system in the figure is the *identity*. It is a simple exercise to show that the system in question is indeed an LTI system. If we denote the product $F(z) \cdot H(z) = G(z)$, then system from Fig.1.6(a) is equivalent to the one in Fig.1.6(b), where $G_0(z)$ denotes the zeroth polyphase component of $G(z)$ with respect to M. Therefore, $F(z)$ and $H(z)$ are said to form a *biorthogonal pair* (biorthogonal partner relationship is symmetric) with respect to M if

$$G_0(z) = [F(z)H(z)]_{\downarrow M} = 1. \tag{1.5}$$

In the time domain (1.5) implies that $g(n)$, the impulse response of $G(z)$, satisfies the Nyquist(M) condition demonstrated in Fig.1.7. In other words, the sequence $g(n)$ has zero-crossings at all multiples of M except when $n = 0$. Notice that if M is changed the two filters might not remain partners; however, the term 'with respect to M' is usually omitted whenever no confusion is anticipated.

As mentioned previously, the phrase 'biorthogonal partners' was first introduced in [65]. In the following we motivate this terminology. Consider the perfect reconstruction (PR) or *biorthogonal* filter bank [61] shown in Fig.1.8. Such system is by definition the identity, i.e.,for any input $x(n)$, the output is $x(n)$. Each pair of filters $\{H_k(z), F_k(z)\}$ in such filter bank forms a biorthogonal pair according to the definition (1.5). To see this, append the analysis bank at the output of the PR filter bank as shown in Fig.1.8. The outputs are obviously given by the same $u_i(n)$ that appear in the subbands of the PR filter bank. This is true for any $x(n)$ and thus for any choice of $u_i(n)$. Without loss of generality, let us concentrate on the first channel (see the figure). We observe that the marked system between $u_1(n)$ and $u_1(n)$ is identical to the one in Fig.1.6(a) and is nothing but the identity system. Therefore $H_1(z)$ and $F_1(z)$ are indeed biorthogonal partners with respect to M.

For a more detailed treatment of biorthogonal partners, the reader is referred to [65]. The goal in this section was just to provide some basics that will motivate the extensions of this theory developed in Chapters 2 and 3. Biorthogonal partners and their extensions arise in many diverse contexts such as filter bank theory, exact and least squares signal interpolation and modeling, multiresolution theory as well as channel equalization in digital communications. Although we will touch upon most of these applications in Chapters 2 and 3, the main focus of this thesis is the use of multiresolution methods in digital communications. For this reason, the following section gives a brief overview of some of the important concepts and issues in

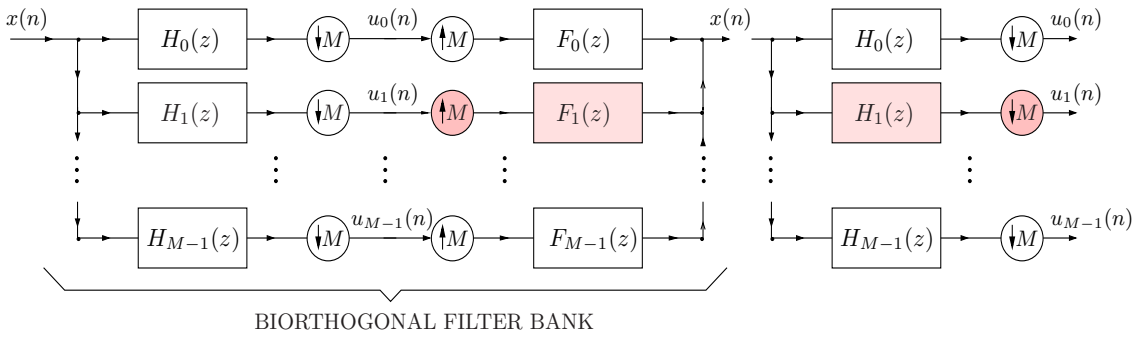

Figure 1.8: Biorthogonal partners in biorthogonal filter banks.

modern communication systems.

1.3 Multirate applications in digital communications

1.3.1 System for digital communication

The block diagram of the communication system that is the focus of this thesis is shown in Fig.1.9. Even though the figure title reads 'general,' numerous variations and extensions are possible [39]. The system focuses on a single user with the corresponding discrete message $s(n)$. This message is to be transmitted to the single receiver, only after sustaining the perturbations introduced by the transmission medium. These perturbations are modeled by the continuous-time LTI channel $c_c(t)$ and the appropriate additive noise at the input of the receiver. The design challenge amounts to ensuring that the received sequence $\widehat{s}(n)$ resembles the original message under some criteria (usually in the ℓ_2 sense). To this end, the receiver often introduces some redundancy combined with the appropriate pre-processing. The goal of this block is to facilitate the signal reconstruction at the transmitter (more about this in the following subsection). The obtained signal $x(n)$ with rate $1/T$ is converted to analog and sent through the medium to the receiver, only after the pulse-shaping. The combined effect of the pulse-shaping and the physical channel is often referred to as the *equivalent channel* and denoted by $f_c(t)$. At the receiver, the corrupted signal is first sampled and digitized, according to the sampling rate q/T. In this thesis we mostly focus on the case when $q > 1$ which corresponds to acquiring 'more information than absolutely necessary' about the signal and the channel. This further facilitates the signal recovery. The corresponding digital equalizer works at the higher rate and that combined with its increased complexity is the price to pay for the improvement in performance achieved by oversampling. Finally, the signal rate needs to be reduced back to the rate of $s(n)$. This is usually achieved after decimating by q and removing the redundancy.

All the signals in Fig.1.9 can be scalars or vectors. Correspondingly, the LTI systems can be SISO or MIMO. The unconventional notation in Fig.1.9 is chosen to reflect these possibilities. Vector signals arise naturally in situations when there is a number of sensors [53], but can also be obtained by blocking scalar signals [39], [49]. The system is further complicated if there is more than one transmitter and/or receiver.

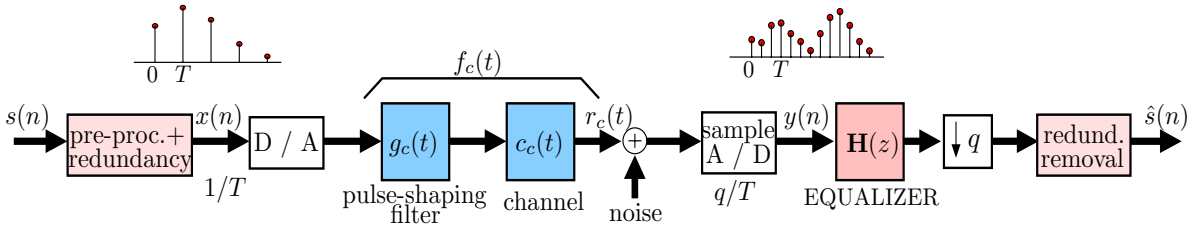

Figure 1.9: Block diagram of a general communications system.

In this thesis we mainly focus on the blocks for redundancy insertion and pre-processing together with the corresponding equalization and redundancy removal (Chapter 4), as well as equalization for different values of the parameter q in the vector and the scalar case (Chapters 2, 3). Also, of special interest will be the system modifications for application in multiuser communications and the corresponding equalization algorithms (Chapter 5). Biorthogonal partners play a special role in the equalizer design whenever $q > 1$, and this is investigated in Chapters 2 and 3. As for the material in the remainder of the thesis, it involves the use of more general multirate structures sometimes called *filter bank precoders*. In the following subsection we provide the corresponding notation and the equivalent representation.

1.3.2 Multirate systems in digital communications: filter bank precoders

As noted in Section 1.1.2, the polyphase representation of digital filters is put to use quite often in multirate DSP. One example is in deriving the equivalence between a bank of filters and the corresponding *polyphase matrix*. Consider the systems on the left-hand side of Fig.1.10. If $P = K = J$, the concatenation of systems in Fig.1.10(b) and Fig.1.10(a) is better known as a P-channel maximally decimated filter bank [61]. However, in most applications in communications P is assumed to be greater than K and J, therefore the structure is sometimes referred to as an overdecimated filter bank. Consider the structure in Fig.1.10(a). It is better known as the filter bank precoder. Note that the rate of $x(n)$ is greater than the combined rates of the signals in the vector $\mathbf{s}(n)$, therefore the structure is often used to introduce redundancy in the data stream at the transmitter side of a communication system. As mentioned in Section 1.3.1, this redundancy proves useful in solving several important practical problems. These include blind channel equalization, equalization of ill-behaved channels and user separation in multiuser systems [18], [19]. We deal with some of these problems in Chapters 4 and 5. At this point we first derive the aforementioned equivalence and then briefly motivate the introduction of redundancy as a remedy for numerous practical problems in digital communications.

Polyphase matrix notation. The overdecimated filter banks in Fig.1.10 are equivalent to the respective systems shown on the right-hand side. Rectangular matrices $\mathbf{R}(z)$ and $\mathbf{E}(z)$ are called polyphase matrices for the corresponding banks of filters. Using the blocking and unblocking definitions as in Fig.1.4 it can be shown that the kth column of $\mathbf{R}(z)$ consists of Type 1 polyphase components of $F_k(z)$ and that the jth row of $\mathbf{E}(z)$ consists of Type 2 polyphase components of $H_j(z)$, both with respect to P. In other words, let

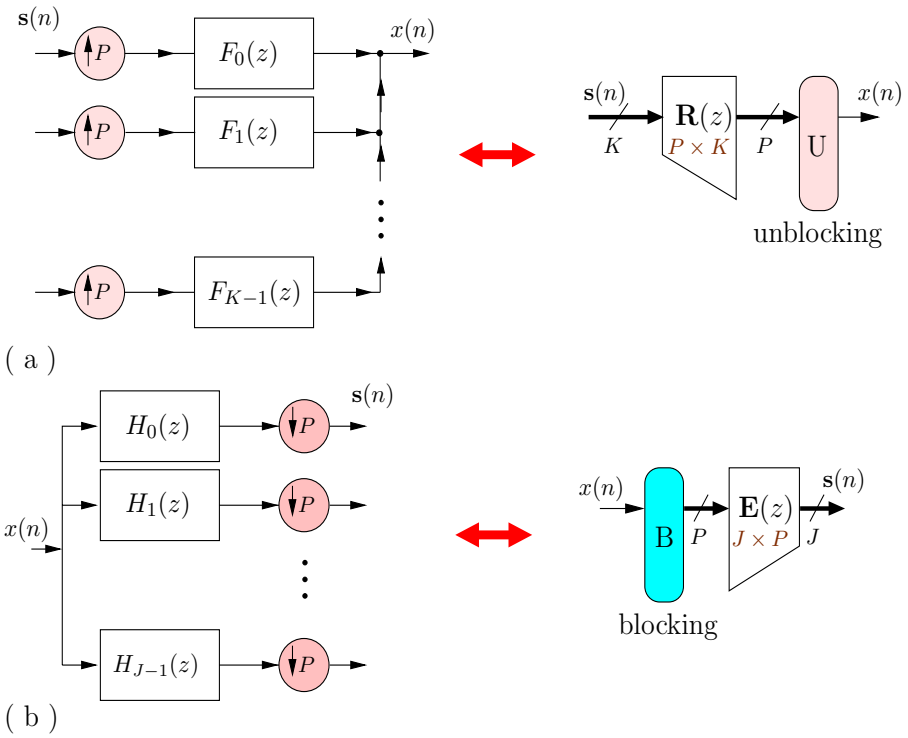

Figure 1.10: Polyphase representations of (a) filter bank precoder and (b) analysis filter bank.

$\mathbf{d}(z) = \begin{bmatrix} 1 & z^{-1} & \cdots & z^{-(P-1)} \end{bmatrix}$; then we have

$$[F_0(z) \;\; F_1(z) \;\; \cdots \;\; F_{K-1}(z)] = \mathbf{d}(z)\mathbf{R}(z^M), \quad \text{and} \quad [H_0(z) \;\; H_1(z) \;\; \cdots \;\; H_{J-1}(z)]^T = \mathbf{E}(z^M)\widetilde{\mathbf{d}}(z). \quad (1.6)$$

In addition to providing a compact notation, the structures on the right-hand side of Fig.1.10 are also efficient from the computational point of view (they promote parallel computations). For example, the rate of the vector signal at the entrance of $\mathbf{R}(z)$ is P times lower than that of the signal at the entrance of the filters $\{F_k(z)\}$. Finally, note that even though the expanders and decimators do not appear explicitly in the diagrams on the right-hand side of Fig.1.10, these are indeed multirate systems by the virtue of the fact that the combined rates at the input and at the output of the systems are not equal.

Significance of filter bank precoders. Precoders find use in solving some of the following problems.

1. *Blind channel equalization.* If the channel is unknown but is assumed to be of finite length, its interference effect is modeled as an unknown FIR filter that should be undone at the receiver. Redundancy introduced by the precoder at the transmitter makes it easier for the receiver to 'guess' this linear transform [17], [42]–[43].

2. *Equalization of ill-behaved channels.* If the channel has zeros outside or close to the unit circle, the inverse filtering required for equalization might be noncausal, unstable, or simply very sensitive to the input noise. Introducing certain redundancy at the transmitter helps avoid inverse filtering altogether.

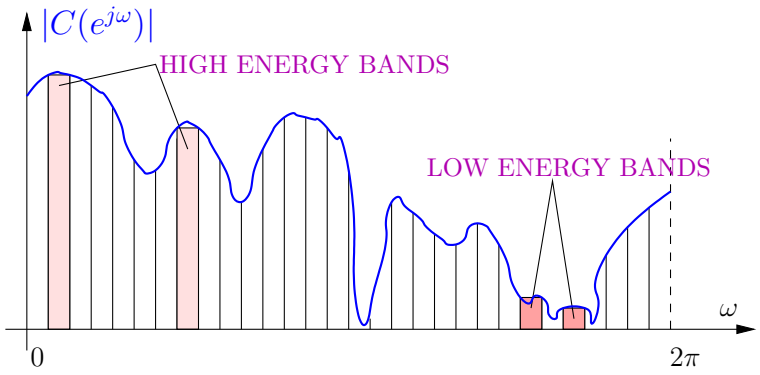

Figure 1.11: Channel magnitude response divided in frequency bands.

Consequently, these alternative equalizers usually perform better in the presence of noise [5], [7], [27], [30], [49].

3. *Power and bit allocation in frequency bands.* Some filter bank precoders together with the corresponding equalization structures at the receiver effectively divide the channel frequency response into a certain number of nonoverlaping channels, corresponding to different frequency bands (see Fig.1.11). The data is then divided according to certain criteria and sent over these independent channels. In order to achieve better performance of the overall system, it proves beneficial to allocate bits and power *nonuniformly* across different bands. The optimal allocation algorithm is a function of the corresponding channel energies and the noise power spectral density (PSD) [5], [7]–[9], [27], [62]. Optimal precoding in this context is the subject of Chapter 4.

4. *User separation in multiuser systems.* Consider the 'uplink scenario' when M different users simultaneously send messages to the common receiver. How to extract the message from user m, i.e.,cancel the interference from the other users without compromising the quality of the desired signal? This problem is investigated in Chapter 5. It is further complicated when different users communicate through different, possibly unknown and time-varying channels. One approach involves using a filter bank precoder for introducing the controlled redundancy which serves as a *signature* distinguishing the desired user from the interfering ones [20]–[21], [41].

1.4 Outline of the thesis

1.4.1 MIMO biorthogonal partners: theory and applications (Chapter 2)

The material in Chapters 2 and 3 presents the extension of the concept of biorthogonal partners to the case of vector signals and noninteger decimation ratios. Chapter 2 deals with multiple input—multiple output (MIMO) biorthogonal partners. As mentioned previously, they arise in many different contexts. The central application considered here is that of MIMO channel equalization, especially with *fractionally*

spaced equalizers. Returning to the general communication system from Fig.1.9, this scenario corresponds to communicating with vector signals and sampling the received signal at rate q/T, for some integer $q > 1$. In this context we assume that no additional redundancy has been inserted in the data stream and that there is no precoding in the system.

Chapter 2 is initiated by deriving the comprehensive theory of MIMO biorthogonal partners and answering some of the most important questions inherited from the scalar case. What are the conditions for the existence of MIMO biorthogonal partners and what is their most general form? Under what conditions do rational matrix transfer functions have polynomial (or FIR) biorthogonal partners? When are these FIR partners unique? How to construct the most general FIR partner (of a given order)? After deriving the theoretical framework of MIMO biorthogonal partners, we consider some of their applications. In MIMO channel equalization, we exploit the inherent *non-uniqueness* of biorthogonal partners and construct fractionally spaced equalizers (FSEs) that perfectly eliminate the inter-symbol interference (ISI) introduced by the channel, and at the same time minimize the noise power at the receiver. Comparing the performance of these flexible FSEs to the symbol-spaced solutions and FSEs without noise optimization, we conclude that significant improvements in performance are possible with minimal or no increase in the receiver complexity.

Several other applications of MIMO biorthogonal partners are considered next. We review their role in the least squares approximation of vector signals. In this context the least squares problem is limited to that of finding the approximation for a vector signal $\mathbf{x}(n)$ within a class of signals described by a multirate model. The optimal solution involves a certain form of biorthogonal partners. Finally, we consider the relation between biorthogonal partners and multiwavelets, especially the multiwavelet prefiltering.

1.4.2 Fractional biorthogonal partners and applications (Chapter 3)

The work in Chapter 3 is yet another extension of the notion of biorthogonal partners to the case where the upsampling and downsampling ratios are not integers but *rational numbers*. Hence the name fractional biorthogonal partners (FBPs). The conditions for the existence of stable and of FIR FBPs are derived. It is also shown that FIR solutions (when they exist) are not unique. The construction algorithm for FIR FBPs is presented that captures the non-uniqueness of these solutions in the form of a polynomial factor to be adjusted. This flexibility in the FBP design proves useful in solving the problem of scalar equalization with oversampling at the receiver. In this case, however, the amount of oversampling (parameter q in Fig.1.9) is not an integer but a rational number. We show that it is possible to optimize FIR FBPs so that when acting as zero-forcing FSEs they also reduce the noise power at the receiver. The performance of such optimized equalizers is evaluated by comparing it to the performance of several other equalization methods including the minimum mean-squared error (MMSE) equalizer. Another application considered is the all-FIR interpolation technique with the minimum amount of oversampling required in the input signal. Finally, we also consider the extension of the least squares approximation problem to the setting of fractional biorthogonal partners. The rest of the thesis deals with more general multirate structures in digital communications.

1.4.3 Precoding in cyclic prefix-based communication systems (Chapter 4)

The focus of Chapter 4 is on the equalization techniques based on cyclic prefix which are widely used in high speed data transmission over frequency selective channels, such as twisted pair channels in telephone cables [5], [49]. Their use in conjunction with DFT filter banks is especially attractive, given the low complexity of implementation. Some examples include the DFT-based DMT systems. In this chapter we consider a general cyclic prefix based system for communications and show that the equalizer performance can be improved by simple pre- and post-processing aimed at reducing the noise power at the receiver. This processing is done independently of the channel equalization performed by the frequency domain equalizer. Drawing the analogy to the system in Fig.1.9, the work in this chapter is focused on designing the optimal precoder (for noise reduction) if the redundancy comes in the form of a cyclic prefix and there is no oversampling at the receiver ($q = 1$). Perhaps not surprisingly, if the channel noise is uncorrelated, the optimal precoder is shown to perform the optimal power allocation across frequency bands (see Fig.1.11), however according to a somewhat less intuitive allocation procedure.

1.4.4 Equalization with oversampling in multiuser communications (Chapter 5)

Chapter 5 differs in theme from the earlier ones since it studies the communication systems with *multiple users*, i.e.,multiple transmitters and receivers. Such systems are invariably present in modern wireless communications. Some of the major challenges in the design of these systems are the suppression of multiuser interference (MUI) and inter-symbol interference (ISI) within a single user created by the multipath propagation. Both of these problems were addressed successfully in a recent design of a mutually-orthogonal usercode-receiver (AMOUR) for code division multiple access (CDMA) systems [18]–[21]. While AMOUR is successful in converting a multiuser CDMA system into parallel single-user systems with no ISI *regardless of the communication medium*, the noise amplification at the receiver can be significant in some multipath channels. In this chapter we provide an alternative approach to understanding AMOUR CDMA systems and propose a modified receiver that incorporates signal oversampling by integer or rational factors. Comparing the performance of such fractionally spaced AMOUR (FSAMOUR) systems to the conventional ones we conclude that their robustness in noisy environments can be significantly improved at the cost of slightly increased complexity of the receiver. The main scope of this chapter, therefore, is to provide a contribution to the ongoing task of designing efficient and robust multiuser communication systems.

1.5 Notation

In general, notation in this thesis closely parallels that in [61]. Superscripts (*) and (^{T}) denote the complex conjugate and matrix (or vector) transpose respectively, while superscript dagger (†) denotes the conjugate transpose. Boldface letters are used for matrices and vectors. Lowercase letters are used for discrete sequences, while uppercase letters are used for Fourier and z-transforms. If not stated otherwise, all matrices

in the thesis are rectangular. The identity matrix of size $N \times N$ is denoted by $\mathbf{I}_N$. Let $r(z)$ be the rank of a polynomial matrix in z. The *normal rank* is defined as the maximum value of $r(z)$ in the entire z plane. For LTI transfer matrices $\mathbf{H}(z)$, the 'paraconjugate' $\mathbf{H}^\dagger(1/z^*)$ is denoted by $\widetilde{\mathbf{H}}(z)$; thus $\widetilde{\mathbf{H}}(e^{j\omega}) = \mathbf{H}^\dagger(e^{j\omega})$. Equations (1.1), (1.2) together with Fig.1.2 establish notation for decimators and expanders. In the block diagram vector and scalar expanders are denoted as in Fig.1.3. In the time domain the decimated and expanded sequences are denoted by $[x(n)]_{\downarrow M}$ and $[x(n)]_{\uparrow M}$ respectively. Notice that

$$\big[X(z^M)Y(z)\big]_{\downarrow M} = X(z)\,[Y(z)]_{\downarrow M}\,, \quad \text{and} \quad \big[X(z^M)Y(z)\big]_{\downarrow M\uparrow M} = X(z^M)\,[Y(z)]_{\downarrow M\uparrow M}\,.$$

The Kronecker delta function is denoted by $\delta(\cdot)$ and defined as: $\delta(0) = 1$ and $\delta(x) = 0$ if $x \neq 0$. We denote by $\mathrm{diag}(\mathbf{A})$ the column vector consisting of the diagonal entries of the square matrix $\mathbf{A}$ and by $\mathrm{diag}(\mathbf{a})$ the square diagonal matrix whose diagonal elements are given by the vector $\mathbf{a}$. The *trace* matrix operator, denoted by $\mathrm{Tr}\{\cdot\}$ calculates the sum of the diagonal elements. A square polynomial matrix is said to be *unimodular* if its determinant is a nonzero constant. A rectangular matrix is called *fat* if it has more columns than rows; otherwise it is said to be *tall*. Throughout the thesis, by 'existence of a biorthogonal partner' we actually mean 'existence of a *stable* biorthogonal partner.'

Chapter 2 MIMO biorthogonal partners: theory and applications

The theory of biorthogonal partners has been developed in [65] and reviewed in Section 1.2 for the simple, single input-single output (SISO) case. Multiple input—multiple output (MIMO) biorthogonal partners can be defined using a similar approach. One distinction between scalar and vector biorthogonal partners should be clearly noted. While it is understood that scalar biorthogonal partners can interchange places without violating the Nyquist condition (1.5), in the MIMO case the biorthogonal partner relation is not symmetric. Therefore, we distinguish between a *left biorthogonal partner* (**LBP**) and a *right biorthogonal partner* (**RBP**). In this chapter we first derive some theoretical properties of MIMO biorthogonal partners. Many of these properties are extensions to the vector case of some known results from the case of scalar signals [65]. However, some of the properties take a different form in the case of vector signals and, furthermore, lead to several new applications. One of the applications of MIMO biorthogonal partners that will be explored in the following is the equalization of vector digital communication channels. Specifically, we are interested in zero-forcing fractionally spaced MIMO equalizers. Fractionally spaced equalizers (**FSE**) demonstrate many advantages over symbol spaced equalizers (**SSE**), such as the existence of an FIR solution and reduced sensitivity to the shift in sampling instances [39]. Moreover, FSEs turn out to be nothing but biorthogonal partners of the equivalent channel transfer matrix and therefore we can resort to the theory of MIMO biorthogonal partners in the process of equalizer design. The content of the chapter is mainly drawn from [80] and its portions have been presented at [83], [85] and [81].

2.1 Chapter outline and relation to previous work

In Section 2.2 we introduce the precise definition of MIMO biorthogonal partners. We derive a general closed form expression for a MIMO transfer function $\mathbf{H}(z)$ to be a biorthogonal partner of $\mathbf{F}(z)$. We also derive a set of necessary and sufficient conditions on $\mathbf{F}(z)$ which allow for the existence of its MIMO biorthogonal partner.

In Section 2.3 we consider FIR MIMO biorthogonal partners in greater detail. A set of necessary and sufficient conditions for the existence of FIR MIMO biorthogonal partners is derived. We especially concentrate on the fact that FIR MIMO biorthogonal partners, when they exist, are not unique. In Section 2.4 we exploit this non-uniqueness in order to reduce the noise power at the output of fractionally spaced equalizers for vector channels. Finally, we address the performance of our algorithm through simple design examples of FSEs for vector channels.

In Section 2.5 we deal with other possible applications of MIMO biorthogonal partners. In particular, we review their role in the least squares approximation of vector signals. For the purpose of this chapter, the least squares problem is limited to that of finding the approximation for a vector signal $\mathbf{x}(n)$ within a certain class of signals. In the scalar case the idea originated in the context of spline interpolation [6], where it was suggested that the signal corrupted by noise could be approximated with an oversampled spline. We show that in the vector case the solution to this problem involves a particular form of MIMO biorthogonal partners. This is also closely related to the concept of oblique projections studied intensively in [3] and [4]. Finally, we consider the relation between biorthogonal partners and multiwavelets. In one of the pioneering works on the subject [90], the use of prefiltering for multiwavelet transform was introduced. Here we consider the prefiltering problem in the light of biorthogonal partners and draw the connection between the two. The majority of the results in Section 2.5 are not new to the signal processing community. However, the significant contribution of this section is in placing some of the well-known results in the biorthogonal partner setting.

2.2 MIMO biorthogonal partners: definition and properties

We start the discussion in this section by defining the notion of a MIMO biorthogonal partner.

Definition 2.1. MIMO biorthogonal partners. A MIMO transfer function $\mathbf{H}(z)$ is said to be a left biorthogonal partner (LBP) of $\mathbf{F}(z)$ with respect to an integer M if

$$[\mathbf{H}(z)\mathbf{F}(z)]_{\downarrow M} = \mathbf{I}. \tag{2.1}$$

Similarly, a MIMO transfer function $\mathbf{H}(z)$ is said to be a right biorthogonal partner (RBP) of $\mathbf{F}(z)$ with respect to an integer M if $[\mathbf{F}(z)\mathbf{H}(z)]_{\downarrow M} = \mathbf{I}$.

The interpretation of the first part of the above definition is shown in Fig.2.1. Recall that the multirate system in Fig.2.1 is just an LTI system with transfer function $[\mathbf{H}(z)\mathbf{F}(z)]_{\downarrow M}$, which under the condition (2.1) becomes the identity. It can be seen that if $\mathbf{H}(z)$ is an LBP of $\mathbf{F}(z)$ this implies that $\mathbf{F}(z)$ is an RBP of $\mathbf{H}(z)$, but it does not imply that $\mathbf{H}(z)$ is also an RBP of $\mathbf{F}(z)$. The latter would happen if, for example, the two matrices commuted. The other important point to make here is that if M is changed, the two filters might not remain partners. However, we will often omit the term 'with respect to M,' since it will usually be understood from the context.

In the following we concentrate on the existence issues and on the general form of MIMO biorthogonal partners. The first result gives the most general form of a biorthogonal partner. In the subsequent discussion, the question of uniqueness of biorthogonal partners will also be addressed. The second result states necessary and sufficient conditions on a transfer matrix $\mathbf{F}(z)$ and integer M such that there exists a biorthogonal partner of $\mathbf{F}(z)$ with respect to M.

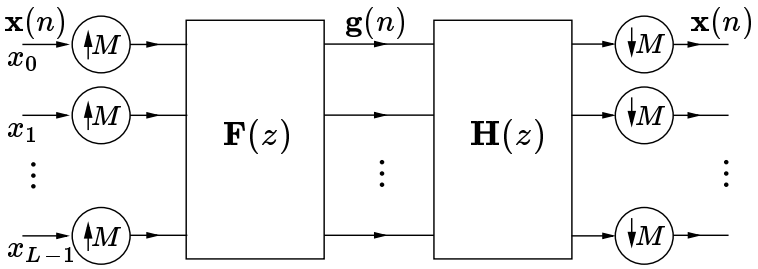

Figure 2.1: Block diagram interpretation of a left biorthogonal partner.

2.2.1 General expression

We first derive a general expression for $\mathbf{H}(z)$ in terms of $\mathbf{F}(z)$ in Fig.2.1. The theorem has two parts, one for left biorthogonal partners and the other for right biorthogonal partners. It is very intuitive that whatever holds for LBPs should also hold for RBPs (in a slightly modified form), and this comes into play in the proof of Theorem 2.1.

Theorem 2.1. General form of biorthogonal partners.

1. A MIMO transfer function $\mathbf{H}(z)$ is an LBP of $\mathbf{F}(z)$ if and only if it can be written in the form

$$\mathbf{H}(z) = \left([\mathbf{G}(z)\mathbf{F}(z)]_{\downarrow M\uparrow M}\right)^{-1}\mathbf{G}(z) \tag{2.2}$$

   for some MIMO transfer function $\mathbf{G}(z)$.

2. A MIMO transfer function $\mathbf{H}(z)$ is an RBP of $\mathbf{F}(z)$ if and only if it can be written in the form

$$\mathbf{H}(z) = \mathbf{G}(z)\left([\mathbf{F}(z)\mathbf{G}(z)]_{\downarrow M\uparrow M}\right)^{-1} \tag{2.3}$$

   for some MIMO transfer function $\mathbf{G}(z)$.

Proof. First we will prove the backward part of the statement one. Given $\mathbf{H}(z)$ as in (2.2), we have

$$[\mathbf{H}(z)\mathbf{F}(z)]_{\downarrow M} = \left([\mathbf{G}(z)\mathbf{F}(z)]_{\downarrow M\uparrow M}\right)^{-1}[\mathbf{G}(z)\mathbf{F}(z)]_{\downarrow M} = \left([\mathbf{G}(z)\mathbf{F}(z)]_{\downarrow M}\right)^{-1}[\mathbf{G}(z)\mathbf{F}(z)]_{\downarrow M} = \mathbf{I}$$

The backward proof of the second statement follows in the same manner. Next we give the forward proof of the **second** statement. For this, first consider Fig.2.2(a). Here $\mathbf{x}_i(n)$ is an arbitrary vector sequence and $\mathbf{g}_i(n)$ is the corresponding output of $\mathbf{H}(z)$. By assumption $\mathbf{H}(z)$ is an RBP of $\mathbf{F}(z)$ and from the definition we have that the output of the system has to be $\mathbf{x}_i(n)$ again. However, this also means that the signal $\mathbf{g}_i(n)$ at the input of the system in Fig.2.2(b) produces $\mathbf{g}_i(n)$ at its output. Thus we have

$$\mathbf{H}(z)[\mathbf{F}(z)\mathbf{G}_i(z)]_{\downarrow M\uparrow M} = \mathbf{G}_i(z). \tag{2.4}$$

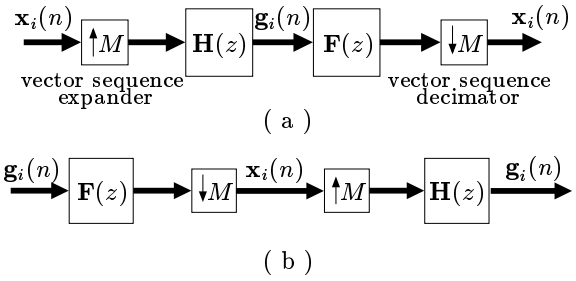

Figure 2.2: Pertaining to the proof of Theorem 2.1.

This equality holds for any $\mathbf{G}_i(z)$ obtained as in Fig.2.2(a). We repeat the procedure sufficient number of times, each time taking $\mathbf{X}_n(z)$ to be linearly independent from the previous vectors $\mathbf{X}_1(z)$, $\mathbf{X}_2(z)$, ... $\mathbf{X}_{n-1}(z)$. Collecting those vectors as columns in a matrix $\mathbf{X}(z)$, and the corresponding vectors $\mathbf{G}_i(z)$ in a matrix $\mathbf{G}(z)$, we have the following

$$\mathbf{H}(z)[\mathbf{F}(z)\mathbf{G}(z)]_{\downarrow M\uparrow M} = \mathbf{G}(z),$$

which after solving for $\mathbf{H}(z)$ gives

$$\mathbf{H}(z) = \mathbf{G}(z)\left([\mathbf{F}(z)\mathbf{G}(z)]_{\downarrow M\uparrow M}\right)^{-1} \tag{2.5}$$

and this concludes the proof of (2.3). Notice that $[\mathbf{F}(z)\mathbf{G}(z)]_{\downarrow M\uparrow M} = [\mathbf{X}(z)]_{\uparrow M}$ so that by choosing the sequences $\mathbf{x}_i(n)$ carefully we can ensure that the matrix inversion in (2.5) is valid. Now we move on to prove the forward direction of the first statement. For this we notice that if $\mathbf{H}(z)$ is an LBP of $\mathbf{F}(z)$, then $\mathbf{H}^T(z)$ is an RBP of $\mathbf{F}^T(z)$. Thus from (2.3) we have

$$\mathbf{H}^T(z) = \mathbf{G}^T(z)\left([\mathbf{F}^T(z)\mathbf{G}^T(z)]_{\downarrow M\uparrow M}\right)^{-1},$$

for some matrix $\mathbf{G}^T(z)$. Finally, taking the transpose of both sides we arrive at (2.2) and this concludes the proof. $\triangledown\triangledown\triangledown$

In the proof of Theorem 2.1 we transposed the result for RBP in order to arrive at a similar result for LBP. The same trick could also be used for other results on MIMO partners and this is why we only consider left biorthogonal partners in the following; very similar results hold for right biorthogonal partners.

Clearly, from the equations (2.2) and (2.3) we have that MIMO biorthogonal partners are in general **not unique**. Any stable matrix transfer function $\mathbf{G}(e^{j\omega})$ such that $\det\left([\mathbf{G}(e^{j\omega})\mathbf{F}(e^{j\omega})]_{\downarrow M}\right)$ is nonzero for all ω gives rise to a stable LBP of $\mathbf{F}(z)$. The similar conclusion holds for right biorthogonal partners. Here are some special cases of interest.

Example 2.1: In the square case, if $\left|\det\left[\mathbf{F}(e^{j\omega})\right]\right| > 0$ for all ω then $\mathbf{H}(z) = \mathbf{F}^{-1}(z)$ is a theoretically stable biorthogonal partner (both LBP and RBP) of $\mathbf{F}(z)$. It can be obtained from (2.2) or (2.3) with the choice $\mathbf{G}(z) = \mathbf{F}^{-1}(z)$. This is conceptually the simplest biorthogonal partner.

Example 2.2: If the construction of biorthogonal partners from Example 2.1 does not work for a particular $\mathbf{F}(z)$, we can try the following. Suppose that $\det\left[[\mathbf{F}(e^{j\omega})]_{\downarrow M}\right]$ is nonzero for all ω. Then, substituting $\mathbf{G}(z) = \mathbf{I}$ in (2.2) or (2.3) we get a biorthogonal partner $\mathbf{H}(z) = \left([\mathbf{F}(z)]_{\downarrow M\uparrow M}\right)^{-1}$.

Example 2.3: To get yet another solution for an LBP, consider the matrix filter

$$\mathbf{H}(z) = \left([\widetilde{\mathbf{F}}(z)\mathbf{F}(z)_{\downarrow M\uparrow M}\right)^{-1}\widetilde{\mathbf{F}}(z),$$

This solution is obtained from (2.2) with $\mathbf{G}(z) = \widetilde{\mathbf{F}}(z)$, and is valid as long as $\det\left(\mathbf{F}^{\dagger}(e^{j\omega})\mathbf{F}(e^{j\omega})]_{\downarrow M}\right)$ is nonzero on the unit circle. It plays a significant role in the rest of this chapter, since it occurs in several different contexts.

2.2.2 Existence

In the following, we look into the problem of the existence of biorthogonal partners more closely. Consider a MIMO transfer function $\mathbf{F}(z)$ with the Type 2 polyphase representation

$$\mathbf{F}(z) = \sum_{k=0}^{M-1} z^k \mathbf{F}_k(z^M). \tag{2.6}$$

We present a necessary and sufficient condition for the existence of its MIMO biorthogonal partner $\mathbf{H}(z)$.

Theorem 2.2. Existence of LBP. A MIMO transfer function $\mathbf{F}(z)$ given by (2.6) has an LBP if and only if the following implication holds for each ω in $0 \le \omega < 2\pi$

$$\mathbf{C}^T(e^{j\omega})[\mathbf{F}_0^T(e^{j\omega}) \;\; \mathbf{F}_1^T(e^{j\omega}) \;\; \cdots \;\; \mathbf{F}_{M-1}^T(e^{j\omega})] = \mathbf{0} \;\; \Rightarrow \;\; \mathbf{C}(e^{j\omega}) = \mathbf{0}.$$

Therefore, for any fixed ω there cannot exist a nonzero common annihilating vector $\mathbf{C}(e^{j\omega})$ for all M polyphase components of $\mathbf{F}(e^{j\omega})$. Note that in order for $\mathbf{F}(z)$ to have an *inverse* we need to have $\det[\mathbf{F}(e^{j\omega})] \neq 0$, for all ω, and that condition is stricter than the one in Theorem 2.2.

Proof. We start by proving the forward part of the theorem, i.e., supposing $\mathbf{H}(z)$ is a stable LBP of $\mathbf{F}(z)$, we need to show that there cannot exist a nonzero common annihilating vector $\mathbf{C}(e^{j\omega})$. By the supposition, we have that $[\mathbf{H}(z)\mathbf{F}(z)]_{\downarrow M} = \mathbf{I}$, which implies that there cannot exist a nonzero vector $\mathbf{C}(z)$ such that $\mathbf{F}(z)\mathbf{C}(z^M) = \mathbf{0}$. Indeed, if we assume there exists such nonzero vector $\mathbf{C}(z)$, we end up with the following contradiction

$$\mathbf{0} = [\mathbf{H}(z)\mathbf{F}(z)\mathbf{C}(z^M)]_{\downarrow M} = \mathbf{C}(z).$$

Rewriting $\mathbf{F}(z)$ in the Type 2 polyphase form (2.6) we then have that there cannot exist a nonzero vector

$\mathbf{C}(z)$ such that

$$\sum_{k=0}^{M-1} z^k \mathbf{F}_k(z^M)\mathbf{C}(z^M) = \mathbf{0}$$

or equivalently, such that

$$\mathbf{F}_k(z)\mathbf{C}(z) = \mathbf{0} \quad \forall k, \quad 0 \le k \le M-1.$$

Therefore, if there is a stable LBP of $\mathbf{F}(z)$, there cannot exist a common nonzero annihilating vector $\mathbf{C}(e^{j\omega})$ for all M polyphase components $\mathbf{F}_k(e^{j\omega})$.

Next we proceed to prove the converse. To that end, we suppose that for no ω does there exist a common nonzero vector $\mathbf{C}(e^{j\omega})$ that annihilates all M polyphase components $\mathbf{F}_k(e^{j\omega})$. That is to say, given any $\omega \in [0, 2\pi)$ such that $\mathbf{C}(e^{j\omega}) \neq \mathbf{0}$, there exists k, satisfying $0 \le k \le M-1$, such that $\mathbf{F}_k(e^{j\omega})\mathbf{C}(e^{j\omega}) \neq \mathbf{0}$. This implies that the following matrix $\mathbf{S}(\omega)$ is positive definite for all ω

$$\mathbf{S}(\omega) = \sum_{k=0}^{M-1} \mathbf{F}_k^{\dagger}(e^{j\omega})\mathbf{F}_k(e^{j\omega}). \tag{2.7}$$

To justify this, observe that for any vector $\mathbf{C}(e^{j\omega})$ and $\mathbf{S}(\omega)$ as in (2.7), the entity $\mathbf{C}^{\dagger}(e^{j\omega})\mathbf{S}(\omega)\mathbf{C}(e^{j\omega})$ is a summation of nonnegative terms. Moreover, as asserted previously, for any nonzero choice of $\mathbf{C}(e^{j\omega})$ at least one of those terms is strictly positive, so that the overall result is positive. Now we observe that the matrix $\mathbf{S}(\omega)$ defined by (2.7) can be rewritten as $\mathbf{S}(\omega) = [\mathbf{F}^{\dagger}(e^{j\omega})\mathbf{F}(e^{j\omega})]_{\downarrow M}$ and from the previous discussion we have that

$$\det\left([\mathbf{F}^{\dagger}(e^{j\omega})\mathbf{F}(e^{j\omega})]_{\downarrow M}\right) > 0. \tag{2.8}$$

The final conclusion is that if there does not exist a common nonzero annihilating vector $\mathbf{C}(e^{j\omega})$ for all M polyphase components $\mathbf{F}_k(e^{j\omega})$ then $\mathbf{F}(z)$ has a stable LBP. In particular, one such LBP is obtained as in Example 2.3 and is given by

$$\mathbf{H}(z) = \left([\widetilde{\mathbf{F}}(z)\mathbf{F}(z)_{\downarrow M}\right)^{-1}_{\uparrow M} \widetilde{\mathbf{F}}(z). \tag{2.9}$$

This concludes the proof. $\bigtriangledown\bigtriangledown\bigtriangledown$

In the following we will see that the LBP given by (2.9) has some other interesting properties. The next corollary asserts that if $\mathbf{F}(z)$ has any stable LBP, the choice (2.9) will be a valid one.

Corollary 2.1. A MIMO transfer function $\mathbf{F}(z)$ has a left biorthogonal partner if and only if $\mathbf{S}(\omega) = [\mathbf{F}^{\dagger}(e^{j\omega})\mathbf{F}(e^{j\omega})]_{\downarrow M}$ is a positive definite matrix for all ω in the range $[0, 2\pi)$.

Proof. If $[\mathbf{F}^{\dagger}(e^{j\omega})\mathbf{F}(e^{j\omega})]_{\downarrow M}$ is a positive definite matrix for all ω then (2.8) holds and thus (2.9) is a valid choice for LBP. Conversely, suppose that there exists a stable LBP of $\mathbf{F}(z)$. Consider $\mathbf{S}(\omega)$, which is obviously a positive semi-definite matrix for all ω. Writing $\mathbf{S}(\omega)$ as in (2.7) and recalling from Theorem 2.1 that the polyphase components $\mathbf{F}_k(e^{j\omega})$ cannot have a common annihilating vector we finally conclude that $\mathbf{S}(\omega)$ has to be positive definite, which concludes the proof. $\bigtriangledown\bigtriangledown\bigtriangledown$

2.3 Existence of FIR LBP

In Theorem 2.2 and Corollary 2.1, we saw the necessary and sufficient conditions for a matrix transfer function $\mathbf{F}(z)$ to have a biorthogonal partner. In practice the situation of most significance is when $\mathbf{F}(z)$ is a rational function of z. A question of considerable interest is the following: Under what conditions does a rational function $\mathbf{F}(z)$ have an FIR biorthogonal partner $\mathbf{H}(z)$? In fact it suffices to pose the previous question for any *FIR* filter $\mathbf{F}(z)$, which is evident by the following reasoning. Let $\mathbf{F}_r(z)$ be an arbitrary rational transfer matrix and let $D(z)$ be the least common multiple of the polynomials appearing in the denominators of the rational entries of $\mathbf{F}_r(z)$. Then we can write $\mathbf{F}_r(z) = \mathbf{F}(z)/D(z)$, where $\mathbf{F}(z)$ is an FIR matrix. If there exists an FIR biorthogonal partner $\mathbf{H}(z)$ of $\mathbf{F}(z)$, then $\mathbf{H}_r(z) = \mathbf{H}(z)D(z)$ is the corresponding FIR biorthogonal partner of $\mathbf{F}_r(z)$.

In view of all this, we begin the discussion in this section by finding the conditions for the existence of an FIR biorthogonal partner of an FIR transfer matrix. To this end we need to revisit the notion of *greatest right common divisors* (**GRCD**) of polynomial matrices [61], [26]. In the linear systems literature, GRCDs are most commonly defined for square matrices. In this setting, we will extend this definition to the case of rectangular matrices. In principle, we can define the GRCD of a $p_1 \times r$ polynomial matrix $\mathbf{A}(z)$ and a $p_2 \times r$ polynomial matrix $\mathbf{B}(z)$ to be any $m \times r$ polynomial matrix $\mathbf{R}(z)$ such that

1. $\mathbf{R}(z)$ is a common right divisor of $\mathbf{A}(z)$ and $\mathbf{B}(z)$, i.e., there exist polynomial matrices $\mathbf{A}_1(z)$ and $\mathbf{B}_1(z)$ such that $\mathbf{A}(z) = \mathbf{A}_1(z)\mathbf{R}(z)$ and $\mathbf{B}(z) = \mathbf{B}_1(z)\mathbf{R}(z)$;

2. If $\mathbf{R}_1(z)$ is another $m_1 \times r$ common right divisor of $\mathbf{A}(z)$ and $\mathbf{B}(z)$, then $\mathbf{R}_1(z)$ is a right divisor of $\mathbf{R}(z)$, i.e., there exists an $m \times m_1$ polynomial matrix $\mathbf{T}(z)$ such that $\mathbf{R}(z) = \mathbf{T}(z)\mathbf{R}_1(z)$.

However, for the purpose of our discussion it is enough to consider only square GRCDs $\mathbf{R}(z)$, so from now on by GRCD we shall mean *square* GRCD. Now we can state the following result.

Theorem 2.3. Existence of FIR LBP. Suppose $\mathbf{F}(z)$ is a causal and FIR $p \times r$ matrix, given by (2.6). Then there exists a causal FIR $r \times p$ matrix $\mathbf{H}(z)$ such that $[\mathbf{H}(z)\mathbf{F}(z)]_{\downarrow M} = \mathbf{I}$ if and only if GRCD$[\mathbf{F}_0(z), \mathbf{F}_1(z), \ldots \mathbf{F}_{M-1}(z)]$ is a unimodular matrix $\mathbf{R}(z)$.

Before proceeding to the proof of Theorem 2.3, several comments are due. Given an arbitrary MIMO transfer function, the GRCD-condition is almost always satisfied. For example, let

$$\mathbf{F}(z) = \begin{bmatrix} 3 + 2z^{-1} + z^{-2} & 2 + 3z^{-1} + z^{-2} \\ 1 + 3z^{-2} & 2 + z^{-1} + 3z^{-2} \end{bmatrix}.$$

The trivial biorthogonal partner (as in Example 2.1) is IIR in this case, since $\det[\mathbf{F}(z)] = 4 + 4z^{-1} + 6z^{-2} - 2z^{-3}$. However, it can be verified that the GRCD of the two polyphase components of $\mathbf{F}(z)$ is unimodular,

with one solution being (for a review on the construction of GRCDs, see [26])

$$\mathbf{R}(z) = -2 \begin{bmatrix} 4 & 2 \\ 0 & 1 \end{bmatrix}.$$

Therefore, an FIR LBP for $M = 2$ indeed exists and one possibility is (see the proof of Theorem 2.3)

$$\mathbf{H}(z) = \frac{1}{16} \begin{bmatrix} 8 + 4z^{-1} + 3z^{-2} & -8 - z^{-2} \\ -4 - 8z^{-1} - 6z^{-2} & 12 + 2z^{-2} \end{bmatrix}.$$

In the statement of Theorem 2.3 we have not assumed anything about the integers p and r - the dimensions of $\mathbf{F}(z)$. It will soon become clear that the necessary relation between them is given by

$$r \leq Mp. \tag{2.10}$$

Also, the constraint on $\mathbf{F}(z)$ and its LBP to be causal is unnecessary; it can be avoided if we allow the determinant of $\mathbf{R}(z)$ to be of the form cz^k, with $k \in \mathbb{Z}$, rather than just a constant.

Proof of Theorem 2.3. First we consider the case $M = 2$. If $\mathbf{F}_0(z)$ and $\mathbf{F}_1(z)$ are right coprime [which is equivalent to saying that $\mathbf{R}(z) = \text{GRCD}[\mathbf{F}_0(z), \mathbf{F}_1(z)]$ is unimodular] then there exist polynomial matrices $\mathbf{H}_0(z)$ and $\mathbf{H}_1(z)$ such that

$$\mathbf{H}_0(z)\mathbf{F}_0(z) + \mathbf{H}_1(z)\mathbf{F}_1(z) = \mathbf{I}. \tag{2.11}$$

This follows from the *simple Bezout identity* [26], extended to the rectangular case. (Although the extension is straightforward, we summarize these results in the Appendix for convenience.) In fact, from the construction of GRCDs [26] it follows that there exists a unimodular matrix $\mathbf{W}(z)$ such that

$$\underbrace{\begin{matrix} r \\ 2p-r \end{matrix}\!\!\begin{bmatrix} \overset{p}{\mathbf{W}_{11}(z)} & \overset{p}{\mathbf{W}_{12}(z)} \\ \mathbf{W}_{21}(z) & \mathbf{W}_{22}(z) \end{bmatrix}}_{\mathbf{W}(z)} \begin{bmatrix} \overset{r}{\mathbf{F}_0(z)} \\ \mathbf{F}_1(z) \end{bmatrix} \begin{matrix} p \\ p \end{matrix} = \begin{bmatrix} \overset{r}{\mathbf{R}(z)} \\ \mathbf{0} \end{bmatrix} \begin{matrix} r \\ 2p-r \end{matrix} \tag{2.12}$$

with indicated sizes of the building blocks. From (2.12) it is easy to see that we can choose

$$\mathbf{H}_0(z) = \mathbf{R}^{-1}(z)\mathbf{W}_{11}(z), \quad \mathbf{H}_1(z) = \mathbf{R}^{-1}(z)\mathbf{W}_{12}(z) \tag{2.13}$$

and that these are indeed polynomial (actually causal, FIR) matrices since $\mathbf{R}(z)$ is unimodular.

So far we have considered the $M = 2$ case, but the extension to arbitrary M follows readily by applying the rule

$$\text{GRCD}_{0 \leq k \leq M-1}[\mathbf{F}_k(z)] = \text{GRCD}\ \{\mathbf{F}_{M-1}(z), \quad \text{GRCD}_{0 \leq k \leq M-2}[\mathbf{F}_k(z)]\}. \tag{2.14}$$

Now, suppose by contradiction that $\mathbf{F}(z)$ has a causal FIR LBP $\mathbf{H}(z)$, but that

$$\mathrm{GRCD}[\mathbf{F}_0(z), \mathbf{F}_1(z), \dots \mathbf{F}_{M-1}(z)] = \mathbf{C}(z)$$

is not unimodular and let $\mathbf{F}_k(z) = \widehat{\mathbf{F}}_k(z)\mathbf{C}(z)$. Writing $\mathbf{H}(z)$ in the Type 1 polyphase form (1.3) we have

$$\mathbf{I} = [\mathbf{H}(z)\mathbf{F}(z)]_{\downarrow M} = \sum_{k=0}^{M-1} \mathbf{H}_k(z)\mathbf{F}_k(z) = \left(\sum_{k=0}^{M-1} \mathbf{H}_k(z)\widehat{\mathbf{F}}_k(z) \right) \mathbf{C}(z) \tag{2.15}$$

and it follows that

$$\sum_{k=0}^{M-1} \mathbf{H}_k(z)\widehat{\mathbf{F}}_k(z) = \mathbf{C}^{-1}(z).$$

The left-hand side of the above equation is a causal FIR matrix (since all $\mathbf{H}_k(z)$ and $\widehat{\mathbf{F}}_k(z)$ are causal FIR), but the right-hand side is not. This contradiction concludes the proof. $\triangledown\triangledown\triangledown$

Notice that (2.12) readily implies that $r \leq 2p$ in order for this particular construction to work. To see that (2.10), when $M = 2$, has to hold for *any* FIR LBP to exist, observe that (2.11) can be rewritten as

$$\begin{bmatrix} \mathbf{H}_0(z) & \mathbf{H}_1(z) \end{bmatrix} \underbrace{\begin{bmatrix} \mathbf{F}_0(z) \\ \mathbf{F}_1(z) \end{bmatrix}}_{\mathbf{P}(z)} = \mathbf{I}.$$

If $r > 2p$, the matrix $\mathbf{P}(z)$ above becomes fat, i.e., has no left inverse, thus in this case there is no FIR LBP of $\mathbf{F}(z)$. We revisit this relation for a general integer M in Section 2.4.2.

It is important to notice here that, if it exists, FIR LBP is not unique. There are two reasons for this. Firstly, the GRCD of two matrices is unique only up to a premultiplication by a unimodular matrix. Secondly, there are many unimodular matrices $\mathbf{W}(z)$ that satisfy (2.12) and each of them provides a valid solution. The issue of parameterization of these solutions will be treated in the following section. Also, notice that in the successive applications of the construction (2.12), as implied by the right-hand side of (2.14), GRCDs of rectangular $p \times r$ matrices $\mathbf{F}_i(z)$ and square $r \times r$ matrices $\mathbf{R}(z)$ are computed. The result will again be a $r \times r$ matrix, and the necessary condition now becomes $r \leq p + r$, which is always satisfied. The sizes of the building blocks $\mathbf{W}_{ij}(z)$ from (2.12) will also need to be adjusted accordingly.

2.4 Application in channel equalization

In the following, we consider the case where an FIR LBP is used as a MIMO channel equalizer. We will show that the flexibility in the choice of $\mathbf{H}(z)$ can be exploited in order to reduce the undesirable amplification of the channel noise. But, before proceeding to these results, we give a brief overview of some equalization techniques for the vector channels.

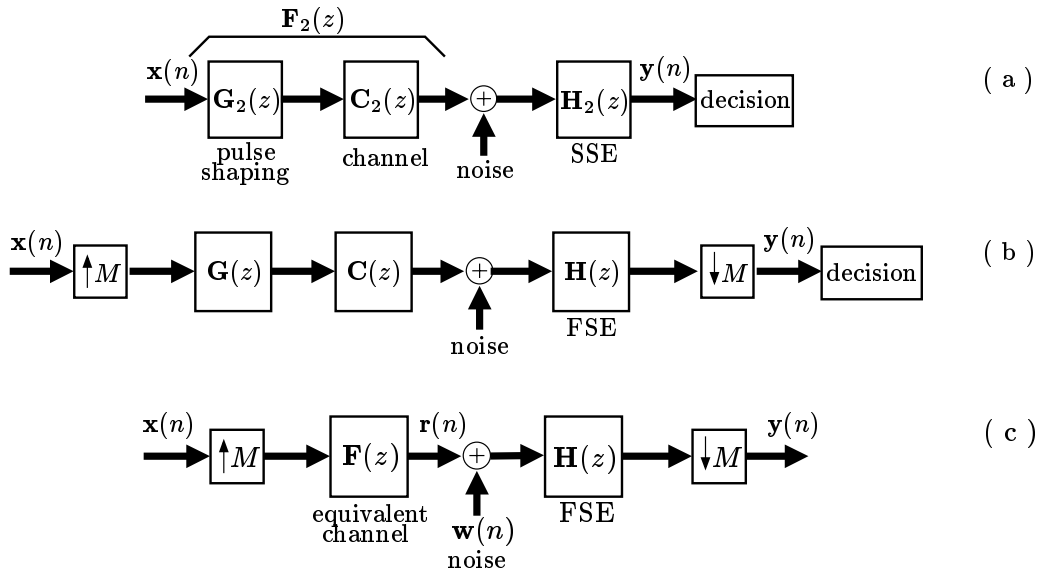

Figure 2.3: (a) Discrete-time equivalent of a digital communication system with SSE; the equivalent channel is $\mathbf{F}_2(z) = \mathbf{C}_2(z)\mathbf{G}_2(z)$. (b) Digital communication system from (a), now equalized with FSE $\mathbf{H}(z)$. (c) Further simplification of the system from (b); the equivalent channel is $\mathbf{F}(z) = \mathbf{C}(z)\mathbf{G}(z)$.

The discrete-time equivalent of an MIMO digital communication system with a symbol spaced equalizer (**SSE**) [39] is shown in Fig.2.3(a). The vector symbol rate at the input $\mathbf{x}(n)$ is $1/T$. Notice that the equalizer $\mathbf{H}_2(z)$ works at the same rate (thus the name symbol spaced equalizer). The discrete versions of the pulse shaping filter and the channel, $\mathbf{G}_2(z)$ and $\mathbf{C}_2(z)$, respectively, are obtained by sampling the corresponding continuous-time impulse responses also at the rate $1/T$. We will refer to their cascade $\mathbf{F}_2(z) = \mathbf{C}_2(z)\mathbf{G}_2(z)$ as the equivalent channel for the SSE case. Therefore, as for the signal $\mathbf{x}(n)$, the system from Fig.2.3(a) can be represented as a cascade of the equivalent channel $\mathbf{F}_2(z)$ and a SSE $\mathbf{H}_2(z)$. An ideal equalizer (or a zero-forcing equalizer [39]) $\mathbf{H}_2(z)$ is then obtained as a *left inverse* of the equivalent channel $\mathbf{F}_2(z)$.

From this discussion, several drawbacks of symbol spaced equalizers are apparent. The MIMO transfer function $\mathbf{F}_2(z)$ does not have a left inverse if it is a fat matrix. Even if the matrix is not fat, its invertibility will depend on the rank. Furthermore, if $\mathbf{F}_2(z)$ is invertible, its inverse is most probably IIR, which often amplifies the noise at the receiver. Finally, it has been observed that the ISI suppression achieved by this equalizer is very sensitive to the phase of the sampling at the receiver [39], [57]. For all these reasons, a popular alternative is to use a so called fractionally spaced equalizer (**FSE**). It can be shown to be far less sensitive to the sampling phase [57], it can be used with fat channel transfer functions, and it often allows for FIR solutions while SSE does not.

The idea behind an FSE is to let the equalizer work at a higher rate. Because of this additional redundancy, FSEs are both more flexible and more robust than SSEs. In a continuous-time communication system, FSE is realized by sampling the received waveform at M times the symbol rate, and feeding such oversampled signal to the equalizer, which now operates at the rate M/T. In this chapter, the oversampling

ratio M is assumed to be an integer. In discrete time, this is modeled as shown in Fig.2.3(b). The discrete transfer functions $\mathbf{G}(z)$ and $\mathbf{C}(z)$ are obtained after sampling the corresponding continuous-time impulse responses at the rate M/T. Thus, the equivalent channel $\mathbf{F}(z)$ in this case is such that $\mathbf{F}_2(z) = [\mathbf{F}(z)]_{\downarrow M}$ and the simplified scheme is shown in Fig.2.3(c). Note that the noise also needs to be modified, but this is not the main point of discussion here. We recall from Section 2.3 that a zero-forcing FSE $\mathbf{H}(z)$ in Fig.2.3(c) is nothing but an LBP of the channel matrix $\mathbf{F}(z)$. In this section we will exploit the non-uniqueness of this biorthogonal partner with the aim of minimizing the noise power at the receiver.

The concept of fractionally spaced equalization is by no means new [57]; however, the original contribution of this section is the attempt to parameterize the FIR FSE solutions, making the search for the 'best' solution analytically tractable. On the other hand, the optimization of MIMO systems of the type shown in Fig.2.3(a) has been considered by several authors in many different contexts (e.g., [32], [42], [91]). The authors in [91] derive the optimal transmitter *and* receiver for a given channel in the sense of minimizing the overall mean squared error. This MMSE solution clearly outperforms any zero-forcing equalizer, however the price is paid in terms of complexity: the solution in [91] involves ideal filtering. Here we have taken a simplistic approach of decoupling the problems of ISI and noise suppression. Moreover, the system shown in Fig.2.3(b) brings in an additional element of freedom, which is exploited in the following.

2.4.1 Optimizing LBP for channel equalization ($M = 2$)

The size of the channel $\mathbf{F}(z)$ will be assumed to be $p \times r$, with $r \leq Mp$. We will first motivate the LBP optimization assuming M is equal to 2 (see Fig.2.4(a)). Later on we derive the optimal solution for a general M. The system from Fig.2.4(a) can be redrawn as in Fig.2.4(b). Here $\mathbf{w}_0(n)$ and $\mathbf{w}_1(n)$ are the corresponding polyphase components of the noise vector sequence $\mathbf{w}(n)$ from Fig.2.4(a), while $\mathbf{F}_0(z)$, $\mathbf{F}_1(z)$ and $\widehat{\mathbf{H}}_0(z)$, $\widehat{\mathbf{H}}_1(z)$ are the polyphase components of $\mathbf{F}(z)$ and $\widehat{\mathbf{H}}(z)$, respectively. Recall that if the conditions of Theorem 2.2 are satisfied, then $\mathbf{H}_0(z)$ and $\mathbf{H}_1(z)$ as in (2.13) lead to one possible solution for $\widehat{\mathbf{H}}(z)$. However, from (2.12) we see that

$$\mathbf{W}_{21}(z)\mathbf{F}_0(z) + \mathbf{W}_{22}(z)\mathbf{F}_1(z) = \mathbf{0},$$

and therefore another class of solutions for $\widehat{\mathbf{H}}(z)$ is given by

$$\widehat{\mathbf{H}}_0(z) = \mathbf{H}_0(z) + \mathbf{A}(z)\mathbf{W}_{21}(z), \quad \widehat{\mathbf{H}}_1(z) = \mathbf{H}_1(z) + \mathbf{A}(z)\mathbf{W}_{22}(z) \tag{2.16}$$

for an *arbitrary* $r \times 2p - r$ matrix $\mathbf{A}(z)$ and matrices $\mathbf{W}_{ij}(z)$ defined by (2.12). The optimization problem reduces to that of designing $\mathbf{A}(z)$ such that the noise component of $\mathbf{y}(n)$ in Fig.2.4(a) is minimized. To facilitate this, we consider the noise model for the system shown in Fig.2.4(b). It is obtained by setting

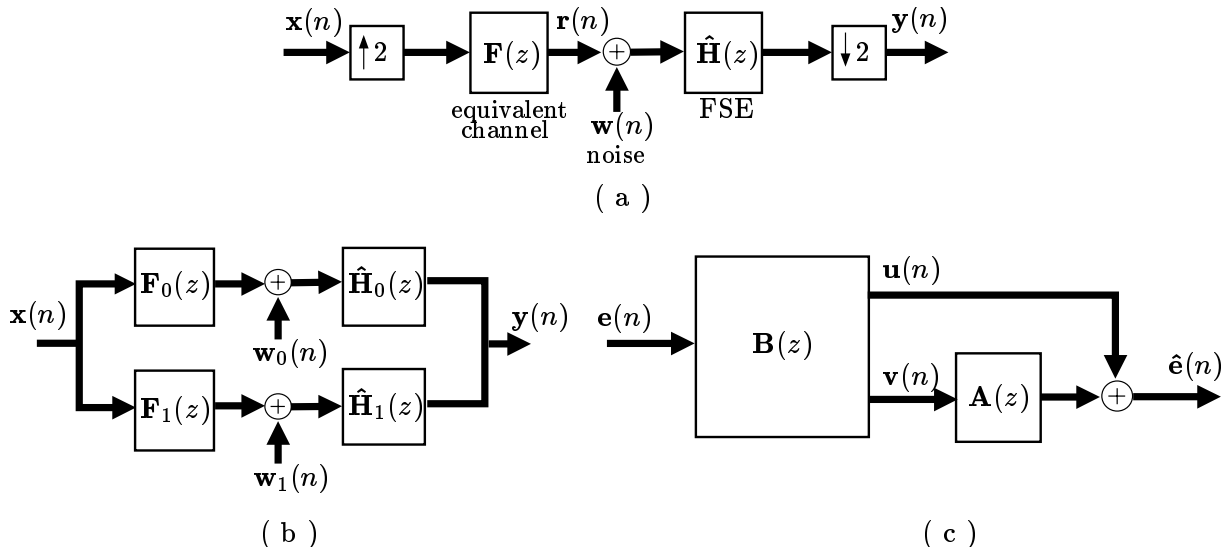

Figure 2.4: Block diagram interpretation of the construction of FSE for $M = 2$. (a) Discrete-time equivalent communication channel with FSE, (b) equivalent of (a) obtained using noble identities [61], and (c) equivalent model for noise.

$\mathbf{x}(n) = 0$. Let us define

$$\mathbf{e}(n) = \begin{bmatrix} \mathbf{w}_0(n) \\ \mathbf{w}_1(n) \end{bmatrix}, \quad \mathbf{B}(z) = \begin{bmatrix} \mathbf{H}_0(z) & \mathbf{H}_1(z) \\ \mathbf{W}_{21}(z) & \mathbf{W}_{22}(z) \end{bmatrix}. \tag{2.17}$$

Then, the equivalent of the noise model from Fig.2.4(b) is shown in Fig.2.4(c). The task is now to find the matrix $\mathbf{A}(z) = \sum_{i=0}^{N_A-1} \mathbf{A}_i z^{-i}$ such that the norm of

$$\widehat{\mathbf{e}}(n) = \mathbf{u}(n) + \sum_{i=0}^{N_A-1} \mathbf{A_i}\mathbf{v}(n-i)$$

is smaller than the corresponding norm when any other polynomial matrix $\bar{\mathbf{A}}(z)$ of the same or lower order is used. That turns out to be equivalent to the problem of finding the best linear estimator of order $N_A - 1$ for the vector process $-\mathbf{u}(n)$ given the observations $\mathbf{v}$(n). Rather than solving this problem for $M = 2$, we will formulate and solve the equivalent problem for a general oversampling ratio M.

2.4.2 LBP optimization for general M

Consider the second equality in (2.15). If $\mathbf{H}(z)$ is an LBP of $\mathbf{F}(z)$, its Type 1 polyphase components need to satisfy

$$\sum_{k=0}^{M-1} \mathbf{H}_k(z)\mathbf{F}_k(z) = \mathbf{I}. \tag{2.18}$$

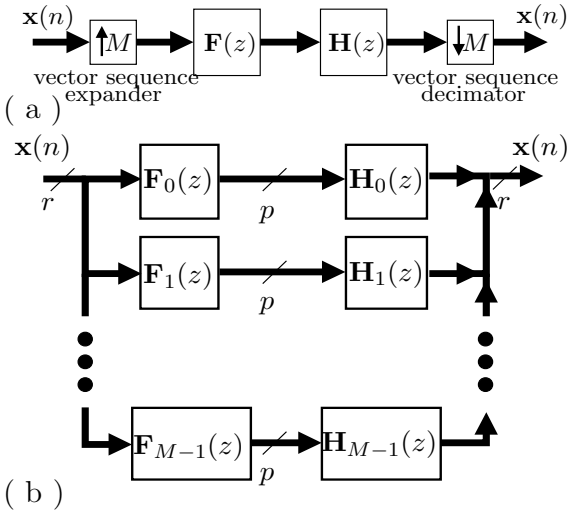

Figure 2.5: (a)-(b) Equivalent structures for FIR LBPs.

In view of (2.18) we can redraw the structure from Fig.2.5(a) as shown in Fig.2.5(b). Next, we define the $Mp \times r$ and $r \times Mp$ polynomial matrices $\mathbf{E}(z)$ and $\mathbf{R}(z)$ as

$$\mathbf{E}(z) \stackrel{\triangle}{=} [\mathbf{F}_0^T(z) \;\; \mathbf{F}_1^T(z) \;\; \cdots \;\; \mathbf{F}_{M-1}^T(z)]^T, \;\; \mathbf{R}(z) \stackrel{\triangle}{=} [\mathbf{H}_0(z) \;\; \mathbf{H}_1(z) \;\; \cdots \;\; \mathbf{H}_{M-1}(z)]. \tag{2.19}$$

From Fig.2.5 we conclude that constructing an FIR LBP $\mathbf{H}(z)$ is absolutely *equivalent* to finding a left polynomial inverse of $\mathbf{E}(z)$, namely, $\mathbf{R}(z)$. This is possible as long as $Mp \geq r$ and the greatest common divisor (GCD) of all the $M \times M$ minors of $\mathbf{E}(z)$ is a delay [14], [89]. From the previous discussion we conclude that this condition is equivalent to GRCD$[\mathbf{F}_0(z), \mathbf{F}_1(z), \cdots, \mathbf{F}_{M-1}(z)]$ being a unimodular matrix.

In order to find the general form of a left FIR inverse, we consider the Smith form [26] of $\mathbf{E}(z)$

$$\mathbf{E}(z) = \mathbf{U}(z)\mathbf{\Gamma}(z)\mathbf{V}(z). \tag{2.20}$$

Here $\mathbf{U}(z)$ and $\mathbf{V}(z)$ are $Mp \times Mp$ and $r \times r$ unimodular matrices respectively and $\mathbf{\Gamma}(z)$ is an $Mp \times r$ diagonal matrix. If $\mathbf{F}(z)$ has an FIR LBP, the elements on the main diagonal of $\mathbf{\Gamma}(z)$ are nonzero constants or delays, but without loss of generality we can assume that they are all constants [namely, any possible delays can readily be 'absorbed' into $\mathbf{U}(z)$ or $\mathbf{V}(z)$]. In other words, $\mathbf{\Gamma}(z) = [\mathbf{\Gamma} \;\; \mathbf{0}]^T$, where $\mathbf{\Gamma}$ is an $r \times r$ constant diagonal matrix. Now from (2.20) we have that the most general form for an FIR left inverse of $\mathbf{E}(z)$ is given by

$$\mathbf{R}(z) = \mathbf{V}^{-1}(z)[\mathbf{\Gamma}^{-1} \;\; \mathbf{A}(z)]\mathbf{U}^{-1}(z), \tag{2.21}$$

where $\mathbf{A}(z)$ is an *arbitrary* $r \times (Mp - r)$ polynomial matrix. It is important to note here that although (2.21) represents the general form of the solution for FIR LBPs, it still does not provide the complete parameterization of all valid solutions. The reason for this is the fact that even though the Smith form

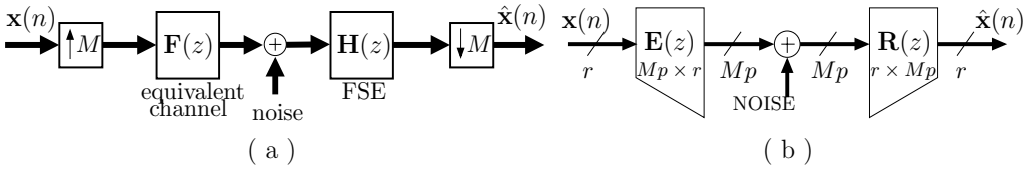

Figure 2.6: (a)-(b) MIMO FSEs and MIMO LBPs.

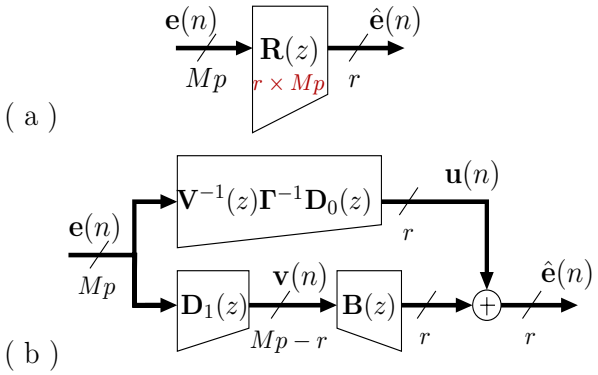

Figure 2.7: (a)-(b) Finding the optimal FIR LBP.

decomposition is unique, the unimodular matrices $\mathbf{U}(z)$ and $\mathbf{V}(z)$ in (2.20) are **not**; moreover their complete parameterization is still an *open problem*.

Next, we consider the problem of finding the optimal $\mathbf{A}(z)$ in (2.21) that results in the zero-forcing equalizer $\mathbf{H}(z)$ [see Fig.2.6(a)] minimizing the output noise power. From the previous discussion it follows that the simplified communication system from Fig.2.6(a) can be redrawn as in Fig.2.6(b). We proceed in a fashion previously described in Section 2.4.1: by considering the noise model of the equivalent system from Fig.2.6(b). This noise model is shown in Fig.2.7(a). Let us define the polynomial matrices $\mathbf{D}_0(z)$, $\mathbf{D}_1(z)$ and $\mathbf{G}(z)$

$$[\underbrace{\mathbf{D}_0^T(z)}_{r} \quad \underbrace{\mathbf{D}_1^T(z)}_{Mp-r}]^T = \mathbf{D}(z) \triangleq \mathbf{U}^{-1}(z), \quad \mathbf{G}(z) \triangleq \mathbf{V}^{-1}(z). \tag{2.22}$$

Now, we can rewrite (2.21) as

$$[\mathbf{H}_0(z) \quad \mathbf{H}_1(z) \quad \cdots \quad \mathbf{H}_{M-1}(z)] = \mathbf{G}(z)\mathbf{\Gamma}^{-1}\mathbf{D}_0(z) + \underbrace{\mathbf{G}(z)\mathbf{A}(z)}_{\triangleq \mathbf{B}(z)}\mathbf{D}_1(z). \tag{2.23}$$

Using (2.23), Fig.2.7(a) can be equivalently presented as in Fig.2.7(b). The $r \times (Mp-r)$ polynomial matrix of free parameters, $\mathbf{A}(z)$, is now replaced by another $r \times (Mp-r)$ polynomial matrix of free parameters, $\mathbf{B}(z)$, and our goal is to find the optimal $\mathbf{B}(z)$ of a given order $N_B - 1$ that will minimize the noise power. Note that *any* $\mathbf{B}(z)$ produces a valid ZFE $\mathbf{H}(z)$. From Fig.2.7(b) we see that the optimal $\mathbf{B}(z)$ is nothing but a matrix Wiener filter, or a linear estimator for recovering the desired vector signal $-\mathbf{u}(n)$ given the

vector process $\mathbf{v}(n)$. The solution for the optimal $\mathbf{B}(z)$ of a given order $N_B - 1$ can be readily obtained using the orthogonality principle [54]. The details of the derivation are omitted for clarity and can be found in the appendix. At this point it should only be noted that the final solution depends only on the statistics of the input noise ($\mathcal{R}_\epsilon$) and the elements of the previously determined matrices $\mathbf{U}(z)$, $\mathbf{V}(z)$ and $\mathbf{\Gamma}$. It is to be expected that the performance of the equalizer $\mathbf{H}(z)$ will improve with the increasing order of $\mathbf{B}(z)$ and this is investigated in the section with experimental results.

2.4.3 Experimental results

In the following we present the results of numerical simulations. The system under investigation is the one described in Fig.2.3. The input sequence $\mathbf{x}(n)$ consisted of vectors of length three, with the independent, identically distributed scalar component sequences. The oversampling ratio was $M = 2$. The signal-to-noise ratio (SNR) used in the experiments was obtained as [see Fig.2.4(a)]

$$\text{SNR} = 20 \log_{10} \frac{||\mathbf{r}||_2}{||\mathbf{w}||_2}.$$

In the **first experiment**, the elements were drawn with equal probability from a 64-QAM constellation [39]. We compare the performance of four different equalization methods:

1. traditional IIR SSE [Fig.2.3(a)],
2. plain FIR FSE (without optimization) obtained as an LBP with $\mathbf{B}(z)$ set to zero in (2.23),
3. optimized FIR FSE obtained by finding the optimal third order $\mathbf{A}(z)$ in Fig.2.4(c), and
4. optimized FIR FSE as in Section 2.4.2 with $\mathbf{B}(z)$ of order three obtained as in (2.44).

The corresponding scattering diagrams of the equalized signals are shown in Fig.2.8, with the probabilities of error (clockwise in Fig.2.8) given by 0.24, 0.0036, 5.33×10^{-5} and 5.26×10^{-6} . The equivalent channel $\mathbf{F}(z)$ in Fig.2.6(a) was a 3×3 polynomial matrix of order three and can be found at [92]. The transfer function $\mathbf{F}_2(z)$ of the equivalent channel in the SSE case [see Fig.2.3(a)] was chosen in such way that the inverse matrix $\mathbf{H}_2(z)$ is stable, but with two poles very close to the unit circle. This leads to its poor performance in the presence of noise. The noise was white with SNR = 28 dB.

Matrix $\mathbf{W}(z)$ in (2.12) was obtained using the GRCD construction algorithm from [26]. As mentioned in Sec. 2.4.2, matrices $\mathbf{U}(z)$ and $\mathbf{V}(z)$ in (2.20) are not unique and this is exploited in the equalization example 4. Notice that there is an improvement by a factor of 10 in the probability of error with respect to the method based on Fig.2.4 and this can mostly be attributed to the choice of $\mathbf{U}(z)$ and $\mathbf{V}(z)$. However, at this point it is still unclear how to choose the optimal $\mathbf{U}(z)$ and $\mathbf{V}(z)$. The three unimodular matrices used in this experiment [$\mathbf{W}(z)$, $\mathbf{U}(z)$ and $\mathbf{V}(z)$] can be found at [92].

In the **second experiment**, we investigate the behavior of the optimal linear estimator $\mathbf{B}(z)$ as a function of its order $N_B - 1$. The input signal elements were drawn from a 16-QAM constellation. We evaluate our

algorithm on two MIMO channels: a square 3×3 channel $\mathbf{F}_{sq}(z)$ and a rectangular, fat 2×3 channel $\mathbf{F}_{rec}(z)$. For simplicity $\mathbf{F}_{rec}(z)$ was chosen such that it consists of the first two rows of $\mathbf{F}_{sq}(z)$. The MIMO channel $\mathbf{F}_{sq}(z)$ was characterized by a 3×3 matrix polynomial of order 6 and the corresponding coefficients can also be found at [92]. The noise was taken to be white.

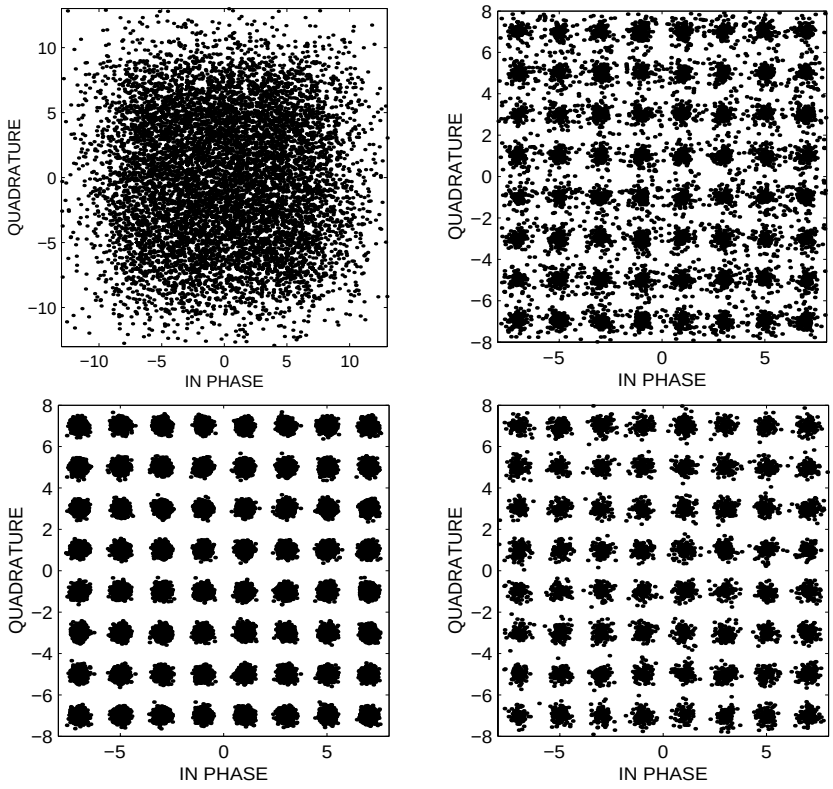

Figure 2.8: Equalization results. Clockwise, starting from upper left: SSE, plain FIR FSE, optimized FIR FSE as in Section 2.4.1, and optimized FIR FSE as in Section 2.4.2.

While it is intuitive that the higher order estimators $\mathbf{B}(z)$ should lead to a better performance than the lower order ones, it is still of importance to quantitatively evaluate this improvement in performance. What we have noticed in our examples is that, with increasing N_B-1, the performance of the equalizer *does not improve much* after a certain point (see Fig.2.9). This is because all the terms in impulse response matrices $\mathbf{B}_k$ tend to decay very rapidly for large values of k and their influence on the equalizer performance diminishes in a similar fashion.

In the left part of Fig.2.9, we plotted the experimentally determined probability of error at the detector in the 3×3 channel case as a function of the order of estimator N_B-1. The probability of error is obtained as the average value of the error probabilities in each of the three channels. The first measurement, for $N_B-1=-1$ corresponds to the case when there is no optimization of the equalizer, i.e., where $\mathbf{B}(z)$ is a zero matrix. The probability of error in this case with SNR = 18 dB was equal to 0.82 percent. Interestingly, the probability of error can be reduced by several orders of magnitude by employing just the *zeroth order* (constant) matrix $\mathbf{B}(z)$. Only two out of 10^5 symbols were misinterpreted in this case. However, there is

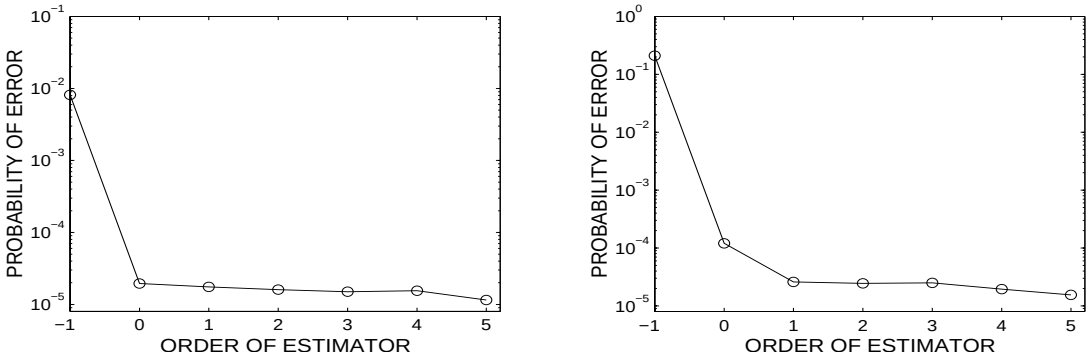

Figure 2.9: Probability of error as a function of the estimator order: (left) square 3×3 channel, and (right) rectangular 2×3 channel—see the text.

not much improvement as the order increases.

Very similar findings hold in the rectangular case as well. Although a *left inverse does not exist in this case*, it is still possible to equalize the 2×3 channel $\mathbf{F}_{rec}(z)$ with oversampling just by two [92]. However, the default equalizer obtained by the LBP construction as in Section 2.3 does not perform very well. As shown in the right part of Fig.2.9, for no estimator correction $\mathbf{B}(z)$ employed, the error rate was more than 20 percent for SNR = 32 dB. However, even the constant correction $\mathbf{B}_0$ resulted in a dramatic decrease in the probability of error to about 10^{-4}, while the higher order corrections kept the error probability below 4×10^{-5}. This, together with the previous, square, example stands to show that exploiting the redundancy of LBP even to the smallest extent can prove to be very fruitful.

2.5 Some further applications of biorthogonal partners

In this section we will consider two other situations where we encounter MIMO biorthogonal partners. In both of these instances, the solutions are already well-known and our intention here is to place them in the context of biorthogonal partners.

2.5.1 Least squares signal approximation

First we will address the problem of least squares signal approximation for vector signals. In the scalar case, a similar problem is very common in multiresolution theory [31] as well as in the spline approximation theory [59], [65]. This topic has been treated extensively in the mathematics literature, in the more general setting of *oblique projections* [3], [4]. The article by Aldroubi and Unser [4] is especially insightful and is closely connected to the material in this section. Another issue related to the design of projection prefilters is the problem of *energy compaction*. The interested reader is referred to [55].

Suppose we are given the signal model as shown in Fig.2.10(a). The vector signal $\mathbf{y}(n)$ is obtained by upsampling the vector sequence $\mathbf{c}(n)$ and passing the result through the matrix transfer function $\mathbf{F}(z)$. Now,

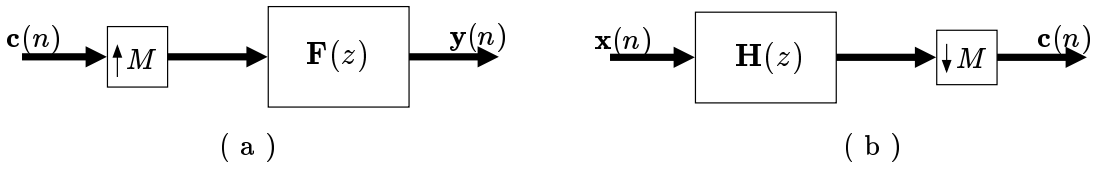

Figure 2.10: Least squares signal modeling: (a) signal model and (b) least squares solution (see text).

given a vector signal $\mathbf{x}(n)$, suppose we want to approximate it by a signal $\mathbf{y}(n)$ admitting the described model

$$\mathbf{y}(n) = \sum_{k\in\mathbb{Z}} \mathbf{F}(n - kM)\mathbf{c}(k), \tag{2.24}$$

or in the z-domain

$$\mathbf{Y}(z) = \mathbf{F}(z)\mathbf{C}(z^M). \tag{2.25}$$

It turns out that the optimum vector sequence $\mathbf{c}(n)$ can be determined as in Fig.2.10(b). The prefilter $\mathbf{H}(z)$ turns out to be a particular form of a MIMO biorthogonal partner of $\mathbf{F}(z)$. In the following we refer to this as the least squares problem.

A very similar problem arises in multiwavelet theory (see [90] and also the next section). Consider the two-band multiwavelet transform. The multiresolution space V_0 is spanned by N scaling functions and their integer shifts. Similarly, the space W_0 is spanned by N wavelets and their integer shifts. Those two spaces together form a finer resolution space V_1. Suppose we have a signal $x_1(n)$ belonging to the space V_1 and we want to find a coarser signal $x_0(n)$ from V_0 such that the distance (in the ℓ_2 sense) from the signal $x_1(n)$ is minimized. This problem can be formulated as a vector valued least squares problem, so the solution is again given by Fig.2.10.

We first state the vector least squares problem in a more general form. Consider the space $\mathcal{F}$ of all vector signals $\mathbf{y}(n)$ satisfying the model (2.24), where $\mathbf{c}(n)$ is an arbitrary ℓ_2 vector sequence.[1] This situation is depicted in Fig.2.10(a). Here $\mathbf{F}(z)$ is a given MIMO transfer function. The problem is as follows. Given any vector signal $\mathbf{x}(n)$, we want to find the corresponding **projection** in $\mathcal{F}$, i.e., the vector signal $\mathbf{y}(n) \in \mathcal{F}$ such that

$$\sum_n \|\mathbf{y}(n) - \mathbf{x}(n)\|^2 \tag{2.26}$$

is minimized. Here $\|\cdot\|$ denotes the vector norm in ℓ_2. The following theorem describes the algorithm by which this is achieved and the corresponding corollary will address the uniqueness of the proposed solution.

Theorem 2.4. Solution of the least squares problem. Given a MIMO transfer function $\mathbf{F}(z)$ and assuming that $\mathbf{S}(e^{j\omega}) = [\mathbf{F}^\dagger(e^{j\omega})\mathbf{F}(e^{j\omega})]_{\downarrow M}$ is a positive definite matrix for all ω, we define the (orthogonal)

[1] This means that all the scalar sequences corresponding to the vector entries are square summable.

projection filter by

$$\mathbf{H}(z) = \left([\widetilde{\mathbf{F}}(z)\mathbf{F}(z)]_{\downarrow M}\right)^{-1}_{\uparrow M} \widetilde{\mathbf{F}}(z). \tag{2.27}$$

If we pass the vector signal $\mathbf{x}(n)$ through the projection filter and decimate the outputs by M we get the optimal driving sequence $\mathbf{c}(n)$ [see Fig.2.10(b)]. This $\mathbf{c}(n)$ can be used to find the least squares approximation $\mathbf{y}(n)$ as in Fig.2.10(a).

Notice that the projection filter is equal to the generic LBP given by (2.9). The positive-definiteness condition is necessary only to ensure the stability of $\mathbf{H}(z)$. The proof of Theorem 2.4 is provided in the appendix.

The next corollary states that the least squares solution proposed by Theorem 2.4 is unique. While the proposed proof provides an elegant argument, the result of Corollary 2.2 also follows from the uniqueness of the orthogonal projection onto a closed subspace [4].

Corollary 2.2. Uniqueness of projection filter. Consider Fig.2.10. For fixed $\mathbf{F}(z)$ satisfying the condition of Theorem 2.4 and $\mathbf{x}(n) \in \ell_2$, the least squares approximation $\mathbf{y}(n)$ is unique. Next, suppose the prefilter $\mathbf{H}(z)$ in Fig.2.10(b) is such that the output of $\mathbf{F}(z)$ [Fig.2.10(a)] is the least squares approximation of $\mathbf{x}(n)$ for *any* choice of the ℓ_2 input $\mathbf{x}(n)$. Then $\mathbf{H}(z)$ is unique and is therefore given by (2.27).

Proof. The uniqueness of $\mathbf{c}(n)$ and thus of $\mathbf{y}(n)$ follows from the proof of Theorem 2.4. Next, let two different prefilters $\mathbf{H}(z)$ and $\mathbf{H}_1(z)$ both be optimal for all $\mathbf{x}(n) \in \ell_2$. Thus by the uniqueness of $\mathbf{c}(n)$ we have that

$$[(\mathbf{H}(z) - \mathbf{H}_1(z))\mathbf{X}(z)]_{\downarrow M} = \mathbf{0}$$

for any choice of $\mathbf{X}(z)$. The choice $\mathbf{X}(z) = z^k\mathbf{e}_i$, where $\mathbf{e}_i$ is the ith unit vector (i.e., the ith column of the identity matrix), implies that the kth polyphase component of the ith column of $\mathbf{H}(z) - \mathbf{H}_1(z)$ is zero. This holds for all i and k, so the conclusion is that all the polyphase components of all columns of $\mathbf{H}(z) - \mathbf{H}_1(z)$ are zero, and thus $\mathbf{H}(z) = \mathbf{H}_1(z)$, i.e., the prefilter is indeed unique. $\triangledown\triangledown\triangledown$

2.5.2 Multiwavelets and prefiltering

Multiwavelet theory emerged recently as the extension of wavelet theory to the case where there is more than one scaling function and mother wavelet. It has been shown [52] that multiwavelets have some advantages over the conventional wavelets, especially in data compression. In this section we provide the connection between MIMO biorthogonal partners and prefilters employed in multiwavelet theory. To that end, we first give a brief overview of some of the results in this area. For a more thorough and comprehensive exposition to multiwavelets, reader is referred to the works by Geronimo *et al.* [15], [12], Xia et al. [90], [88], Vetterli and Strang [73], [29], [51], and Selesnick [46], [45].

Consider the set of N scaling functions $\{\phi_n(t)\}$, $0 \le n \le N-1$ and the corresponding set of N mother wavelets $\{\psi_n(t)\}$. The scaling functions are chosen in such way that their integer shifts $\{\phi_n(t-k)\}$, together with the shifts of the dilated versions $\{\phi_n(2^j t - k)\}$ span a sequence of nested subspaces of L_2. These

subspaces $V_j \subset V_{j+1}$, $j \in \mathbb{Z}$ (integer j is called the *scale*) form a multiresolution analysis [15] of L_2. Some of the desirable properties of the scaling functions are linear phase, orthogonality and compact support. In the scalar case (for $N = 1$) these properties occur simultaneously only in the Haar basis, while in the multiwavelet case ($N > 1$) many such examples are known [15], [51], [46]. In the following we will assume that the scaling functions are orthogonal and compactly supported. Let $x_c(t)$ be a continuous-time signal contained in V_0. Then it can be written as

$$\begin{aligned} x_c(t) &= \sum_{n=0}^{N-1} \sum_{k\in\mathbb{Z}} c_{0,n}(k)\phi_n(t-k) \\ &= \sum_{n=0}^{N-1} \sum_{k\in\mathbb{Z}} c_{J_0,n}(k)2^{J_0/2}\phi_n(2^{J_0}t-k) + \sum_{n=0}^{N-1} \sum_{J_0\le j<0} \sum_{k\in\mathbb{Z}} d_{j,n}(k)2^{j/2}\psi_n(2^j t-k), \end{aligned} \tag{2.28}$$

where $J_0, j < 0$. This decomposition algorithm suggests possibilities for a tree-like signal decomposition in terms of the coefficients at coarser scales. In fact, given the coefficients $\{c_{0,n}(k)\}$ the corresponding coefficients $\{c_{j,n}(k)\}$ and $\{d_{j,n}(k)\}$, $j < 0$ can be found using the concept of vector-valued wavelets and filterbanks (see [90] and references therein). Let us denote the vectors of stacked coefficients at scale j

$$\mathbf{c}_j(k) = [c_{j,0}(k) \;\; c_{j,1}(k) \;\; \cdots \;\; c_{j,N-1}(k)]^T, \;\; \mathbf{d}_j(k) = [d_{j,0}(k) \;\; d_{j,1}(k) \;\; \cdots \;\; d_{j,N-1}(k)]^T.$$

Starting from the dilation equation on scaling functions and wavelets, it can be shown that

$$\mathbf{c}_{j-1}(k) = \sum_{m\in\mathbb{Z}} \mathbf{H}_m \mathbf{c}_j(2k-m) \;\; \text{and} \;\; \mathbf{d}_{j-1}(k) = \sum_{m\in\mathbb{Z}} \mathbf{G}_m \mathbf{c}_j(2k-m)$$

for some appropriate matrix polynomials $\mathbf{H}(z) = \sum_m \mathbf{H}_m z^{-m}$ and $\mathbf{G}(z) = \sum_m \mathbf{G}_m z^{-m}$. In other words, this gives rise to the vector-valued filterbank pyramid for decomposition, as shown in Fig.2.11. From the orthogonality condition on the scaling functions it follows [90] that the reconstruction part is as shown in the lower part of Fig.2.11.

The initial step in the multiwavelet decomposition is the so-called **prefiltering** [90], [88] and is not shown in Fig.2.11. In order to understand the nature of this operation, consider again the first equality in (2.28) and rewrite it at instances $t = \frac{n}{M}$ (the significance of the factor M will be clear shortly)

$$x(n) \stackrel{\triangle}{=} x_c(\frac{n}{M}) = \sum_{k\in\mathbb{Z}} \boldsymbol{\phi}_c^T(\frac{n}{M} - k)\mathbf{c}_0(k), \tag{2.29}$$

where we introduced the column vector $\boldsymbol{\phi}_c(t) = [\phi_0(t) \;\; \phi_1(t) \;\; \cdots \;\; \phi_{N-1}(t)]^T$. Now, let us define

$$\boldsymbol{\phi}_M(n) \stackrel{\triangle}{=} \boldsymbol{\phi}_c(\frac{n}{M}), \;\; \text{with} \;\; \boldsymbol{\Phi}_M(z) = \sum_{k\in\mathbb{Z}} \boldsymbol{\phi}_M(n) z^{-n}. \;\; \text{Then we have}$$

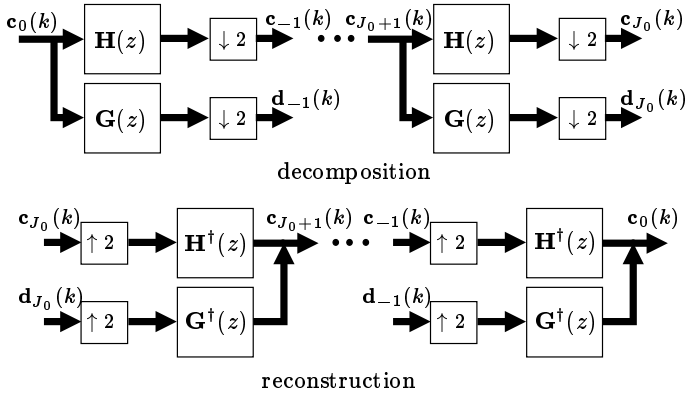

Figure 2.11: Vector-valued wavelet pyramid: decomposition to coarser scales and reconstruction.

$$x(n) = \sum_{k\in\mathbb{Z}} \boldsymbol{\phi}_M^T(n - kM)\mathbf{c}_0(k), \quad \text{or} \quad X(z) = \boldsymbol{\Phi}_M^T(z)\mathbf{C}_0(z^M). \tag{2.30}$$

This is depicted in Fig.2.12(a). Notice here that $x(n)$ is a sequence of samples of $x_c(t)$ oversampled by M. **The purpose of prefiltering** is to obtain the multiwavelet coefficients $\mathbf{c}_0(k)$ at scale 0 from the signal samples $x(n)$. This prefiltering is unnecessary in the case of the so called interpolating multiwavelets [45]. The scaling functions there are chosen such that the multiwavelet coefficients are equal to signal samples. Balanced multiwavelets [29], [46] present similar attempts at circumventing the prefiltering operation, however they are in general only approximate methods. Therefore, in the most general multiwavelet setting the prefiltering operation is unavoidable. To understand how this operation is performed, we define the scalar filter $F_n(z)$ to be the nth entry in the column vector $\boldsymbol{\Phi}_M(z)$. In other words we have

$$F_n(z) = \sum_{k\in\mathbb{Z}} \phi_n(\frac{k}{M})z^{-k}.$$

Now we can redraw the signal model from Fig.2.12(a) as in the left half of Fig.2.12(b). Notice how this figure resembles the transmultiplexer [61], where the composite signal $x(k)$ is obtained as the sum of signals $c_{0,n}(k)$ modulated by filters $F_n(z)$, for $n = 0, 1, \ldots, N-1$. The recovery of partial signals $c_{0,n}(k)$ is then achieved as in the right part of Fig.2.12(b), for appropriately chosen filters $H_n(z)$. In order to find those *prefilters* $H_n(z)$, we present both filterbanks from Fig.2.12(b) in terms of their polyphase matrices, which is shown in Fig.2.12(c). They are defined as

$$\mathbf{P}(z) = \begin{bmatrix} F_{0,0}(z) & F_{0,1}(z) & \cdots & F_{0,N-1}(z) \\ F_{1,0}(z) & F_{1,1}(z) & \cdots & F_{1,N-1}(z) \\ & & & \\ F_{M-1,0}(z) & F_{M-1,1}(z) & \cdots & F_{M-1,N-1}(z) \end{bmatrix}, \tag{2.31}$$

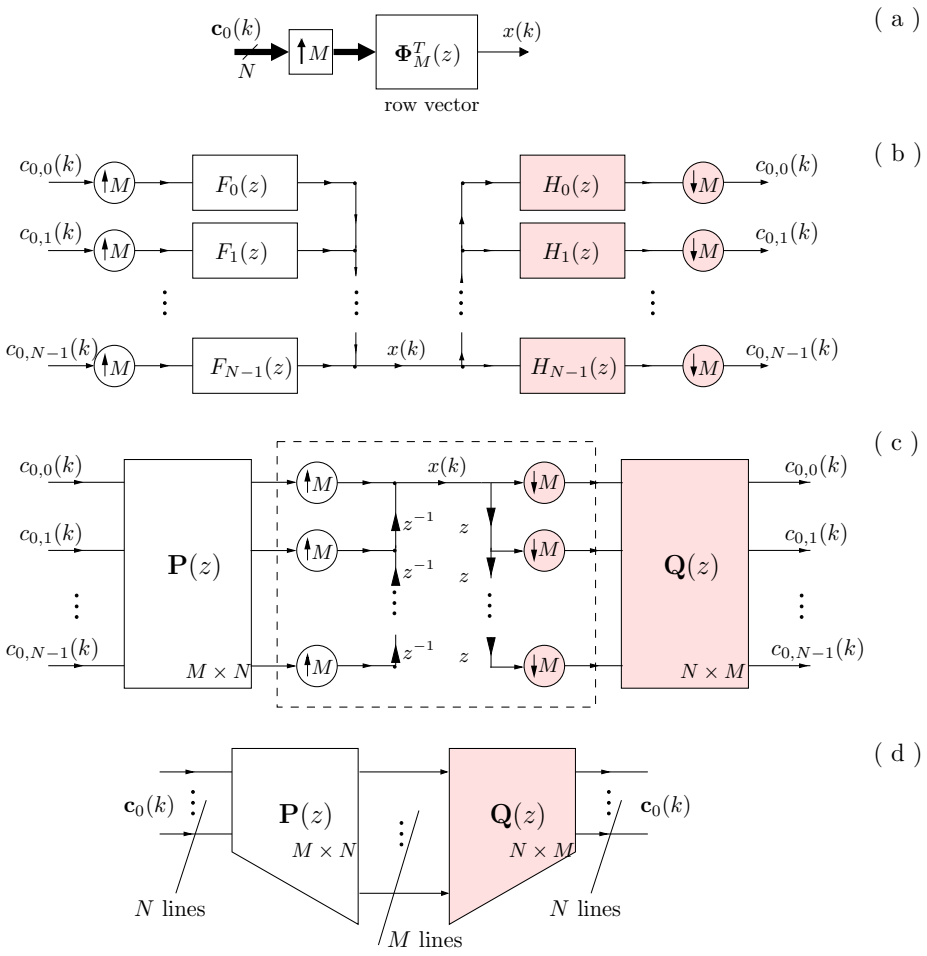

Figure 2.12: Prefiltering for multiwavelet transform. (a) Signal model. (b) Equivalent drawing of (a) together with the prefiltering part. (c) Equivalent drawing using polyphase matrices. (d) Final form of the traditional method for prefiltering by left-inverting the polyphase matrix. See text.

and

$$\mathbf{Q}(z) = \begin{bmatrix} H_{0,0}(z) & H_{0,1}(z) & \cdots & H_{0,M-1}(z) \\ H_{1,0}(z) & H_{1,1}(z) & \cdots & H_{1,M-1}(z) \\ & & & \\ H_{N-1,0}(z) & H_{N-1,1}(z) & \cdots & H_{N-1,M-1}(z) \end{bmatrix}. \tag{2.32}$$

and their entries are nothing but the Type 1 and Type 2 polyphase components of order M of filters $F_n(z)$ and $H_n(z)$. Now we see that given the samples $x_c(\frac{n}{M})$, we can obtain the corresponding multiwavelet coefficients $\mathbf{c}_0(n)$ at scale 0 as shown in the right half of Fig.2.12(c). Notice here that $\mathbf{P}(z)$ is a known $M \times N$ matrix and $\mathbf{Q}(z)$ is an unknown $N \times M$ matrix, which describes the prefiltering operation. Next we note that the middle part of Fig.2.12(c) (enclosed in a dashed box) is equivalent to the identity, since it is a cascade of unblocking and blocking operators. Therefore, this is equivalently redrawn as in Fig.2.12(d). The matrix

$\mathbf{Q}(z)$ is, therefore, nothing but a **left inverse** of $\mathbf{P}(z)$, i.e., $\mathbf{Q}(z)\mathbf{P}(z) = \mathbf{I}$. From here it immediately follows that the minimum amount of oversampling $M \geq N$ is necessary, since we need $\mathbf{P}(e^{j\omega})$ to have rank N on the unit circle.

As argued in Section 2.3, the polynomial matrix inversion problem and the problem of constructing MIMO biorthogonal partners are completely equivalent. In the following we demonstrate this point by reducing the problem of finding a left inverse $\mathbf{Q}(z)$ to the equivalent biorthogonal partner problem. For simplicity, in the following we assume that M is an even integer, i.e., $M = 2L$. Then, we can redraw Fig.2.12(b) as in Fig.2.13(a). Now we consider the middle part of Fig.2.13(a) (enclosed in a dashed box) and present it using the polyphase matrices of filters $F_n(z)$ and $H_n(z)$, only now with respect to $L = \frac{M}{2}$. This is shown in Fig.2.13(b), with

$$\bar{\mathbf{P}}(z) = \begin{bmatrix} \bar{F}_{0,0}(z) & \bar{F}_{0,1}(z) & \cdots & \bar{F}_{0,N-1}(z) \\ \bar{F}_{1,0}(z) & \bar{F}_{1,1}(z) & \cdots & \bar{F}_{1,N-1}(z) \\ & & & \\ \bar{F}_{L-1,0}(z) & \bar{F}_{L-1,1}(z) & \cdots & \bar{F}_{L-1,N-1}(z) \end{bmatrix}, \quad \text{and} \tag{2.33}$$

$$\bar{\mathbf{Q}}(z) = \begin{bmatrix} \bar{H}_{0,0}(z) & \bar{H}_{0,1}(z) & \cdots & \bar{H}_{0,L-1}(z) \\ \bar{H}_{1,0}(z) & \bar{H}_{1,1}(z) & \cdots & \bar{H}_{1,L-1}(z) \\ & & & \\ \bar{H}_{N-1,0}(z) & \bar{H}_{N-1,1}(z) & \cdots & \bar{H}_{N-1,L-1}(z) \end{bmatrix}, \tag{2.34}$$

and the entries in the above matrices satisfying

$$F_n(z) = \sum_{k=0}^{L-1} \bar{F}_{k,n}(z^L) z^{-k}, \quad H_n(z) = \sum_{k=0}^{L-1} \bar{H}_{n,k}(z^L) z^k.$$

Comparing Fig.2.13(b) with Fig.2.1, we see that $\bar{\mathbf{Q}}(z)$ is found as a left biorthogonal partner of $\bar{\mathbf{P}}(z)$ with respect to 2, or $[\bar{\mathbf{Q}}(z)\bar{\mathbf{P}}(z)]_{\downarrow 2} = \mathbf{I}$. Therefore, we conclude that the problem of finding a left inverse $\mathbf{Q}(z)$ as in Fig.2.12(d) is indeed completely equivalent to finding an LBP $\bar{\mathbf{Q}}(z)$ as in Fig.2.13(b). Moreover, comparing (2.33) and (2.34) to (2.31) and (2.32), we can easily verify the following relation

$$\begin{bmatrix} \bar{\mathbf{P}}_0(z) \\ \bar{\mathbf{P}}_1(z) \end{bmatrix} = \mathbf{P}(z), \quad \begin{bmatrix} \bar{\mathbf{Q}}_0(z) & \bar{\mathbf{Q}}_1(z) \end{bmatrix} = \mathbf{Q}(z), \quad \text{with} \tag{2.35}$$

$$\bar{\mathbf{P}}(z) = \bar{\mathbf{P}}_0(z^2) + z^{-1}\bar{\mathbf{P}}_1(z^2), \quad \text{and} \quad \bar{\mathbf{Q}}(z) = \bar{\mathbf{Q}}_0(z^2) + z\bar{\mathbf{Q}}_1(z^2). \tag{2.36}$$

From the relation between the solutions $\mathbf{Q}(z)$ and $\bar{\mathbf{Q}}(z)$, it is evident that many properties of one solution immediately apply to the other as well. For example, if one matrix is rational/FIR, the other will also be rational/FIR. The previous findings are summarized in the following lemma.

Lemma 2.1. Consider the continuous-time signal $x_c(t) \in V_0$, given by its samples $x_c(\frac{k}{M})$. Let the space

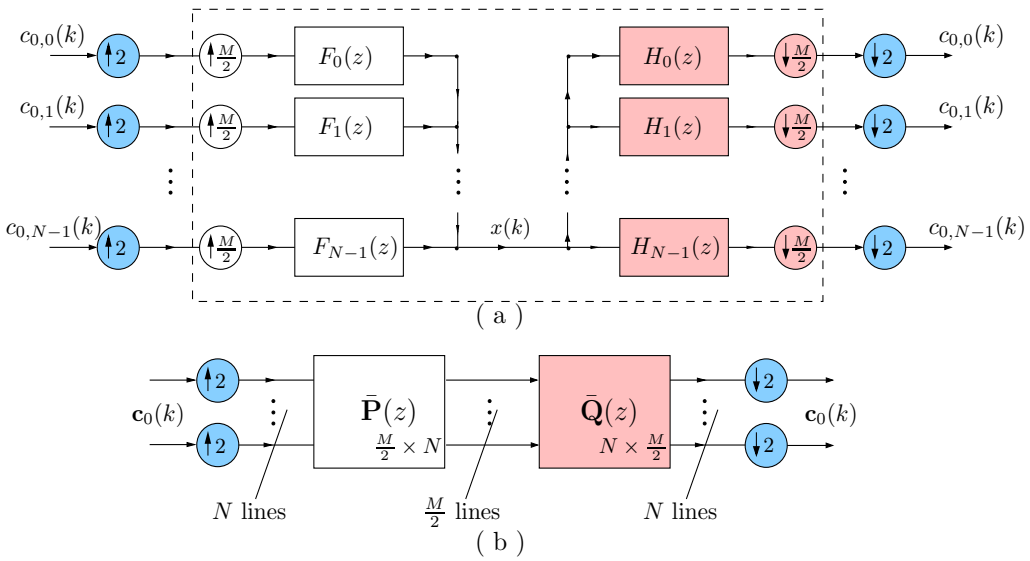

Figure 2.13: Biorthogonal partners in prefiltering for multiwavelet transform. (a) Equivalent of Fig.2.12(b) for even M. (b) Equivalent of Fig.2.12(d) for even M. See text.

V_0 be spanned by a set of N scaling functions $\{\phi_n(t)\}$ and their integer shifts; furthermore, let $M \geq N$ be an even integer and let $\mathbf{P}(z)$ be the corresponding polyphase matrix defined by (2.31). Then there will exist (an FIR) prefilter $\mathbf{Q}(z)$ for the corresponding multiwavelet transform if and only if there exists (an FIR) LBP $\bar{\mathbf{Q}}(z)$ of the $\frac{M}{2} \times N$ polyphase matrix $\bar{\mathbf{P}}(z)$ given by (2.33). The relation between them is given by (2.35) and (2.36).

The significance of Lemma 2.1 lies in the fact that the non-uniqueness and the parameterization of FIR LBPs can be used in the construction of the multiwavelet prefilters. This may become useful in many applications where prefilters are required to have certain properties [29], [90], [88], and is an interesting topic for further investigation.

2.6 Concluding remarks

Multiple input—multiple output (MIMO) biorthogonal partners arise in several signal processing applications including MIMO channel equalization and multiwavelet theory. The theory of MIMO biorthogonal partners is to some extent a natural extension of the SISO case as considered in [65]. However, in the vector case we are presented with additional degrees of freedom which may be useful in some applications. An important application considered in this chapter is the MIMO channel equalization with fractionally spaced equalizers. This problem has been converted to the problem of finding MIMO partners and the optimal solution of a given orders have been derived. While the focus of this chapter has been the extension of scalar biorthogonal partners to the vector case, in Chapter 3 we consider what happens if the decimation and expansion ratios are no longer integers but rational numbers.

2.7 Appendices

Appendix A: The simple Bezout identity

In the first appendix we provide the statement and the proof of the simple Bezout identity for rectangular matrices. This result occurs frequently in linear systems theory (see [26] for example), but is usually stated for the case where one of the matrices is square. In this context (cf. Section 2.3) both matrices are of the same size and are allowed to be rectangular.

Theorem 2.5. Rectangular $p \times r$ polynomial matrices $\mathbf{F}_0(z)$ and $\mathbf{F}_1(z)$ are right coprime if and only if there exist polynomial matrices $\mathbf{H}_0(z)$ and $\mathbf{H}_1(z)$ such that

$$\mathbf{H}_0(z)\mathbf{F}_0(z) + \mathbf{H}_1(z)\mathbf{F}_1(z) = \mathbf{I}.$$

Before proving the simple Bezout identity for rectangular matrices, we need to introduce the following results.

Lemma 2.2. Given any two $p \times r$ polynomial matrices $\mathbf{F}_0(z)$ and $\mathbf{F}_1(z)$, there exists a unimodular matrix $\mathbf{W}(z)$, such that (2.12) holds true for some $\mathbf{R}(z)$. This $\mathbf{R}(z)$ is a GRCD of $\mathbf{F}_0(z)$ and $\mathbf{F}_1(z)$. Furthermore, if $\mathbf{R}_0(z)$ is any GRCD of $\mathbf{F}_0(z)$ and $\mathbf{F}_1(z)$, it can be written as

$$\mathbf{G}_0(z)\mathbf{F}_0(z) + \mathbf{G}_1(z)\mathbf{F}_1(z) = \mathbf{R}_0(z), \tag{2.37}$$

for some polynomial matrices $\mathbf{G}_0(z)$ and $\mathbf{G}_1(z)$.

Proof of Lemma 2.2. The first statement about the existence of a unimodular matrix $\mathbf{W}(z)$ is proved in the general case (see Theorem 2.6.3-2. of [26]). Now, since $\mathbf{W}(z)$ is unimodular, its inverse is a polynomial matrix; call it $\mathbf{V}(z)$. Therefore, from (2.12) we have

$$\begin{bmatrix} \mathbf{F}_0(z) \\ \mathbf{F}_1(z) \end{bmatrix} = \underbrace{\begin{bmatrix} \mathbf{V}_{11}(z) & \mathbf{V}_{12}(z) \\ \mathbf{V}_{21}(z) & \mathbf{V}_{22}(z) \end{bmatrix}}_{\mathbf{V}(z)} \begin{bmatrix} \mathbf{R}(z) \\ \mathbf{0} \end{bmatrix},$$

which implies

$$\mathbf{F}_0(z) = \mathbf{V}_{11}(z)\mathbf{R}(z); \quad \mathbf{F}_1(z) = \mathbf{V}_{21}(z)\mathbf{R}(z).$$

Thus $\mathbf{R}(z)$ is a common right divisor of $\mathbf{F}_0(z)$ and $\mathbf{F}_1(z)$. If $\bar{\mathbf{R}}(z)$ is any other common right divisor, we can write similarly

$$\mathbf{F}_0(z) = \mathbf{X}(z)\bar{\mathbf{R}}(z); \quad \mathbf{F}_1(z) = \mathbf{Y}(z)\bar{\mathbf{R}}(z) \tag{2.38}$$

with the appropriately chosen polynomial matrices $\mathbf{X}(z)$ and $\mathbf{Y}(z)$. Now, reading the first matrix equality from (2.12) we get

$$\mathbf{W}_{11}(z)\mathbf{F}_0(z) + \mathbf{W}_{12}(z)\mathbf{F}_1(z) = \mathbf{R}(z), \tag{2.39}$$

which after substituting (2.38) leads to

$$(\mathbf{W}_{11}(z)\mathbf{X}(z) + \mathbf{W}_{12}(z)\mathbf{Y}(z))\bar{\mathbf{R}}(z) = \mathbf{R}(z),$$

and this proves that $\mathbf{R}$(z) is indeed a GRCD of $\mathbf{F}_0(z)$ and $\mathbf{F}_1(z)$. Finally, we use the fact that any two GRCDs are identical up to a premultiplication by a unimodular matrix [26]. Therefore, an arbitrary GRCD $\mathbf{R}_0(z)$ can be written as $\mathbf{R}_0(z) = \mathbf{T}(z)\mathbf{R}(z)$. Applying this to (2.39) leaves us with

$$\underbrace{\mathbf{T}(z)\mathbf{W}_{11}(z)}_{\mathbf{G}_0(z)}\mathbf{F}_0(z) + \underbrace{\mathbf{T}(z)\mathbf{W}_{12}(z)}_{\mathbf{G}_1(z)}\mathbf{F}_1(z) = \mathbf{R}_0(z),$$

which concludes the proof of Lemma 2.2. $\triangledown\triangledown\triangledown$

Proof of Theorem 2.5. First we give the backward proof. From Lemma 2.2 we have that if $\mathbf{R}(z) = \text{GRCD}[\mathbf{F}_0(z), \mathbf{F}_1(z)]$, then there exist polynomial matrices $\bar{\mathbf{H}}_0(z)$ and $\bar{\mathbf{H}}_1(z)$ such that

$$\bar{\mathbf{H}}_0(z)\mathbf{F}_0(z) + \bar{\mathbf{H}}_1(z)\mathbf{F}_1(z) = \mathbf{R}(z). \tag{2.40}$$

If $\mathbf{F}_0(z)$ and $\mathbf{F}_1(z)$ are right coprime, then $\mathbf{H}_0(z) \stackrel{\triangle}{=} \mathbf{R}^{-1}(z)\bar{\mathbf{H}}_0(z)$ and $\mathbf{H}_1(z) \stackrel{\triangle}{=} \mathbf{R}^{-1}(z)\bar{\mathbf{H}}_1(z)$ are also polynomial matrices. Thus, premultiplying both sides of (2.40) by $\mathbf{R}^{-1}(z)$ concludes the proof.

Conversely, suppose there exist polynomial matrices $\mathbf{H}_0(z)$ and $\mathbf{H}_1(z)$ such that (2.11) holds. Let $\mathbf{R}(z)$ be any GRCD of $\mathbf{F}_0(z)$ and $\mathbf{F}_1(z)$. It follows that $\mathbf{F}_0(z) = \bar{\mathbf{F}}_0(z)\mathbf{R}(z)$ and $\mathbf{F}_1(z) = \bar{\mathbf{F}}_1(z)\mathbf{R}(z)$ for appropriate polynomial matrices $\bar{\mathbf{F}}_0(z)$ and $\bar{\mathbf{F}}_1(z)$. Thus we have

$$[\mathbf{H}_0(z)\bar{\mathbf{F}}_0(z) + \mathbf{H}_1(z)\bar{\mathbf{F}}_1(z)]\mathbf{R}(z) = \mathbf{I}, \quad \text{or} \quad \mathbf{R}^{-1}(z) = \mathbf{H}_0(z)\bar{\mathbf{F}}_0(z) + \mathbf{H}_1(z)\bar{\mathbf{F}}_1(z).$$

Since the right-hand side of the above equation is a polynomial matrix, this shows that $\mathbf{R}(z)$ is a unimodular matrix, which concludes the proof. $\triangledown\triangledown\triangledown$

Appendix B: Optimal linear estimator $\mathbf{B}(z)$

In this appendix we derive the expression for the optimal linear estimator $\mathbf{B}(z)$ from Fig.2.7(b) in the sense defined in Section 2.4.2. Let $\mathbf{C}(z) \stackrel{\triangle}{=} \mathbf{V}^{-1}(z)\mathbf{\Gamma}^{-1}\mathbf{D}_0(z)$ and let the matrices $\mathbf{B}_i$, $\mathbf{C}_i$ and $\mathbf{D}_i$ represent the impulse responses of $\mathbf{B}(z)$, $\mathbf{C}(z)$ and $\mathbf{D}_1(z)$ respectively. Matrices $\mathbf{C}(z)$ and $\mathbf{D}_1(z)$ are FIR by construction and their impulse responses consist of N_C and N_D terms, respectively, while the solution for the optimal matrix polynomial $\mathbf{B}(z)$ depends on its pre-specified order, namely, $N_B - 1$. Next define the $r \times N_C Mp$ matrix $\mathcal{C}$ and the $(Mp - r)N_B \times Mp(N_B + N_D - 1)$ matrix $\mathcal{D}_1$

$$\mathcal{C} \stackrel{\triangle}{=} [\mathbf{C}_0 \;\; \mathbf{C}_1 \;\; \cdots \;\; \mathbf{C}_{N_C-1}],$$

$$\mathcal{D}_1 \stackrel{\triangle}{=} \begin{bmatrix} \mathbf{D}_0 & \dots & \mathbf{D}_{N_D-1} & \mathbf{0} & \dots & \mathbf{0} \\ \mathbf{0} & \mathbf{D}_0 & \dots & \mathbf{D}_{N_D-1} & \dots & \mathbf{0} \\ \vdots & & \ddots & & \ddots & \\ \mathbf{0} & \dots & \mathbf{0} & \mathbf{D}_0 & \dots & \mathbf{D}_{N_D-1} \end{bmatrix}. \tag{2.41}$$

We also define the $N_B(Mp-r)\times 1$ vector process $\mathcal{V}(n)$ and the $r \times N_B(Mp-r)$ matrix $\mathcal{B}$ as

$$\begin{aligned} \mathcal{V}(n) &\stackrel{\triangle}{=} [\mathbf{v}^T(n) \;\; \mathbf{v}^T(n-1) \;\; \cdots \;\; \mathbf{v}^T(n-N_B+1)]^T, \\ \mathcal{B} &\stackrel{\triangle}{=} [\mathbf{B}_0 \;\; \mathbf{B}_1 \;\; \cdots \;\; \mathbf{B}_{N_B-1}]. \end{aligned} \tag{2.42}$$

By the orthogonality principle we have that $E\{[\mathcal{B}\mathcal{V}(n)+\mathbf{u}(n)]\mathcal{V}^\dagger(n)\}=\mathbf{0}$ (here $E\{\cdot\}$ denotes the expectation), which leads to the optimal $\mathcal{B}$ as

$$\mathcal{B} = -E\{\mathbf{u}(n)\mathcal{V}^\dagger(n)\}\cdot\mathcal{R}_{\mathcal{V}\mathcal{V}}^{-1}, \tag{2.43}$$

where $\mathcal{R}_{\mathcal{V}\mathcal{V}}$ is the autocorrelation matrix of $\mathcal{V}(n)$. Given the definitions (2.41) and referring to Fig.2.7(b) we see that $\mathbf{u}(n) = \mathcal{C}\mathcal{E}_{N_C}$ and $\mathcal{V}(n) = \mathcal{D}_1\mathcal{E}_{N_D+N_B-1}$, where $\mathcal{E}_N$ denotes the $NMp\times 1$ vector of concatenated input noise vectors $\mathbf{e}(n-i)$, $0\le i\le N-1$. Substituting in (2.43) we get the optimal $\mathbf{B}(z)$ to be given by its impulse response matrix

$$\mathcal{B} = -\mathcal{C}\mathcal{R}_{\epsilon,1}\mathcal{D}_1^\dagger\Big(\mathcal{D}_1\mathcal{R}_\epsilon\mathcal{D}_1^\dagger\Big)^{-1}. \tag{2.44}$$

Here, $\mathcal{R}_\epsilon$ is the $Mp(N_B+N_D-1)\times Mp(N_B+N_D-1)$ noise autocorrelation matrix and $\mathcal{R}_{\epsilon,1}$ is its $N_CMp\times Mp(N_B+N_D-1)$ submatrix consisting of the first N_CMp rows. The solution (2.44) provides the optimal impulse response matrices $\mathbf{B}_i$, and the optimal linear predictor $\mathbf{B}(z)$ is found by

$$\mathbf{B}(z) = \sum_{i=0}^{N_B-1}\mathbf{B}_i z^{-i}.$$

Appendix C: Proof of Theorem 2.4

The error (2.26) that needs to be minimized can be rewritten in the frequency domain

$$\sum_n \|\mathbf{y}(n)-\mathbf{x}(n)\|^2 = \int_0^{2\pi}\|\mathbf{Y}(e^{j\omega})-\mathbf{X}(e^{j\omega})\|^2\frac{d\omega}{2\pi} = \int_0^{2\pi}\underbrace{\|\mathbf{F}(e^{j\omega})\mathbf{C}(e^{j\omega M})-\mathbf{X}(e^{j\omega})\|^2}_{\mathcal{E}(\omega)}\frac{d\omega}{2\pi}.$$

Note that $\mathbf{C}(e^{j\omega M})$ appearing in the integrand is periodic with period $2\pi/M$, and thus can be chosen independently only in the range $0\le\omega\le 2\pi/M$. That is why the integrand can be rewritten as

$$\mathcal{E}(\omega) = \sum_{k=0}^{M-1}\|\mathbf{F}(e^{j(\omega+\frac{2\pi k}{M})})\mathbf{C}(e^{j\omega M})-\mathbf{X}(e^{j(\omega+\frac{2\pi k}{M})})\|^2.$$

For each ω in $0 \leq \omega \leq 2\pi/M$ we can choose $\mathbf{C}(e^{j\omega M})$ such that the nonnegative integrand $\mathcal{E}(\omega)$ is minimized and that would in turn minimize the projection error (2.26). Define the vector $\mathbf{a}(\omega)$ and the matrix $\mathbf{B}(\omega)$ as

$$\mathbf{a}(\omega) = [\mathbf{X}^T(e^{j\omega}) \;\; \mathbf{X}^T(e^{j(\omega+\frac{2\pi}{M})}) \ldots \mathbf{X}^T(e^{j(\omega+\frac{2\pi(M-1)}{M})})]^T$$

$$\mathbf{B}(\omega) = [\mathbf{F}^T(e^{j\omega}) \;\; \mathbf{F}^T(e^{j(\omega+\frac{2\pi}{M})}) \ldots \mathbf{F}^T(e^{j(\omega+\frac{2\pi(M-1)}{M})})]^T.$$

The problem now reduces to that of minimizing

$$\begin{aligned}
\mathcal{E}(\omega) &= \|\mathbf{B}(\omega)\mathbf{C}(e^{j\omega M}) - \mathbf{a}(\omega)\|^2 \\
&= [\mathbf{C}^\dagger(e^{j\omega M}) - \mathbf{a}^\dagger(\omega)\mathbf{B}(\omega)\mathbf{S}^{-1}(\omega)]\mathbf{S}(\omega)[\mathbf{C}(e^{j\omega M}) - \mathbf{S}^{-1}(\omega)\mathbf{B}^\dagger(\omega)\mathbf{a}(\omega)] \\
&\quad +\mathbf{a}^\dagger(\omega)\mathbf{a}(\omega) - \mathbf{a}^\dagger(\omega)\mathbf{B}(\omega)\mathbf{S}^{-1}(\omega)\mathbf{B}^\dagger(\omega)\mathbf{a}(\omega) \qquad (2.45)
\end{aligned}$$

where $\mathbf{S}(\omega) = \mathbf{B}^\dagger(\omega)\mathbf{B}(\omega)$. The form (2.45) was obtained by the 'completion of squares.' Consider the right-hand side of the last equality in (2.45). It consists of two parts; the first part depends on the choice of $\mathbf{C}(e^{j\omega M})$ and the second part does not. Since the first part is always nonnegative, we should choose $\mathbf{C}(e^{j\omega M})$ such that it becomes zero. Note that the matrix $\mathbf{S}(\omega) = \mathbf{B}^\dagger(\omega)\mathbf{B}(\omega)$ is positive definite, which follows from the assumption $[\mathbf{F}^\dagger(e^{j\omega})\mathbf{F}(e^{j\omega})]_{\downarrow M} > 0$. Therefore, the only way to make the first part zero is to choose $\mathbf{C}(e^{j\omega M}) = \left(\mathbf{B}^\dagger(\omega)\mathbf{B}(\omega)\right)^{-1}\mathbf{B}^\dagger(\omega)\mathbf{a}(\omega)$. In order to rewrite this solution in terms of multirate building blocks, we note from (1.2) that for any transfer function $\mathbf{A}(e^{j\omega})$

$$[\mathbf{A}(e^{j\omega})]_{\downarrow M} = \frac{1}{M}\sum_{k=0}^{M-1}\mathbf{A}(e^{j\frac{\omega+2\pi k}{M}}).$$

Therefore

$$\mathbf{B}^\dagger(\omega)\mathbf{B}(\omega) = \sum_{k=0}^{M-1}\mathbf{F}^\dagger(e^{j(\omega+\frac{2\pi k}{M})})\mathbf{F}(e^{j(\omega+\frac{2\pi k}{M})}) = M[\mathbf{F}^\dagger(e^{j\omega})\mathbf{F}(e^{j\omega})]_{\downarrow M\uparrow M},$$

$$\mathbf{B}^\dagger(\omega)\mathbf{a}(\omega) = \sum_{k=0}^{M-1}\mathbf{F}^\dagger(e^{j(\omega+\frac{2\pi k}{M})})\mathbf{X}(e^{j(\omega+\frac{2\pi k}{M})}) = M[\mathbf{F}^\dagger(e^{j\omega})\mathbf{X}(e^{j\omega})]_{\downarrow M\uparrow M}.$$

The optimal $\mathbf{C}(e^{j\omega M})$ is therefore

$$\mathbf{C}(e^{j\omega M}) = \left[\left([\mathbf{F}^\dagger(e^{j\omega})\mathbf{F}(e^{j\omega})]_{\downarrow M}\right)^{-1}_{\uparrow M}\mathbf{F}^\dagger(e^{j\omega})\mathbf{X}(e^{j\omega})\right]_{\downarrow M\uparrow M}.$$

Thus we have $\mathbf{C}(z) = [\mathbf{H}(z)\mathbf{X}(z)]_{\downarrow M}$, with $\mathbf{H}(z)$ given by (2.27). This concludes the proof. $\triangledown\,\triangledown\,\triangledown$

Chapter 3 Fractional biorthogonal partners and applications

While one of the applications of biorthogonal partners proposed originally in [65] was the reconstruction of signals oversampled by integer amounts, in the following we extend this reasoning to the case when the oversampling ratio is a rational number (or a fraction). This gives rise to the definition of *fractional* biorthogonal partners (**FBP**s in the following). The chapter starts by providing a motivation for the study of FBPs and defining them formally. Next we show a way to construct fractional biorthogonal partners. This discussion leads to deriving the conditions for the existence of FIR FBPs and of stable FBPs. An immediate consequence of the construction procedure is that FIR FBPs (when they exist) are not unique. This property is used in the channel equalization in a similar way as in the previous chapter. Namely, it is shown that, if the *amount of oversampling at the receiver is a rational number*, the problem of fractionally spaced equalization in communications can be posed in terms of fractional biorthogonal partners. The advantage of this approach is that many results developed in this and the previous chapter can be employed in FSE design. For example, the flexibility in the choice of FBPs will again translate to the non-uniqueness in the equalizer design. Moreover, as it was the case in Chapter 2, we will pose the problem of finding a fractionally spaced equalizer that in addition to being zero-forcing also combats the channel noise. This design procedure follows closely the one from Section 2.4.2. Another application of FBPs that is considered is spline interpolation of slightly oversampled signals using exclusively FIR filtering. This technique is illustrated through an image interpolation example. We also consider the least squares approximation problem in the setting of fractional biorthogonal partners. The content of the chapter is drawn mainly from [77] and its portions have been presented at [76] and [78].

3.1 Chapter outline and relation to past work

The relation between biorthogonal partners and biorthogonal filter banks was pointed out in Chapter 1. An extension of filter banks to the case when the decimation ratios in subbands are rational numbers instead of integers, namely, perfect reconstruction *rational* filter banks were treated by many authors [36], [28]. It can be shown that every pair of filters $\{H_k(z), F_k(z)\}$ in a perfect reconstruction rational filter bank forms a *fractional biorthogonal partner* pair. However, the properties of such filters considered *outside* the filter bank setup were not addressed previously and constitute a major part of this chapter. In addition to this, the reader will find that the theory as well as the applications presented here are quite different from the results on rational PR filter banks and are more related to the theory of biorthogonal [65] and MIMO biorthogonal

partners.

In Section 3.2 we introduce the precise definition of fractional biorthogonal partners. We describe the construction procedure for finding an FBP of a discrete-time filter $F(z)$. Moreover, we derive a set of necessary and sufficient conditions for the existence of stable and of FIR FBPs. One of the results which follow from this derivation is that FIR FBPs (if they exist) are not unique.

Section 3.3 considers one of the applications of FBPs—the channel equalization with fractionally spaced equalizers. The idea of signal oversampling at the receiver for the purpose of FIR equalization was motivated in Chapter 2. A similar idea has also been used for blind channel identification [56], [47], [48]. In the context of FBPs we are interested in fractionally spaced equalizers with *fractional* amount of oversampling at the receiver. After reviewing the characteristics of FSEs, especially those with fractional amount of oversampling, we draw a parallel between FSEs and FBPs. From the findings of Chapter 2 it is to be expected that it is possible to optimize FIR FBPs for the purpose of zero-forcing equalization. The performance of such optimized equalizers is evaluated in the section with experimental results where we compare it to the performance of several other equalization methods including the minimum mean-squared error (MMSE) equalizer.

In Section 3.4 we consider another application of FBPs, namely, the interpolation of signals described by oversampled models. This method is a modification of the well-known spline interpolation technique [25], [44] which requires the use of non-causal IIR filters. Efficient implementation of this filtering is treated in [59]. Here we show that by assuming even a slightly oversampled model for the signal, *exact* spline interpolation is possible using only FIR filters. This approach is thus different from another all-FIR spline interpolation method described in [74] where certain approximations were introduced.

Approximation of arbitrary signals by signals admitting a described oversampled model is treated in Section 3.5. This discussion is an extension to rational oversampling ratios of a similar method for vector signals treated in Chapter 2. Not surprisingly, the solution to this problem involves the use of fractional biorthogonal partners. This solution makes use of the corresponding results in the MIMO biorthogonal partner setting, even though the initial problem formulation seems rather different. In Section 3.6 we extend the concept of scalar FBPs to the vector case.

3.2 Fractional biorthogonal partners

Biorthogonal partners as originally introduced in [65] arise in many different contexts. One of those not treated in Chapter 2 is the reconstruction of continuous time signals admitting the model

$$x(t) = \sum_{k=-\infty}^{\infty} c(k)\phi(t-k). \tag{3.1}$$

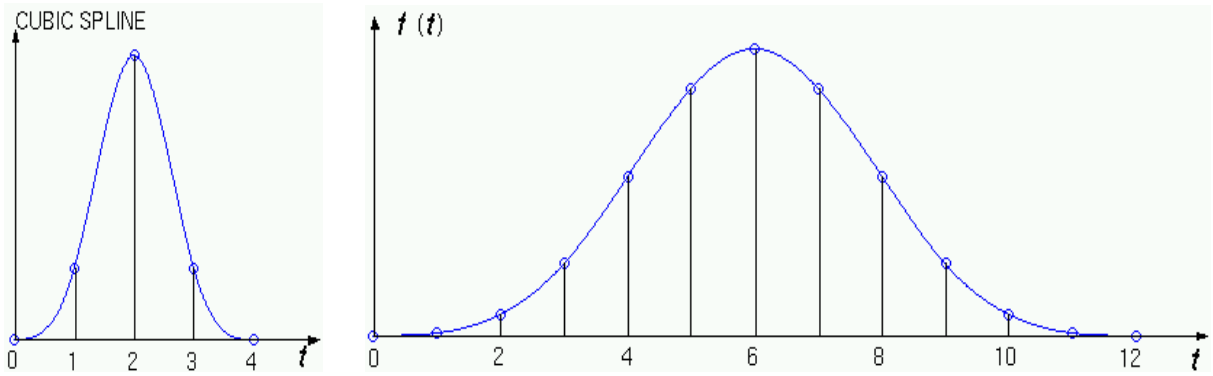

Figure 3.1: Example of a generating function $\phi(t)$ (cubic spline) and its three times 'stretched' version $f(t)$.

Given the integer samples of $x(t)$ admitting the model (3.1), namely

$$x(n) = \sum_{k=-\infty}^{\infty} c(k)\phi(n-k) \tag{3.2}$$

the reconstruction of the driving sequence $c(n)$ and thus of $x(t)$ is obtained by inverse filtering $1/\Phi(z)$, with $\Phi(z)$ denoting the z-transform of $\phi(n)$. This is a direct consequence of (3.2). It has been shown [65] that the IIR reconstructive filtering $1/\Phi(z)$ can often be replaced by simple FIR filtering if the continuous time signal $x(t)$ is sampled L times more densely (for an integer $L \geq 2$). This is motivated in Fig.1.5. The FIR filter is nothing but a biorthogonal partner of the corresponding oversampled version of $\Phi(z)$ with respect to an integer L. In the following we consider the case where $x(t)$ is oversampled by a *rational number*, possibly less than two. We shall see that FIR reconstruction is often possible even under these relaxed conditions.

Suppose we are given the discrete-time signal $y(n)$ that is obtained by sampling $x(t)$ from (3.1) at the rate L/M, i.e., $y(n) = x(nM/L)$. For obvious reasons we will assume that M and L are coprime. We shall see later that in most of the applications considered here $L > M$ is required as well, although in principle it is not necessary. Notice that $y(n)$ is obtained by *oversampling* $x(t)$ with respect to the usual integral sampling strategy by a factor of L/M. Therefore we have

$$\begin{aligned} y(n) &= x(\frac{M}{L}n) = \sum_{k=-\infty}^{\infty} c(k)\phi(\frac{M}{L}n - k) \\ &= \sum_{k=-\infty}^{\infty} c(k) f(Mn - kL), \end{aligned} \tag{3.3}$$

where $f(t) \stackrel{\triangle}{=} \phi(t/L)$ is the generating function 'stretched' by a factor of L. This is shown in Fig.3.1 for the case where $\phi(t)$ is a cubic spline [25] and $L = 3$. The signal $y(n)$ from (3.3) can thus be obtained as shown in Fig.3.2(a).

Now consider the problem of signal reconstruction [recovering $c(n)$ from $y(n)$]. We look for the solution

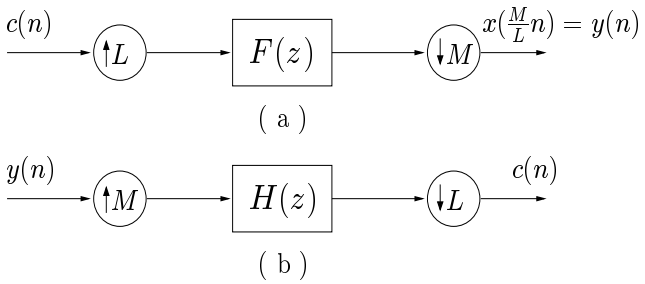

Figure 3.2: (a) Signal model. (b) Scheme for reconstruction.

in the form depicted in Fig.3.2(b). It will be shown that under some mild assumptions this solution [i.e., filter $H(z)$] exists. Further, we establish the conditions under which an FIR filter $F(z)$ yields an FIR solution for $H(z)$.

3.2.1 Definition

The preceding discussion leads naturally to the definition of fractional biorthogonal partners.

Definition 3.1. Transfer function $H(z)$ is said to be a *right fractional biorthogonal partner* (RFBP) of $F(z)$ with respect to the fraction L/M if the system shown in Fig.3.3(a) is the identity. Under these conditions $F(z)$ is also said to be a *left fractional biorthogonal partner* (LFBP) of $H(z)$ with respect to L/M.

This definition includes the notion of (integral) biorthogonal partners [65] as a special case when $M = 1$. As mentioned in Chapter 1, the system in Fig.3.3(a) is LTI whenever M divides L. However, in general it is not. Also, note that (similar to the MIMO case) we need to distinguish between left and right FBPs. The results that hold for RFBPs can easily be modified to accommodate LFBPs, and therefore we only focus on RFBPs in the following. It is important to note the distinction between this definition and a similar definition of left (right) biorthogonal partners in the MIMO case. Right FBP appears on the right-hand side in the *diagram* in Fig.3.3(a), while right MIMO biorthogonal partner appears on the right-hand side in the equivalent *transfer function* (thus on the left-hand side in the diagram). The reason for this inconsistency is that in general for $M > 1$ the system with fractional biorthogonal partners in Fig.3.3(a) is not LTI, so we cannot write its transfer function. As a final remark, we note that the FBP relationship depends on the fraction L/M. Nevertheless, this number will be omitted whenever no confusion is anticipated.

Returning to the previous discussion we see that the reconstruction of $x(t)$ given by the model (3.1) from its samples $y(n)$ obtained at rate L/M is possible if $F(z)$ has a stable RFBP $H(z)$. Similarly, it is possible to perform an FIR reconstruction whenever there exists an FIR RFBP. In the following we describe a way of constructing fractional biorthogonal partners. This will result in a set of conditions for the existence of FIR or just stable FBPs. Even though this introductory material might seem rather familiar, the reader will soon discover that the FBP construction is rather different from the methods used in Chapter 2.

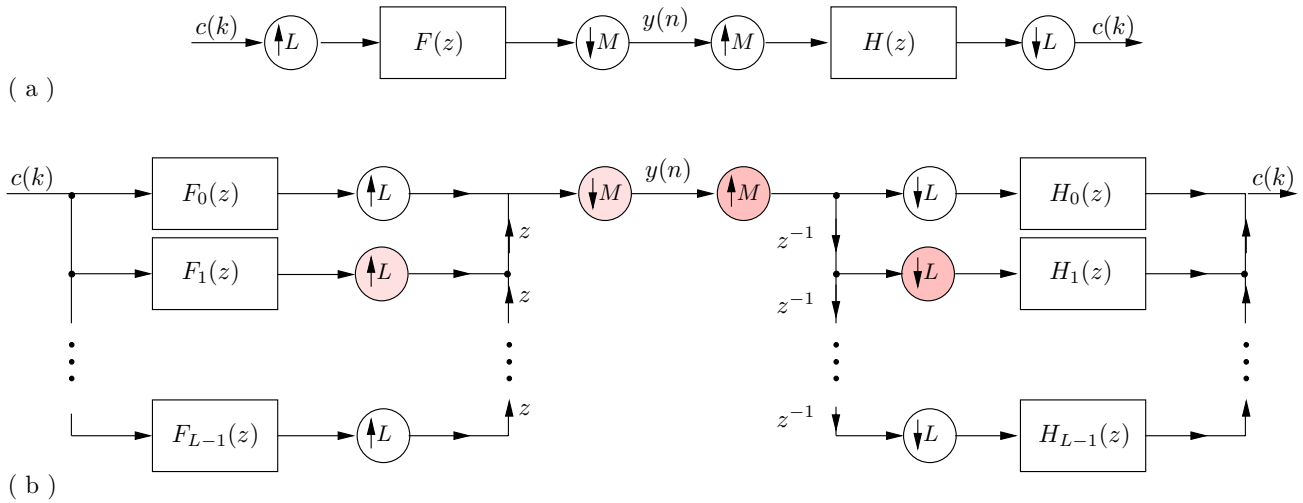

Figure 3.3: (a)-(b) Equivalent presentations of fractional biorthogonal partners.

3.2.2 Existence and construction of FBPs

Consider the system in Fig.3.3(a). Write the filters $F(z)$ and $H(z)$ in terms of their Type 2 and Type 1 polyphase components

$$F(z) = \sum_{k=0}^{L-1} F_k(z^L) z^k, \quad \text{and} \quad H(z) = \sum_{k=0}^{L-1} H_k(z^L) z^{-k}. \tag{3.4}$$

Then we can redraw the system as shown in Fig.3.3(b). Next, consider the left-hand side of Fig.3.3(b) and focus on the system between the output of the ith filter $F_i(z)$ and $y(n)$, namely, a cascade of an expander by L, advance operator z^i and a decimator by M [see Fig.3.4(a)]. Since we assumed M and L are coprime, there exist integers m and l such that

$$lL + mM = 1. \tag{3.5}$$

In fact, the unique solution for the smallest m and l can be obtained by the Euclid's algorithm. Writing the delay $z^i = z^{ilL} \cdot z^{imM}$, we can easily prove the multirate identity depicted in Fig.3.4(a). Similarly, it can be shown that the system between $y(n)$ and the input to $H_i(z)$ can be equivalently presented as in Fig.3.4(b).

Substituting the described identities back to Fig.3.3(b) we obtain the equivalent structure shown in Fig.3.5(a). Let us define

$$P_k(z) \triangleq z^{kl} F_k(z), \quad \text{and} \quad Q_k(z) \triangleq z^{-kl} H_k(z), \tag{3.6}$$

for $0 \le k \le L-1$. Since L and M are coprime, it follows that L and m are coprime as well. Under these circumstances it can be shown that the $L \times L$ system shown in Fig.3.5(a) within the dashed box is the identity. Thus, the whole structure can be redrawn as in Fig.3.5(b). It is important to notice here that the original filters $F(z)$ and $H(z)$ are FIR if and only if the banks of filters $\{P_k(z)\}$ and $\{Q_k(z)\}$ are FIR for all k. The structure from Fig.3.5(b) is an L-channel, uniform, nonmaximally decimated filter bank. In our

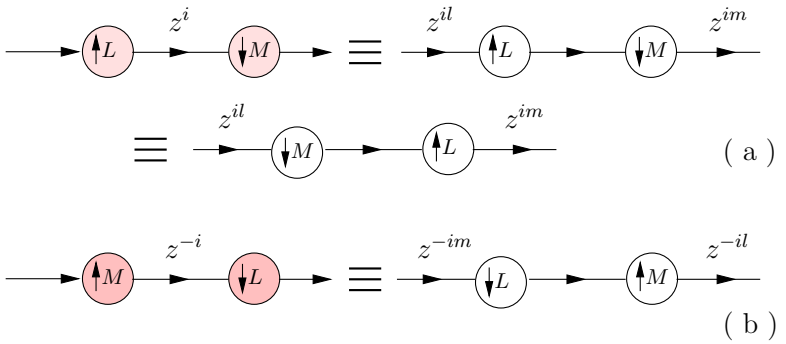

Figure 3.4: (a)-(b) Some multirate identities.

setting one side (analysis or synthesis) of this filter bank is usually known, and the task is to construct the other side so that the whole system has perfect reconstruction property. For example, in the problem of signal reconstruction, $F(z)$ and thus $\{P_k(z)\}$ are known and the goal is to find the corresponding synthesis bank $\{Q_k(z)\}$. Recall that at the same time this is exactly the problem of constructing an RFBP $H(z)$, since it is uniquely defined by the filters $\{Q_k(z)\}$. Recalling the discussion in Section 1.3.2, we resort to the polyphase matrix notation. Define the $L \times M$ analysis and the $M \times L$ synthesis polyphase matrices $\mathbf{E}(z)$ and $\mathbf{R}(z)$ respectively

$$\mathbf{E}(z) = \begin{bmatrix} E_{0,0}(z) & E_{0,1}(z) & \cdots & E_{0,M-1}(z) \\ E_{1,0}(z) & E_{1,1}(z) & \cdots & E_{1,M-1}(z) \\ \vdots & \vdots & \vdots & \vdots \\ E_{L-1,0}(z) & E_{L-1,1}(z) & \cdots & E_{L-1,M-1}(z) \end{bmatrix}, \quad \text{and}$$

$$\mathbf{R}(z) = \begin{bmatrix} R_{0,0}(z) & R_{0,1}(z) & \cdots & R_{0,L-1}(z) \\ R_{1,0}(z) & R_{1,1}(z) & \cdots & R_{1,L-1}(z) \\ \vdots & \vdots & \vdots & \vdots \\ R_{M-1,0}(z) & R_{M-1,1}(z) & \cdots & R_{M-1,L-1}(z) \end{bmatrix}, \tag{3.7}$$

containing the Type 1 and Type 2 polyphase components (of order M this time) $E_{i,j}(z)$ and $R_{i,j}(z)$ defined by

$$P_k(z) = \sum_{j=0}^{M-1} E_{k,j}(z^M) z^{-j}, \quad \text{and} \quad Q_k(z) = \sum_{i=0}^{M-1} R_{i,k}(z^M) z^i, \tag{3.8}$$

for $0 \le k \le L-1$. Now the system in Fig.3.5(b) can be equivalently redrawn as in Fig.3.5(c). We see that the problem of finding an RFBP of $F(z)$ becomes equivalent to that of finding a *left inverse* $\mathbf{R}(z)$ of an $L \times M$ matrix $\mathbf{E}(z)$. Obviously, when computing an LFBP, we would need to find a right matrix inverse of $\mathbf{R}(z)$. At this point it should be clear why the condition $L > M$ was included in the problem formulation.

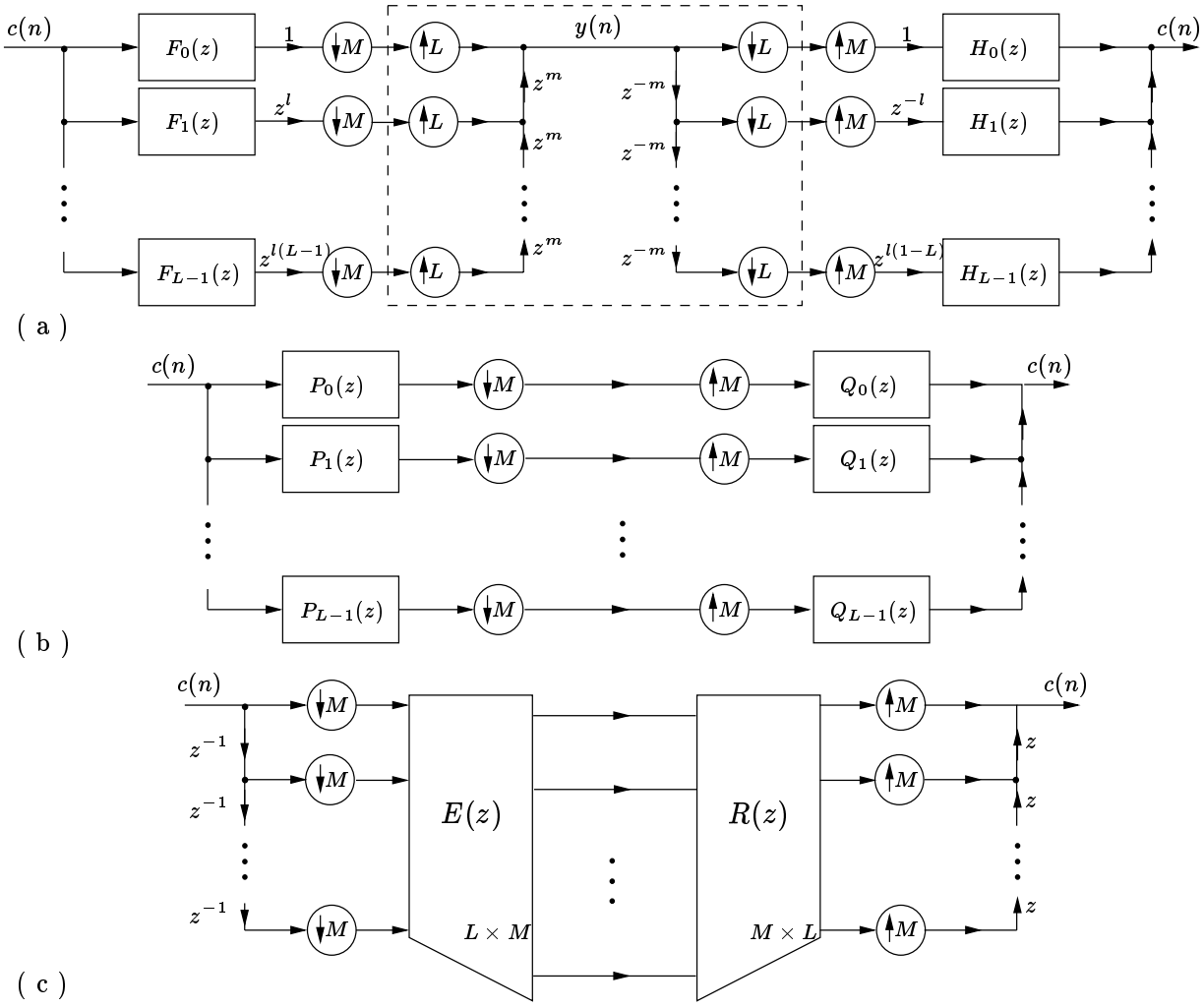

Figure 3.5: (a)-(c) Further simplifications of fractional biorthogonal partners.

For $L < M$, the polyphase matrices $\mathbf{E}(z)$ and $\mathbf{R}(z)$ do not have the corresponding inverses; in other words, there is not enough information in the samples $y(n)$ to reconstruct $x(t)$. On the other hand, when $L = M$ the system in Fig.3.3(a) is just a cascade of two LTI systems [namely, the zeroth polyphase components of $F(z)$ and $H(z)$], so the unique FBP is obtained by filter inversion. Based on the previous findings we prove the following theorem.

Theorem 3.1. Given the transfer function $F(z)$ and two coprime integers L and M, there exists a *stable* right fractional biorthogonal partner of $F(z)$ if and only if $L > M$, and the minimum rank of $\mathbf{E}(e^{j\omega})$ pointwise in ω is M. For an FIR filter $F(z)$ there exists an *FIR* right fractional biorthogonal partner if and only if $L > M$, and the greatest common divisor (GCD) of all the $M \times M$ minors of $\mathbf{E}(z)$ is a delay. Here, the polyphase matrix $\mathbf{E}(z)$ is defined by (3.7)–(3.8). Analogous results hold for left FBPs as well.

Proof. We have shown that there exists a stable (FIR) RFBP of $F(z)$ if and only if there exists a stable

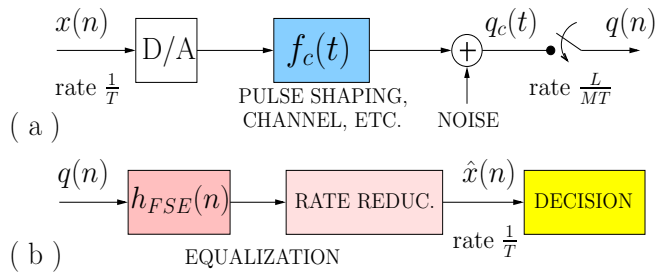

Figure 3.6: Continuous-time communication system. (a) Transmitter and channel. (b) Receiver.

(polynomial) left inverse of a (polynomial) matrix $\mathbf{E}(z)$. We know that fat matrices do not have left inverses, so we immediately have $L > M$ as a necessary condition ($L = M$ is eliminated for the reasons explained earlier). Next, for the inverse of $\mathbf{E}(e^{j\omega})$ to be stable, we need the full column rank of $\mathbf{E}(e^{j\omega})$ pointwise in ω, which is the same as saying that the minimum rank over all ω is M. Finally, using the result mentioned in Section 2, we have that there is a left polynomial inverse of a $L \times M$ polynomial matrix if and only if the GCD of all its $M \times M$ minors is a delay [14], [63]. $\triangledown\triangledown\triangledown$

Due to a rather complicated relation between the starting filters $F(z)$ and $H(z)$ and the polyphase matrices $\mathbf{E}(z)$ and $\mathbf{R}(z)$, it is not clear how the conditions appearing in Theorem 3.1 can be translated into the corresponding conditions on the filters $F(z)$ and $H(z)$. Note that whenever the conditions for the existence of FIR FBPs are satisfied, these solutions are not unique. This is a consequence of the construction for left polynomial inverses of tall polynomial matrices, or equivalently right polynomial inverses of fat polynomial matrices. In the next section we exploit this non-uniqueness in the process of constructing FIR zero-forcing fractionally spaced equalizers for communication channels.

3.3 Channel equalization with fractionally spaced equalizers

Consider the continuous-time baseband communication system shown in Fig.3.6, where $f_c(t)$ denotes the combined effect of the reconstruction filter from the D/A converter, pulse shaping filter as well as the continuous-time channel. After passing through the channel, signal is corrupted by the additive noise and the received waveform $q_c(t)$ is sampled at the rate $(L/M)/T$ to produce the received sequence $q(n)$. Recall that if the ratio L/M is equal to 1, the equalizer at the receiver from Fig.3.6(b) is a symbol spaced equalizer (SSE). As mentioned previously, the receiver in this case becomes very sensitive to the phase shift at the sampling device; also, sampling at exactly the symbol rate may create some aliasing problems. In addition to this, the zero-forcing SSE is nothing but the channel inverse, which is almost always IIR and sometimes introduces stability issues, as demonstrated in Section 2.4.3. For all these reasons, the preferred alternative is to keep $L > M$, giving rise to the receiver structure called the *fractionally oversampled* fractionally spaced equalizer (**FoFSE**), or just FSE in this chapter. The received sequence $q(n)$ with the denser spacing (higher rate) enters the FoFSE $h_{FSE}(n)$, which now has to operate at a slightly higher rate. Accompanied with this

process, some rate reduction also needs to take place at the receiver so that the final sequence $\widehat{x}(n)$ entering the decision device has exactly the same rate $1/T$ as the information sequence $x(n)$.

FSEs are the preferred alternative to traditional channel equalization since they often lead to well-behaved FIR solutions. Moreover, oversampling at the receiver often allows for *blind* channel identification and equalization [56], [47], [48]. As stated previously, one popular equalization method involves the use of *zero-forcing equalizers* (ZFEs). Note, however that the ZFEs are not necessarily the best solutions. Instead of insisting on $\widehat{x}(n) = x(x)$ in the absence of noise it might be advantageous to take into account the effect of the additive noise as well and thus minimize the overall distortion at the output.

It should be noted that even though there are some similarities between the underlying filter bank structures of the FSE system considered here and the discrete multitone (DMT) system [27], [30], [40], the two problems do not have much in common. DMT systems make use of the transmultiplexer-like structures, whereas this chapter deals with the dual system (analysis/synthesis) and uses fractional decimators. In addition to that, FIR equalization in DMT systems is achieved by introducing some form of redundancy at the transmitter which eventually leads to the *bandwidth expansion*. In contrast, the systems with fractionally spaced equalizers in general do not introduce any bandwidth expansion, but require more computations at the receiver. In this chapter we show that in most cases this computational overhead can be minimal since even the slight amount of oversampling often leads to FIR solutions. This should be compared to FSEs with integer oversampling where $L/M = 2$ is the minimum oversampling ratio and thus results in the minimum computational overhead. FSEs with fractional oversampling were also treated by Ding and Qiu in the context of blind identification [11]. Although the authors there use a different notation, it can be shown that the problem formulation in [11] is equivalent to the one treated in this section. However, the solution presented here is derived in the context of FBPs, which brings many advantages, like the theoretical framework described in the previous section, as well as the the study of the optimal solutions described in Section 3.3.2.

3.3.1 FSEs with fractional oversampling

In the following we first derive the equivalent digital structure of the system in Fig.3.6 and then we construct the best FoFSE and evaluate its performance. As we did before, in the following we assume that $L > M$ and that L and M are coprime. Consider Fig.3.6(a) in the absence of noise. We can see that

$$q(n) = q_c(n\frac{M}{L}T) = \sum_{k=-\infty}^{\infty} x(k) f_c(n\frac{M}{L}T - kT). \tag{3.9}$$

By defining the discrete-time sequence $f(n) \stackrel{\triangle}{=} f_c(nT/L)$, which is actually the function $f_c(t)$ sampled L times more densely than at integers, we have

$$q(n) = \sum_{k=-\infty}^{\infty} x(k) f(nM - kL). \tag{3.10}$$

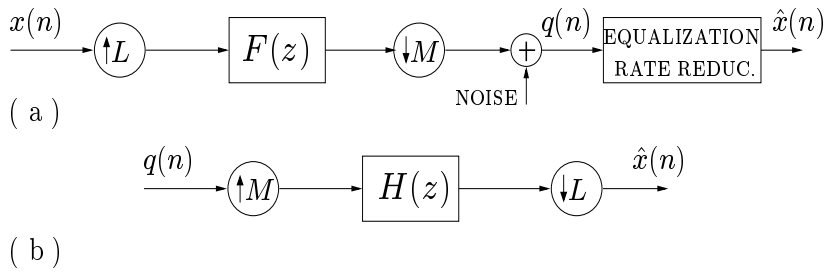

Figure 3.7: FSEs with fractional oversampling. (a) Discrete-time model of the communication system. (b) Form of the proposed equalizer.

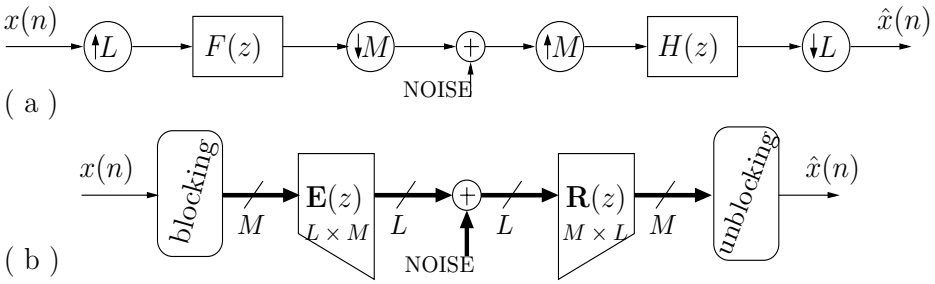

Figure 3.8: Communication system with FoFSEs. (a) FBP form. (b) Blocked equivalent form.

This identity is incorporated in Fig.3.7(a) where we show the discrete-time model of the communication system from Fig.3.6. The discrete-time noise appearing in Fig.3.7(a) is obtained by sampling the corresponding continuous-time noise from Fig.3.6(a) at the rate L/MT. In the following we focus on the box in Fig.3.7(a) labeled 'equalization and rate reduction.' Recalling that in the zero-forcing setting the goal of this block is to make $\widehat{x}(n) = x(n)$ in the absence of noise, we conclude that this block needs to incorporate a right FBP of $F(z)$ with respect to L/M. In other words, we search for the equalizer of the form shown in Fig.3.7(b). For the reasons explained in Chapter 2, of special interest are FIR solutions, and non-uniqueness of these solutions is exploited in the following.

3.3.2 Optimizing FIR RFBPs for channel equalization

It follows from the previous discussion that the discrete-time equivalent communication system with fractionally oversampled FSEs can be drawn as in Fig.3.8(a), which in turn can be equivalently presented as in Fig.3.8(b). Matrices $\mathbf{E}(z)$ and $\mathbf{R}(z)$ are given by (3.7) and construction of the FSE $H(z)$ amounts to finding the appropriate left inverse $\mathbf{R}(z)$ of the matrix $\mathbf{E}(z)$. In the following we assume that the equivalent channel $f_c(t)$ is of finite length, which implies that $\mathbf{E}(z)$ is a polynomial matrix. In practice, this is achieved by applying one of the several methods for channel shortening [2] before equalization. We look for FIR equalizers, implying that the corresponding polyphase matrix $\mathbf{R}(z)$ should be polynomial as well. Since the solution to this problem is not unique, our goal is to find the one that performs favorably with respect to the

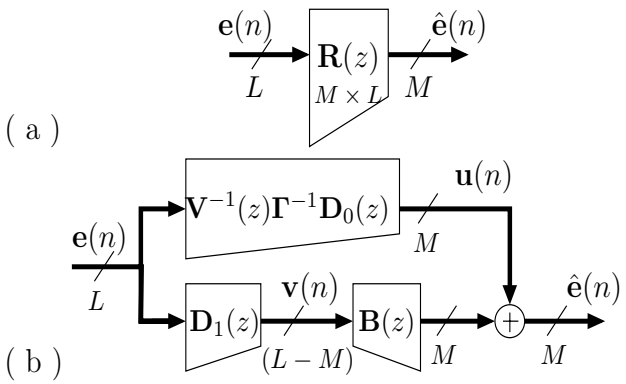

Figure 3.9: (a)-(b) Finding the optimal FIR RFBP. See text.

noise amplification at the receiver. This problem is *equivalent* to the one studied in Section 2.4.2, so here we skip many derivation details.

Consider the system in Fig.3.8(b). The equivalent model for noise is shown in Fig.3.9(a). Using the Smith form decomposition of $\mathbf{E}(z)$ and the same notation as in Chapter 2, it can be shown that the most general form of an FIR ZFE $\mathbf{R}(z)$ is given by Fig.3.9(b) for an *arbitrary* polynomial matrix $\mathbf{B}(z)$. The solution for the optimal $\mathbf{B}(z)$ of a given order $N_B - 1$ is again given by

$$\mathcal{B} = -\mathcal{C} \cdot \mathcal{R}_{\epsilon,1} \cdot \mathcal{D}_1^\dagger \cdot \left(\mathcal{D}_1 \cdot \mathcal{R}_{\epsilon\epsilon} \cdot \mathcal{D}_1^\dagger \right)^{-1}, \tag{3.11}$$

where $\mathcal{R}_{\epsilon\epsilon}$ is now a $L(N_B + N_D - 1) \times L(N_B + N_D - 1)$ autocorrelation matrix of the input noise process, and $\mathcal{R}_{\epsilon,1}$ consists of its first $N_C L$ rows.

3.3.3 MMSE equalizer

As mentioned earlier, although a zero-forcing equalizer completely eliminates the channel distortion, the best equalizer $\mathbf{R}(z)$ of a given order $N_R - 1$ in Fig.3.8(b) is the one that minimizes the mean-squared error between $x(n)$ and $\widehat{x}(n)$. This is nothing but a vector Wiener filter [54] for recovering $\mathbf{x}(n)$ corrupted by a linear distortion $\mathbf{E}(n)$ and an additive noise with the given statistics. Consider Fig.3.8(b). Let the matrices $\mathbf{E}_i$ and $\mathbf{R}_i$ denote the impulse responses of $\mathbf{E}(z)$ and $\mathbf{R}(z)$ respectively and let the $N_R L \times M(N_R + N_E - 1)$ matrix $\mathcal{G}$ be defined as

$$\mathcal{G} \stackrel{\triangle}{=} \begin{bmatrix} \mathbf{E}_0 & \dots & \mathbf{E}_{N_E-1} & \mathbf{0} & \dots & \mathbf{0} \\ \mathbf{0} & \mathbf{E}_0 & \dots & \mathbf{E}_{N_E-1} & \dots & \mathbf{0} \\ \vdots & & \ddots & & \ddots & \\ \mathbf{0} & \dots & \mathbf{0} & \mathbf{E}_0 & \dots & \mathbf{E}_{N_E-1} \end{bmatrix}.$$

It can be shown [54] that the MMSE solution for $\mathbf{R}(z)$ is given by its impulse response

$$\mathcal{P} \stackrel{\triangle}{=} [\mathbf{R}_0 \;\; \mathbf{R}_1 \;\; \cdots \;\; \mathbf{R}_{N_R-1}] = \mathcal{R}_{\mathcal{X},1} \cdot \mathcal{G}^\dagger \cdot \left(\mathcal{G} \cdot \mathcal{R}_{\mathcal{X}\mathcal{X}} \cdot \mathcal{G}^\dagger + \mathcal{R}_{ee} \right)^{-1}. \tag{3.12}$$

Here $\mathcal{R}_{\mathcal{X}\mathcal{X}}$ is a $M(N_R+N_E-1)\times M(N_R+N_E-1)$ autocorrelation matrix of the input sequence $x(n)$, $\mathcal{R}_{\mathcal{X},1}$ consists of its first M rows and $\mathcal{R}_{ee}$ is a $N_RL\times N_RL$ autocorrelation matrix of the noise process.

Even though the MMSE method provides statistically the best solution, the equalizers based on zero-forcing are often preferred for simplicity reasons. Namely, comparing the two solutions (3.11) and (3.12) we see that as opposed to the MMSE method, the optimized FIR RFBP method does not require the knowledge of the signal autocorrelation matrix nor the noise variance, whenever the noise is uncorrelated. The latter can become a significant advantage, especially in a low signal to noise ratio environment, when the matrix inversion in (3.12) depends significantly on the noise power. This point is illustrated in the next subsection. Also, in certain communication systems the transmitter might change the coding technique during the transmission (thus changing the signal covariance matrix), while the equalizer stages of the receiver might not have this information available. This change in $\mathcal{R}_{\mathcal{X}\mathcal{X}}$ would seriously affect the MMSE performance (3.12), however the optimal solution (3.11) would remain unaltered.

3.3.4 Performance evaluation

Using computer simulations, we compare the equalization performance of four different methods

1. Traditional IIR SSE (simply a channel inverse), which corresponds to the case of no oversampling at the receiver, i.e., when $L=M$ (we call this method **SSE**).
2. Simple FIR FSE method using plain RFBPs without the optimization matrix $\mathbf{B}(z)$ in Fig.3.9(b)—**plain RFBP**.
3. Optimized FIR RFBP method described in Section 3.3.2—**optimized RFBP**.
4. MMSE equalizer described in Section 3.3.3—**MMSE**.

The channel sampled at integers was taken to be of the fourth order, with coefficients

$$1.0000 \quad 0.7599 \quad -0.2600 \quad -0.1200 \quad 0.5000$$

and the corresponding sequence $f(n)$ [$f_c(t)$ oversampled by L] was obtained by linear interpolation. Note that two of the four complex zeros of the minimum phase channel lie very close to the unit circle and thus the traditional SSE consists of a barely stable IIR filter which amplifies the channel noise. In all the FoFSE implementations (2–4) we fixed $L=5$ and $M=4$, so that the amount of computational overhead for the fractionally spaced equalizer (with respect to the symbol spaced one) was just 25%. The order of the MMSE solution $\mathbf{R}(z)$ given by (3.12) was $N_R-1=7$. For the fairness of comparison, the optimized FIR RFBP was chosen to be of the same order and thus the order of the linear estimator $\mathbf{B}(z)$ was $N_B-1=3$.

The noise was taken to be white and the signal-to-noise ratio (SNR) measured at the input to the receiver was 29 dB. The obtained probabilities of error for the four methods were 0.0791, 1.4×10^{-3}, 1.19×10^{-5} and 5.0×10^{-6} respectively. The corresponding scattering diagrams for the 64-QAM input constellation

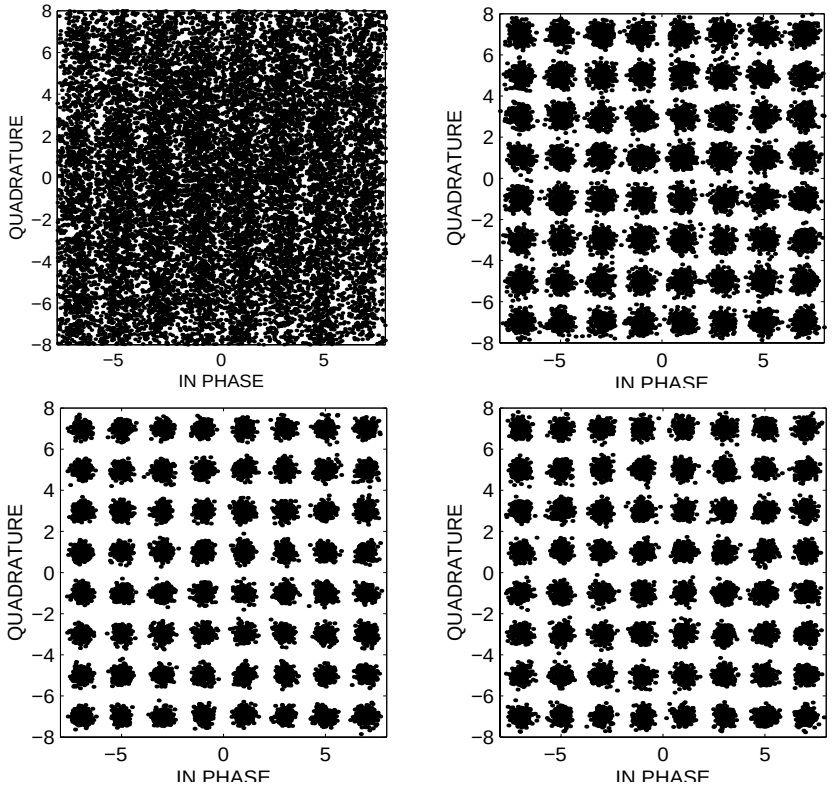

Figure 3.10: Equalization results. Clockwise, starting from upper left: SSE, plain FIR RFBP, optimized FIR RFBP and MMSE methods.

are shown clockwise in Fig.3.10. The diagram presenting the probability of error in the four methods as a function of SNR is shown in Fig.3.11.

The simulation example shows that the improvement in performance achieved by exploiting the redundancy in the construction of FIR RFBPs can be significant. Also, both the plain RFBP and the optimized RFBP methods perform significantly better than the SSE, at the expense of just 25% increase in the clock rate at the receiver. It can also be observed that the method with optimized RFBP equalization does not perform far from the optimal MMSE equalization of the same order, while it requires no knowledge of the input statistics and the noise variance.

In Fig.3.12 we explore the sensitivity of the optimal MMSE equalizer to the estimate of the noise variance at the receiver. Let the ratio between the estimated and the actual noise variances be $\sigma^2_{est}/\sigma^2_{act} = \alpha^2$. In Fig.3.12 we show the probability of error achieved using the equalization methods three and four as a function of the parameter α^2 with a fixed SNR = 29 dB. We can see that whenever the noise variance gets overestimated by a factor of two or more, the MMSE equalizer performance becomes comparable or even worse than the performance of the optimized FIR RFBP equalizer.

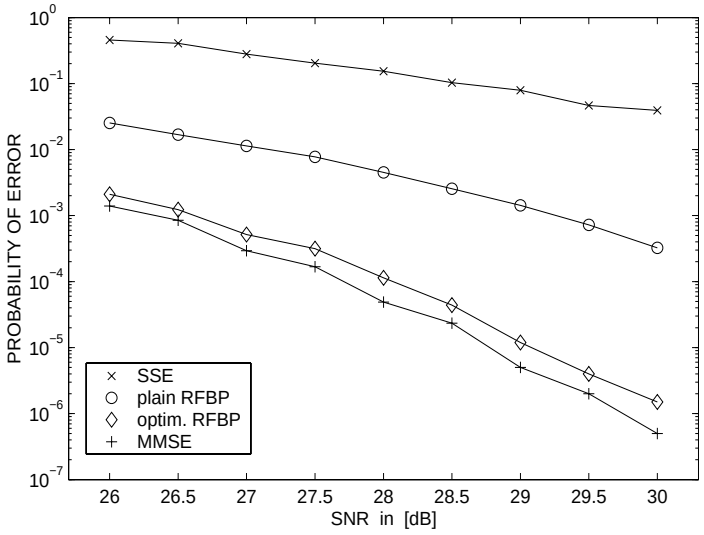

Figure 3.11: Probability of error as a function of SNR in the four equalization methods.

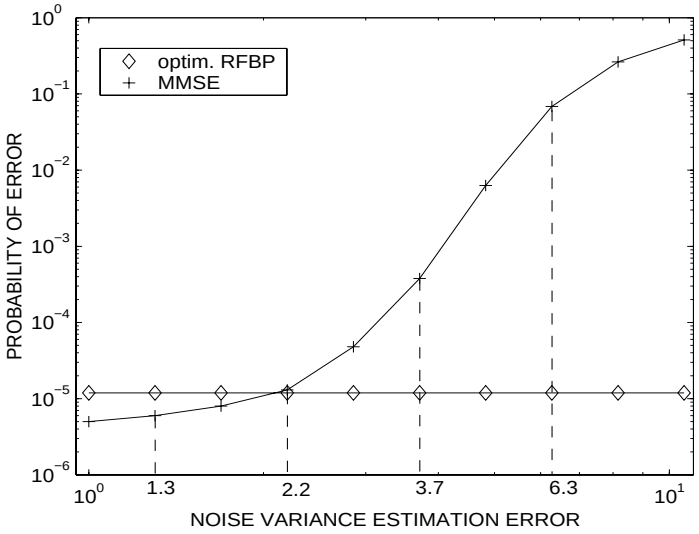

Figure 3.12: Probability of error as a function of noise variance discrepancy α^2.

3.4 Interpolation of oversampled signals

3.4.1 Spline models in conventional interpolation

In this section we consider the problem of linear signal interpolation using continuous-time signal models. We develop the connection between FBPs and the corresponding interpolation systems for slightly oversampled signals. Given a discrete-time signal $x(n)$ and a function $\phi(t)$, we can almost always assume that $x(n)$ is

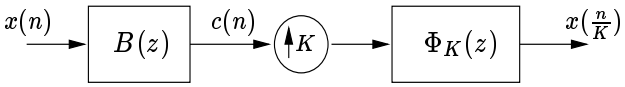

Figure 3.13: Interpolation of discrete signals using digital filtering. In the case of spline interpolation, $\phi_K(t)$ is an oversampled B-spline.

obtained by sampling at integers the continuous-time signal $x(t)$ given by the model (3.1), i.e.

$$x(n) = \sum_{k=-\infty}^{\infty} c(k)\phi(n-k). \tag{3.13}$$

The only condition is that $\Phi(e^{j\omega})$, the discrete-time Fourier transform of $\phi(n)$ is nonzero for all ω [65]. The driving coefficients $c(n)$ can be obtained by the inverse filtering $1/\Phi(e^{j\omega})$, if it is stable. These driving coefficients can then be employed for signal reconstruction as in (3.1) or for the *interpolation* of discrete signals. The signal $x(n)$ interpolated by an integral factor K is obtained by sampling $x(t)$ from (3.1) K times more densely than at integers. Thus, the interpolation process for the signals admitting the model (3.13) is shown in Fig.3.13, with $\phi_K(t) \stackrel{\triangle}{=} \phi(t/K)$ and $B(e^{j\omega}) \stackrel{\triangle}{=} 1/\Phi(e^{j\omega})$.

While in principle $\phi(t)$ can be chosen to be just about any function, various researchers have traditionally used continuously differentiable interpolating functions such as *B-splines* [25], [44] to insure some smoothness properties of the resulting interpolant. The mth order B-spline is given by the m-fold convolution of the unit pulse function

$$p(t) = \begin{cases} 1 & \text{for } t \in [0,1), \\ 0 & \text{otherwise} \end{cases}$$

with itself. The important property of B-splines is that they span the space of continuously differentiable functions—splines [44]. In other words, the $(m-1)$th derivative of $x(t)$ exists and is continuous if $x(t)$ admits the model (3.1), with $\phi(t)$ representing the mth order B-spline. The case when $m = 3$ is called cubic spline interpolation and it has received much attention in the image processing community [59]. The cubic spline $\phi(t)$ and its 3 times stretched version $\phi_3(t)$ are shown in Fig.3.1.

Spline interpolation, though elegant, unfortunately comes at a certain price. It can be shown [59] that in this case the inverse filtering by $B(z) = 1/\Phi(z)$ in Fig.3.13 is not only IIR but noncausal, so recursive implementation [59] is required. The authors in [74] consider one way of modifying the interpolation structure from Fig.3.13 in order to avoid IIR filtering. Although the technique proposed there is shown to produce results very similar to the exact spline interpolation, it is still only an approximation of the exact method and results in a reduced degree of smoothness or irreversibility of the interpolant [74]. In [65], the same problem was considered from a slightly different point of view. It is shown that if $x(n)$ is a spline function *oversampled* by an integer amount, i.e., if $x(n)$ admits the model (3.13), with $\phi(n)$ being a B-spline oversampled by some integer, then the reconstruction prefilter $B(z)$ in Fig.3.13 can be FIR and the system still produces the exact spline interpolant. In the following we extend this work by showing that even if $x(n)$ is a spline oversampled

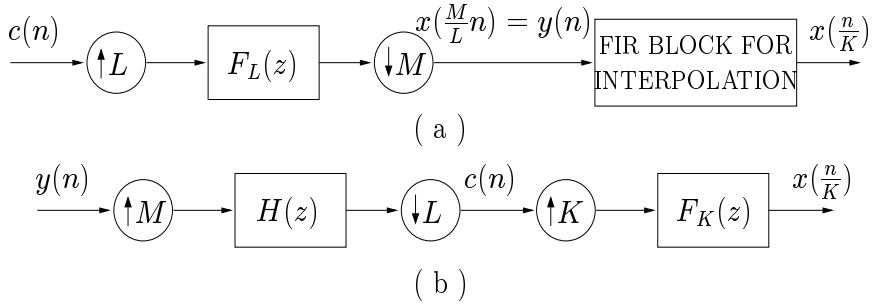

Figure 3.14: (a) Signal model and proposed interpolation. (b) Scheme for all-FIR interpolation.

by an arbitrarily small (rational) amount, the all-FIR interpolation is still possible.

3.4.2 FBPs in all-FIR interpolation of oversampled signals

Let $x(t)$ be a third-order spline given by the model (3.1). Consider the discrete-time signal $y(n) = x(\frac{M}{L}n)$ (for $L > M$) which is obtained by oversampling $x(t)$ by a factor of L/M. The signal $y(n)$ can be constructed as shown in the first half of Fig.3.14(a). Here $F_L(z)$ represents the z-transform of the sequence $\phi_L(n)$, which is obtained by sampling $\phi(t)$ L times more densely than at integers. Our task is to find an interpolation system as in Fig.3.14(a) consisting of FIR filters only, that produces the interpolated version $x(\frac{n}{K})$, for an arbitrary integer K. The interpolation by a rational amount K_1/K_2 can in principle be thought of as an interpolation by K_1 followed by a simple decimation by K_2. Also, note that the oversampled signal $y(n)$ as in Fig.3.14(a) actually gets interpolated by a total factor of MK/L.

Following the discussion from Section 3.2 we conclude that the driving sequence $c(n)$ can be recovered as shown in the first half of Fig.3.14(b), where $H(z)$ is an RFBP of $F_L(z)$ with respect to L/M. It is often possible to find FIR solutions for $H(z)$ as explained in Section 3.2.2. After this is achieved, the interpolation by K is performed as in the second half of Fig.3.14(b), where $F_K(z)$ corresponds to the K-fold oversampled cubic spline (see Fig.3.1). Summarizing, we have achieved an all-FIR spline interpolation, with only one requirement: that the input signal admits a slightly oversampled model. By making $L = M + 1$ and choosing M large enough, this required overhead in the input signal rate can be made insignificant.

In Fig.3.15 we present an example of all-FIR cubic spline interpolation. In this example we used $L = 6$ and $M = 5$. The smaller image is a portion of the *Parrots* image, oversampled by 6/5. In other words, this signal satisfies the model in Fig.3.14(a). It was obtained from the original image using the traditional cubic spline interpolation by a factor of 6/5. Employing the system shown in Fig.3.14(b) with the FIR reconstruction filter $H(z)$ and $K = 2$, this image is next interpolated by a total factor of $MK/L = 5/3$ and the result is also shown in Fig.3.13. We note that this is precisely the same result as the one obtained using recursive IIR filtering in traditional spline interpolation [59]. However, in this case we had to assume a certain signal model, which is not valid for an arbitrary signal. A possible remedy is to *approximate* the starting signal with a signal admitting the model and then proceed with the all-FIR interpolation. In the

Figure 3.15: FIR interpolation example: a region of the image oversampled by $L/M = 6/5$ and its cubic spline interpolation by a factor of $MK/L = 5/3$ obtained using FIR filters.

next section we formally define this approximation problem and derive the solution.

3.5 Least squares signal approximation

Consider the class $\mathcal{F}$ of discrete-time signals $y(n)$ which can be modeled as the output of the system shown in Fig.3.16(a). The signal model from Fig.3.16(a) appears in several different contexts; for example, see the left half of Fig.3.7(a) or the left half of Fig.3.14(a). Here, $c(n)$ is an arbitrary ℓ_2 sequence, and L and M are coprime integers satisfying $L > M$. The problem of least squares approximation is as follows. Given an arbitrary signal $x(n) \in \ell_2$, find a signal $y(n) \in \mathcal{F}$ such that the ℓ_2 distance between these two signals, namely

$$\sum_n |y(n) - x(n)|^2$$

is minimized. Obviously, this problem is the same as finding the optimal driving sequence $c(n)$. The reason for the restrictions on L and M is similar as before; if L and M have a common factor, say P, then the model reduces to a similar one with the expander and decimator ratios L/P and M/P, respectively, and $F(z)$ replaced by its zeroth polyphase component of order P. On the other hand if $L < M$, the class $\mathcal{F}$ almost always incorporates all ℓ_2 signals and the approximation problem becomes degenerate. Note that $y(n)$ is nothing but the *orthogonal projection* of $x(n)$ onto $\mathcal{F}$.

In order to solve the least squares problem, notice that the structure from Fig.3.16(a) can be equivalently redrawn as in Fig.3.16(b). Here $F_i(z)$ for $0 \leq i \leq M-1$ are the Type 1 polyphase components of order M of $F(z)$. Next, notice that the structure between $c(n)$ and the input to the filter $F_i(z)$ is nothing but a

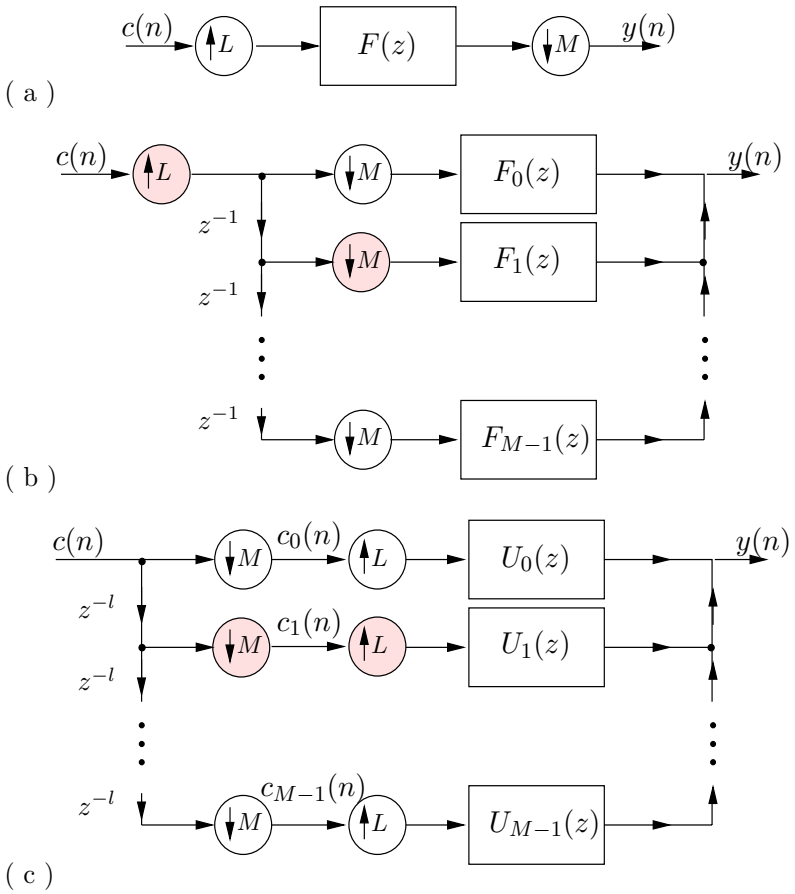

Figure 3.16: Least squares problem. (a) Signal model. (b)-(c) Equivalent drawing.

cascade of an expander by L, delay z^{-i} and a decimator by M. Using the identity shown in Fig.3.4(a), we can redraw Fig.3.16(b) as in Fig.3.16(c). We also used the fact that L and M are coprime, and integers l and m are chosen such that (3.5) is satisfied. Filters $U_i(z)$ are defined as

$$U_i(z) \triangleq z^{-im} \cdot F_i(z).$$

Now, notice that the subsequences $c_i(n)$ represent a complete partitioning of $c(n)$, i.e., $c(n)$ can be recovered from $c_i(n)$ using a generalized unblocking structure shown in the right part of Fig.3.18(a). This is a consequence of the fact that l and M are coprime as well. Therefore, the problem of finding the optimal driving sequence $c(n)$ in Fig.3.16(a) is equivalent to the problem of finding the optimal driving sequences $\{c_i(n)\}$ for $0 \leq i \leq M-1$ in Fig.3.16(c). This problem represents a special, uniform case of a more general multichannel, nonuniform least squares problem considered in [79]. Also, it can be viewed as a special case of the least squares problem considered in the MIMO biorthogonal partner setting (Chapter 2).

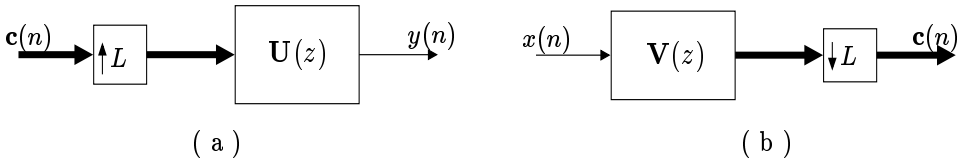

Figure 3.17: Least squares problem revisited in MIMO biorthogonal partner setting. (a) Signal model. (b) Least squares approximation.

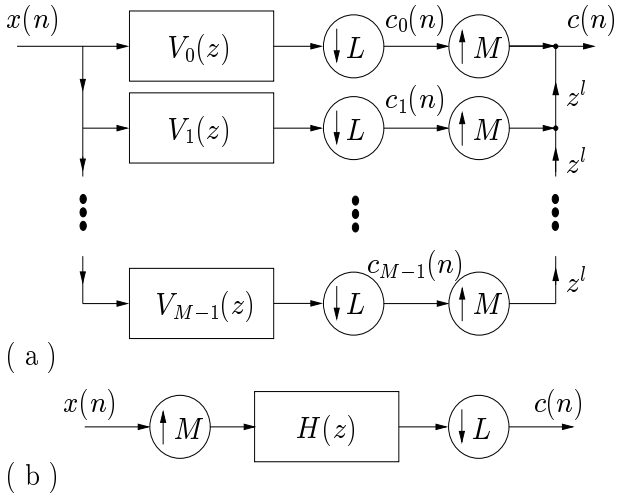

Figure 3.18: (a)-(b) Solution to the least squares problem.

Consider Fig.3.17(a), with the vector sequence $\mathbf{c}(n)$ and MISO filter $\mathbf{U}(z)$ defined by

$$\mathbf{c}(n) \triangleq [c_0(n) \;\; c_1(n) \;\; \cdots \;\; c_{M-1}(n)]^T$$
$$\mathbf{U}(z) \triangleq [U_0(z) \;\; U_1(z) \;\; \cdots \;\; U_{M-1}(z)].$$

It is easily seen that the signal model in Fig.3.17(a) corresponds to the one in Fig.3.16(c) and thus the one in Fig.3.16(a). According to the results in Section 2.5.1, the solution to the corresponding least squares approximation problem is unique and is given by the structure shown in Fig.3.17(b). The SIMO filter $\mathbf{V}(z)$ is defined by

$$\mathbf{V}(z) \triangleq [V_0(z) \;\; V_1(z) \;\; \cdots \;\; V_{M-1}(z)]^T,$$

and can be found as

$$\mathbf{V}(z) = \left([\widetilde{\mathbf{U}}(z) \cdot \mathbf{U}(z)]_{\downarrow L \uparrow L}\right)^{-1} \widetilde{\mathbf{U}}(z). \tag{3.14}$$

Note that two of the necessary conditions for the existence of the matrix inverse in (3.14) are $L \geq M$ and $\left[|F_i(e^{j\omega})|^2\right]_{\downarrow L} > 0$ for all ω and for $0 \leq i \leq M-1$. However, they are not sufficient. On the other hand, if the matrix in question is not of full rank, we can use the Moore-Penrose generalized inverse (pointwise in ω) instead and that would correspond to the least squares solution.

Representing the SIMO system $\mathbf{V}(z)$ in the form of a filter bank, we can redraw the solution from Fig.3.17(b) as in Fig.3.18(a), which also combines the optimal subsequences $\{c_i(n)\}$ back into the driving sequence $c(n)$. We can further simplify this system as shown in Fig.3.18(b), using a similar method as in Fig.3.16. Here, $H(z)$ is the optimum projection prefilter and is defined by

$$H(z) \stackrel{\triangle}{=} \sum_{i=0}^{M-1} z^{i(Mm+1)} \cdot V_i(z^M).$$

Summarizing, the solution to the least squares approximation problem defined by the signal model in Fig.3.16(a) is given by the structure in Fig.3.18(b). Note that $H(z)$ is a particular RFBP of $F(z)$ with respect to L/M, since the cascade of the systems from Fig.3.16(a) and Fig.3.18(b) is equal to the identity.

3.6 Vector signals

The problem of signal reconstruction discussed in Section 3.2 was originally posed for scalar signals. However, an analogous problem can be considered in the case of vector signals as well. Suppose that a $N \times 1$ vector signal $\mathbf{x}(t)$ admits the model

$$\mathbf{x}(t) = \sum_{k=-\infty}^{\infty} \mathbf{\Phi}(t-k)\mathbf{c}(k), \tag{3.15}$$

where $\mathbf{c}(k)$ is a $K \times 1$ vector driving sequence and $\mathbf{\Phi}(t)$ is a $N \times K$ matrix model function. We consider the discrete vector signal $\mathbf{y}(n)$ obtained by sampling $\mathbf{x}(t)$ at multiples of M/L. Thus we have $\mathbf{y}(n) = \mathbf{x}(nM/L)$ and the structure producing $\mathbf{y}(n)$ is shown on the left-hand side of Fig.3.19(a). Here, $\mathbf{F}(z)$ is a z-transform of the integer samples of a $N \times K$ matrix function $\mathbf{F}(t) \stackrel{\triangle}{=} \mathbf{\Phi}(t/L)$. The problem of vector signal reconstruction can now be solved using the structure on the right-hand side of Fig.3.19(a). The matrix transfer function $\mathbf{H}(z)$ for which the complete system shown in Fig.3.19(a) is the identity is called a right *vector* fractional biorthogonal partner (**RVFBP**) with respect to the ratio L/M. In this case we call $\mathbf{F}(z)$ a left *vector* fractional biorthogonal partner (**LVFBP**) with respect to L/M.

Similarly as before, we are usually concerned with the case when L and M are coprime, since otherwise we can reduce both the expander and decimator by a common factor. Using the equivalent reasoning as in the scalar case (Section 3.2), we conclude that the system from Fig.3.19(a) can be equivalently redrawn as in Fig.3.19(b), where the block polyphase matrices (for vector signals) $\mathbf{E}_v(z)$ and $\mathbf{R}_v(z)$ have a form similar to (3.7). The only difference is that the scalar polyphase components of filters $\{P_k(z)\}$ and $\{Q_k(z)\}$ are replaced by the $N \times K$ and $K \times N$ matrix polyphase components of the corresponding matrix filters $\{\mathbf{P}_k(z)\}$ and $\{\mathbf{Q}_k(z)\}$, defined similarly as in the scalar case (3.6). This discussion leads to the conditions for the existence of FIR or just stable RVFBPs, which are summarized in the following theorem.

Theorem 3.2. Given a $N \times K$ matrix transfer function $\mathbf{F}(z)$ and two coprime integers L and M, there exists a *stable* right vector fractional biorthogonal partner of $\mathbf{F}(z)$ if and only if $NL > KM$, and the minimum rank of $\mathbf{E}_v(e^{j\omega})$ [from Fig.3.19(b)] pointwise in ω is M. For an FIR matrix filter $\mathbf{F}(z)$ there exists

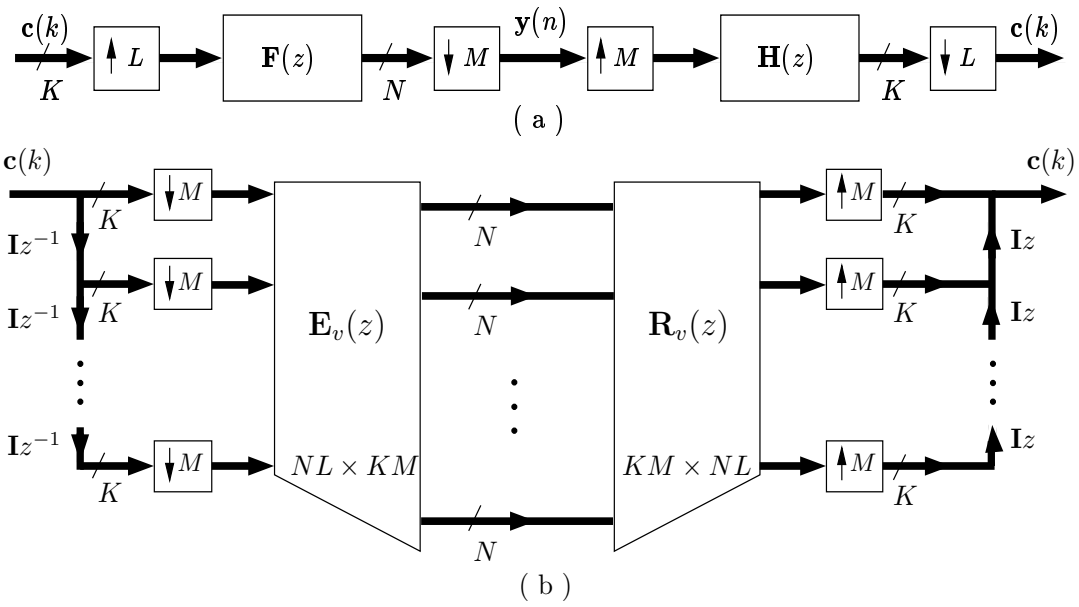

Figure 3.19: (a) Definition of vector FBPs. (b) Construction of vector FBPs.

an *FIR* right vector fractional biorthogonal partner if and only if $NL > KM$, and the greatest common divisor (GCD) of all the $KM \times KM$ minors of $\mathbf{E}_v(z)$ is a delay. Analogous results hold for left vector FBPs as well.

The proof of this theorem is completely equivalent to the proof of Theorem 3.1, and is therefore omitted. Notice that the necessary condition $L > M$ from the scalar case here gets modified into a more general condition $NL > KM$. Similar to the scalar case, we conclude that whenever FIR VFBPs exist they are not unique. However, the degrees of freedom that can be used in the construction of FIR VFBPs now depend on the difference $NL - KM$ rather than $L - M$.

In accordance with the discussion in Section 3.3.1, we can define the problem of *vector* channel equalization using fractionally oversampled MIMO FSEs, and this would correspond to the extension of the material from Chapter 2 to the FoFSE case. Again, the degrees of freedom in this FIR MIMO FoFSE optimization are a consequence of the fact that $NL > KM$.

The other two applications of FBPs, considered in Section 3.4 and Section 3.5 can also be extended easily to the case of vector signals. The interpolation of vector signals has the application whenever the task is to asses the values of some vector-valued process at the instances between consecutive measurements. Of course, in order for the theory of linear interpolation (described in Section 3.4 in the case of scalar signals) to be applicable, the unknown continuous-time vector process should be assumed to satisfy a model of the form similar to (3.15). As for the least squares signal approximation, problem formulation is the same regardless of the dimensionality of the signals, the extension is straightforward and a similar problem has already been treated in Section 2.5.1.

3.7 Concluding remarks

The original theory of biorthogonal partners in the scalar and the vector case was derived from the signal models with integral amount of oversampling. This chapter provides an extension of these results to the case when the oversampling amount is fractional. One of the main conclusions drawn here is that fractional biorthogonal partners always allow for additional flexibility in the design of FIR solutions. This design closely follows the corresponding procedure from Chapter 2. In fact, the design of ZFEs for noise reduction reduces to the problem treated in Section 2.4.2. One contribution of this chapter is that we have compared the performance of FoFSEs to that of more complicated MMSE solutions and shown that the degradation is not significant. Several other applications of fractional biorthogonal partners have also been considered, including all-FIR signal interpolation and least squares signal approximation. The theory of FBPs has been extended to the case of vector signals.

Chapter 4 Precoding in cyclic prefix-based communication systems

In this chapter we consider the digital communication systems with the equalization techniques based on *cyclic prefix*. The application of these techniques to high-speed data transmission over frequency-selective channels, such as twisted pair channels in telephone cables, has attracted considerable attention over the last fifteen years [5], [8]-[9], [27], [49]. Cyclic prefix systems are invariably used in conjunction with the discrete Fourier transform (DFT) matrices, and one example is the DFT-based discrete multitone modulation (DMT) system [9]. Although it has been shown by Kalet [27] that the use of the *ideal* transmit and receive filters in the multitone environment can lead to achieving signal-to-noise ratio (SNR) within 8-9 dB of the channel capacity (depending on the probability of error), in practice the DFT filter bank is most commonly used because of its low complexity. The development of cyclic prefix systems leads, for example, to asymmetric digital subscriber loops (ADSL) and high-speed digital subscriber loops (HDSL) [49], [9].

The initial goal of cyclic prefix based methods for equalization is to cancel the intersymbol interference (ISI) induced by the channel without inverting it. This task is achieved by introducing some redundancy in the form of a cyclic prefix (see Section 4.2). However, depending on the nulls of the channel in question, the noise can get severely amplified even in cyclic prefix based equalizers. In this chapter we consider a general cyclic prefix based system with the aim of further reducing the noise power at the receiver. This is achieved by performing the ISI cancellation and the noise suppression *separately*, in different modules. The main module for ISI cancellation is based on cyclic prefix with the DFT filter bank and is unchanged. It is preceded (followed) by the *optimal precoder* (*equalizer*) for the given input and noise statistics. These blocks are realized by constant matrix multiplications, so that the overall communication system remains of low complexity. We consider two different precoding schemes, which are developed based on two different optimization criteria. In the presence of white noise, both of these reduce to simple power allocation across different subbands of the channel (see Fig.1.11), however these allocation algorithms are different from the classical water-filling solution [27]. Portions of the material in this chapter have been presented at [82] and [68].

4.1 Chapter outline

The chapter begins with a brief overview of cyclic prefix systems with DFT matrices used for ISI cancellation (Section 4.2). Cyclic prefix methods introduced here can in fact be applied in a much broader, filter inversion setting, not necessarily related to digital communications. When it comes to data transmission, cyclic prefix

has traditionally been used after bit parsing, combined with optimal bit allocation resulting in different symbol constellations in different subbands [27], [49], [30]. However, in the setting of this chapter cyclic prefix is directly applied on the data stream. The main thrust of this chapter is towards a better understanding of the communication systems based on cyclic prefix. The authors of several different papers, including [27] and [30] have considered the problem of optimal transmitter and receiver design in this context using the information-theoretic criteria. Here, we consider the same problem from a signal processing point of view, deriving two different solutions, corresponding to the two slightly different sets of objectives.

In Section 4.3 we introduce one way of dealing with noise suppression separately and derive the optimal constrained pair precoder/equalizer for this purpose. The overall system is constrained to be ISI-free in the absence of noise and the precoder is chosen to minimize the noise power at the receiver. The performance of the proposed method is evaluated through computer simulations and a significant improvement over the original system without precoding is demonstrated.

A slightly modified method for optimal pre- and post-processing is presented in Section 4.4. The design procedure here aims at maximizing signal-to-noise ratio at the receiver, under the additional constraint that SNR should be *stationary*, i.e., not time-dependent. Ideally, this approach should also result in minimizing the probability of detection error under the ISI-free condition. Simulation results confirm a significant improvement in performance over the plain channel inversion method. Throughout this chapter we assume that the frequency-selective channel is a *known* FIR system of order L, i.e., it is given by

$$C(z) = \sum_{k=0}^{L} c(k) z^{-k}.$$

4.2 Cyclic prefix systems in digital communications

In this section we give a review of cyclic prefix based systems for channel equalization that employ DFT filter banks. Before deriving the complete communication system, we first introduce the concept of *cyclic prefix*. It presents a way of inserting redundancy into the input data stream which becomes useful in the process of channel equalization as will be explained later. Consider the symbol stream from Fig.4.1(a). It is divided into blocks of length M. The last L symbols from each block are copied and inserted at the beginning of that block (we assume hereafter that the block size M is greater than L). This is achieved by 'squeezing' the samples as explained in Fig.4.1(b)–(c). Obviously, this operation of inserting the redundancy into the input data stream results in bandwidth expansion. In this case the bandwidth expansion ratio is given by $\alpha = (M + L)/M$, which can be made sufficiently small by making M large. The purpose of cyclic prefix insertion is twofold: it allows the receiver to remove ISI using very simple operations, and it guarantees the stability of such equalization regardless of the channel.

As a first step in understanding how this is achieved, consider the system with cyclic prefix in Fig.4.2, ignoring the noise for the time being. The blocks labeled 'blocking' and 'unblocking' were explained in the

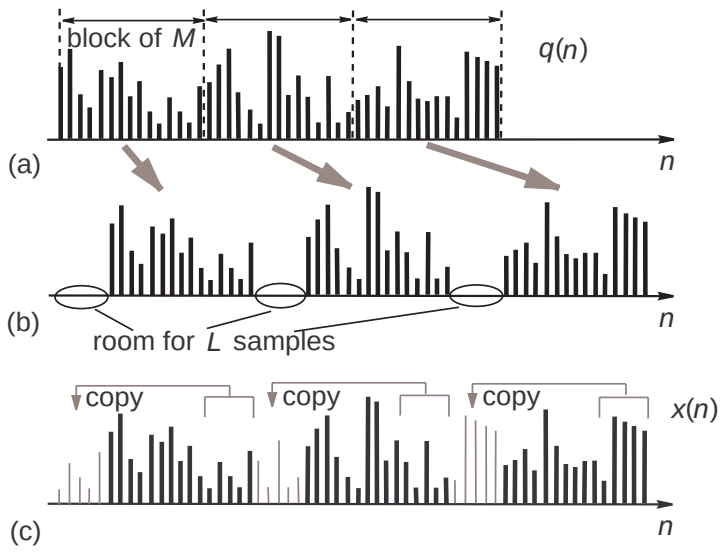

Figure 4.1: (a) Input symbol stream, (b)-(c) explanation of how cyclic prefix is inserted.

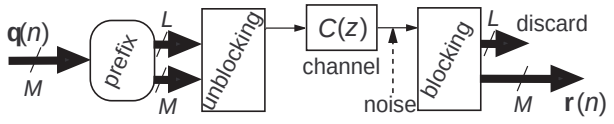

Figure 4.2: Channel with the system for cyclic prefix.

introductory section, while the block 'prefix' inserts a cyclic prefix as described in Fig.4.1. It can be shown that the blocked sequences $\mathbf{q}(n)$ and $\mathbf{r}(n)$ are related through a multiplication by the $M \times M$ *right circulant* [37] channel matrix $\mathbf{C}$. The first column of $\mathbf{C}$ consists of the $L+1$ channel coefficients $c(k)$ followed by $M-L-1$ zeros. for example, if $L=3$ and $M=6$,

$$\mathbf{C} = \begin{bmatrix} c(0) & 0 & 0 & c(3) & c(2) & c(1) \\ c(1) & c(0) & 0 & 0 & c(3) & c(2) \\ c(2) & c(1) & c(0) & 0 & 0 & c(3) \\ c(3) & c(2) & c(1) & c(0) & 0 & 0 \\ 0 & c(3) & c(2) & c(1) & c(0) & 0 \\ 0 & 0 & c(3) & c(2) & c(1) & c(0) \end{bmatrix}. \tag{4.1}$$

Since we can safely assume[1] $c(0) \neq 0$, it follows that $\mathbf{C}$ is nonsingular and the effect of the channel can be neutralized by inverting it. Next, we use the result that any circulant matrix can be *diagonalized* by a DFT matrix [37], in other words we have

$$\mathbf{C} = \mathbf{W}^{-1}\mathbf{\Gamma}_c\mathbf{W}, \tag{4.2}$$

[1]Otherwise we can shorten the impulse response of $C(z)$.

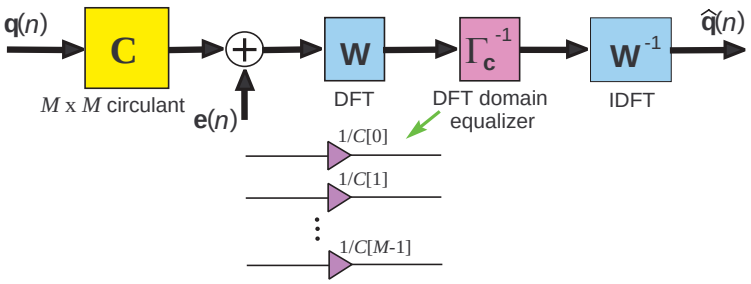

Figure 4.3: Cyclic prefix system with all processing at the receiver.

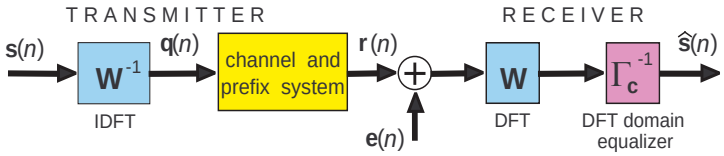

Figure 4.4: Conventional cyclic prefix system with DFT matrices used for ISI cancellation.

where $\mathbf{W}$ is the $M \times M$ DFT matrix and the diagonal matrix $\mathbf{\Gamma}_c$ has the eigenvalues of $\mathbf{C}$ on its diagonal. Those eigenvalues, in turn, are nothing but the M-point DFT coefficients of $c(k)$, thus we have

$$\mathbf{\Gamma}_c = \begin{bmatrix} C_M[0] & 0 & 0 & \dots & 0 \\ 0 & C_M[1] & 0 & \dots & 0 \\ \vdots & & \ddots & \vdots & \\ 0 & 0 & 0 & \dots & C_M[M-1] \end{bmatrix}, \tag{4.3}$$

with $C_M[n] = \sum_{k=0}^{L} c(k) e^{-j2\pi kn/M}$. As noted before, the ISI cancellation is achieved by inverting $\mathbf{C}$ in (4.2). Therefore, the ISI-free communication system is given in Fig.4.3. Notice that in this representation, all the computational complexity of the channel inversion is appointed to the receiver. It is possible to distribute some of this complexity to the transmitter side by noting in Fig.4.3 that $\mathbf{W}^{-1}$ is a square inverse of the matrix $\mathbf{\Gamma}_c^{-1}\mathbf{WC}$. This observation results in the conventional DFT-based cyclic prefix system, shown in Fig.4.4. The block labeled 'channel and prefix system' is given in Fig.4.2. Matrix $\mathbf{\Gamma}_c^{-1}$ is better known as the *frequency domain equalizer* and on its diagonal it contains the reciprocals of the DFT coefficients of the channel. The input vector sequence $\mathbf{s}(n)$ in Fig.4.4 is obtained by blocking the symbol stream into blocks of length M. The noise vector $\mathbf{e}(n)$ is obtained by blocking the discretized channel noise into blocks of length $M + L$ and then discarding L samples out of each block (see Fig.4.2).

The main merit of cyclic prefix systems with DFT matrices lies in their simplicity. From Fig.4.4 we see that the transmitter only needs to perform the inverse DFT operation followed by a cyclic prefix insertion. On the other hand, the receiver removes the cyclic prefix, performs the DFT operation and frequency domain equalization, which simply amounts to multiplying the signal in each channel by a constant (see Fig.4.3).

Moreover, if M is chosen as a power of two, both IDFT and DFT operations can be implemented using the fast radix-2 algorithm.

The noise vector process $\mathbf{e}(n)$ at the receiver passes through the DFT matrix $\mathbf{W}$ and the frequency domain equalizer $\mathbf{\Gamma}_c^{-1}$. Since $\mathbf{W}$ is a scaled unitary matrix, the main contribution to the noise power at the receiver comes from the multipliers $1/C_M[n]$ embedded in $\mathbf{\Gamma}_c^{-1}$. Obviously, if the channel $C(z)$ has zeros near the unit circle, these multipliers can get large, consequently boosting the noise at the receiver and degrading the system performance. In the next section we propose a simple modification of the basic equalization structure from Fig.4.4 that aims at improving the system performance.

4.3 Simple pre- and post-processing for noise suppression

4.3.1 Modified system design

Consider the system shown in Fig.4.5. It consists of the same basic cyclic prefix transceiver (the middle portion) surrounded by the constant matrices $\mathbf{T}^{-1}$ and $\mathbf{T}$. Notice that as for the signal part, this system is completely equivalent to the one from Section 4.2, i.e., the signal still goes through the identity system. Therefore, the only purpose of the *precoder* $\mathbf{T}^{-1}$ and the corresponding *equalizer* $\mathbf{T}$ is to reduce the noise power at the receiver output $\widehat{\mathbf{s}}(n)$. This is shown in Fig.4.6. It is clear that without any additional constraints this task can be trivially accomplished by scaling the matrix $\mathbf{T}$ by a very small constant; without changing the received signal, in this way we could arbitrarily reduce the received noise power. However, this would in turn arbitrarily increase the power of the transmitted signal $\mathbf{x}(n)$, which is of course unacceptable. The remedy, therefore, is to find the optimal precoder/equalizer pair *subject to* the constraint on the transmitted power, proportional to $E[\mathbf{x}^\dagger\mathbf{x}]$. This power constraint is more conveniently rewritten as

$$\mathrm{Tr}\{E[\mathbf{x}\mathbf{x}^\dagger]\} = \mathrm{Tr}\{\mathbf{T}^{-1}\mathcal{R}_{ss}(\mathbf{T}^{-1})^\dagger\} \leq P_x, \tag{4.4}$$

where $\mathcal{R}_{ss}$ denotes the autocorrelation matrix of the input vector process $\mathbf{s}(n)$. Quantity P_x denotes the maximum power in the transmitted signal $\mathbf{x}(n)$. Throughout this chapter we make the assumption that the input symbols are independent, identically distributed, coming from a predefined constellation. Therefore, the autocorrelation matrix becomes $\mathcal{R}_{ss} = P_s\mathbf{I}_M$, where P_s is the power in the input symbol stream. Thus, if the transmitted power needs to be unchanged after employing the precoder, the power constraint becomes

$$\mathrm{Tr}\{\mathbf{T}^{-1}(\mathbf{T}^{-1})^\dagger\} = \mathrm{Tr}\{(\mathbf{T}^{-1})^\dagger\mathbf{T}^{-1}\} = 1, \tag{4.5}$$

using the identity $\mathrm{Tr}\{\mathbf{AB}\} = \mathrm{Tr}\{\mathbf{BA}\}$, for $\mathbf{A}, \mathbf{B}$ square.

According to the *polar decomposition theorem* [24] an arbitrary square matrix $\mathbf{T}$ can be written as a product $\mathbf{T} = \mathbf{UP}$, where $\mathbf{U}$ is unitary and $\mathbf{P}$ a positive semidefinite matrix (in our case, since $\mathbf{T}$ is obviously

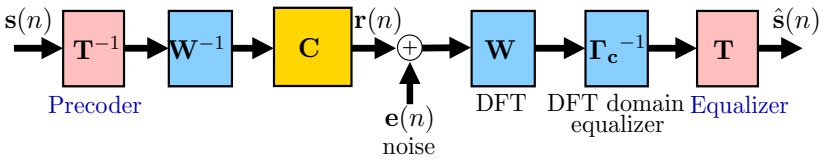

Figure 4.5: Cyclic prefix system with separated ISI cancellation and noise suppression. First method.

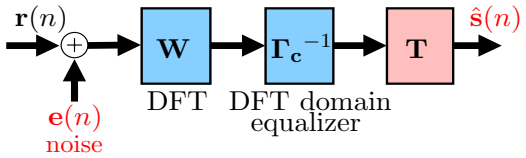

Figure 4.6: Receiver and the noise model.

desired to be nonsingular, $\mathbf{P}$ is positive definite). Therefore, the power constraint (4.5) becomes

$$\mathrm{Tr}\{\mathbf{U}^\dagger\mathbf{U}(\mathbf{P}^{-1})^\dagger\mathbf{P}^{-1}\} = \mathrm{Tr}\{\mathbf{P}^{-2}\} = 1. \tag{4.6}$$

Our objective as mentioned before is to minimize the output noise power (subject to the power constraint). This can be written as

$$\begin{aligned} &\min_{\mathbf{T}} \mathrm{Tr}\{\mathbf{T}\boldsymbol{\Gamma}_c^{-1}\mathbf{W}\mathcal{R}_{ee}\mathbf{W}^\dagger(\boldsymbol{\Gamma}_c^{-1})^\dagger\mathbf{T}^\dagger\}, \quad \text{that is} \\ &\min_{\mathbf{P}} \mathrm{Tr}\{\mathbf{P}^\dagger\mathbf{P}\mathbf{Q}\}, \quad \text{with} \quad \mathbf{Q} \stackrel{\triangle}{=} \boldsymbol{\Gamma}_c^{-1}\mathbf{W}\mathcal{R}_{ee}\mathbf{W}^\dagger(\boldsymbol{\Gamma}_c^{-1})^\dagger. \end{aligned} \tag{4.7}$$

Notice that neither the objective (4.7) nor the constraint (4.6) depend on the choice of the unitary matrix $\mathbf{U}$. This leads us to conclude that without loss of generality we can choose $\mathbf{U} = \mathbf{I}_M$, or $\mathbf{T} = \mathbf{P}$. Furthermore, it follows that we can achieve nothing in terms of noise suppression if $\mathbf{T}$ itself is unitary (this can also be concluded directly from Fig.4.5).

In order to solve this problem of *nonlinear optimization*, namely, minimizing (4.7) subject to (4.6), it is useful to consider the unitary diagonalization of the positive definite matrices

$$\mathbf{P} = \mathbf{U}_p\boldsymbol{\Lambda}_p\mathbf{U}_p^\dagger, \quad \text{and} \quad \mathbf{Q} = \mathbf{U}_q\boldsymbol{\Lambda}_q\mathbf{U}_q^\dagger. \tag{4.8}$$

Namely, in (4.8) $\mathbf{U}_p$ and $\mathbf{U}_q$ are unitary, while $\boldsymbol{\Lambda}_p$ and $\boldsymbol{\Lambda}_q$ are diagonal. Defining another unitary matrix

$$\mathbf{V} \stackrel{\triangle}{=} \mathbf{U}_q^\dagger\mathbf{U}_p, \tag{4.9}$$

the objective function (4.7) can be written as

$$\min_{\mathbf{V},\mathbf{\Lambda}_p} \mathrm{Tr}\{\mathbf{V}^\dagger \mathbf{\Lambda}_q \mathbf{V} \mathbf{\Lambda}_p^2\}. \tag{4.10}$$

Notice that the matrices $\mathbf{V}$ and $\mathbf{\Lambda}_p$ are arbitrary, subject to being unitary and diagonal positive definite, respectively. More importantly, optimal $\mathbf{\Lambda}_p$ can be chosen independently of optimal $\mathbf{V}$. Let us define

$$\mathbf{A} \stackrel{\triangle}{=} \mathbf{V}^\dagger \mathbf{\Lambda}_q \mathbf{V}, \quad \text{with} \quad \mathrm{diag}(\mathbf{A}) = [a_1, a_2, \cdots, a_M]^T \stackrel{\triangle}{=} \mathbf{a}, \tag{4.11}$$

$$\mathrm{diag}(\mathbf{\Lambda}_p) = [\lambda_{p,1}, \lambda_{p,2}, \cdots, \lambda_{p,M}]^T \stackrel{\triangle}{=} \boldsymbol{\lambda}_p, \quad \text{and} \quad \mathrm{diag}(\mathbf{\Lambda}_q) = [\lambda_{q,1}, \lambda_{q,2}, \cdots, \lambda_{q,M}]^T \stackrel{\triangle}{=} \boldsymbol{\lambda}_q. \tag{4.12}$$

When considered as a function of $\{\lambda_{p,i}\}$, the minimization problem becomes

$$\min_{\lambda_{p,i}} \sum_{i=1}^{M} a_i \lambda_{p,i}^2, \quad \text{s.t.} \quad \sum_{i=1}^{M} \lambda_{p,i}^{-2} = 1. \tag{4.13}$$

The problem is conveniently reduced to scalar optimization which can be readily solved using the method of Lagrange multipliers. The optimal solution for $\{\lambda_{p,i}\}$ as a function of the diagonal elements of $\mathbf{A}$ is given by

$$\lambda_{p,i}^{(opt)} = \left(\frac{\sqrt{a_i}}{\sum_{i=1}^{M} \sqrt{a_i}} \right)^{-1/2}. \tag{4.14}$$

The next step is to find the optimal set of diagonal elements of $\mathbf{A}$, namely, $\{a_i\}$ that minimize the objective (4.13). After substituting the solution for $\{\lambda_{p,i}\}$, the problem becomes

$$\min_{a_i} \left[\sum_{i=1}^{M} a_i + \sum_{i \neq j} \sqrt{a_i a_j} \right]. \tag{4.15}$$

Notice from (4.11) that

$$\sum_{i=1}^{M} a_i = \mathrm{Tr}\{\mathbf{\Lambda}_q\} = \text{const.} \tag{4.16}$$

since $\mathbf{Q}$ is fixed, so that the objective given by (4.15) becomes that of minimizing

$$f(\mathbf{a}) \stackrel{\triangle}{=} \sum_{i \neq j} \sqrt{a_i a_j}, \tag{4.17}$$

with the vector $\mathbf{a}$ defined in (4.11). It is important here to notice that $f(\cdot)$ is a *concave* function of $\mathbf{a}$ (see Fig.4.7), since it is a positive linear combination of concave functions of the form $\sqrt{a_i a_j}$. If we denote by

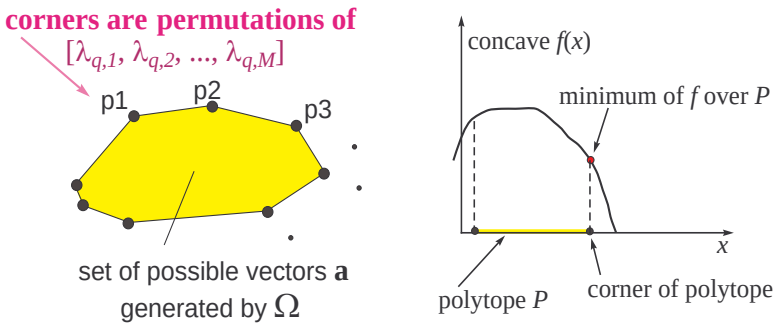

Figure 4.7: Convex polytope defined by the doubly stochastic matrix $\mathbf{\Omega}$ (left), and concave function $f(\cdot)$ defined over this polytope (right).

$v_{i,j}$ the (i,j)th element of $\mathbf{V}$ defined previously, then from (4.11) we have

$$a_i = \sum_{k=1}^{M} |v_{k,i}|^2 \lambda_{q,k},$$

or in other words

$$\mathbf{a} = \mathbf{\Omega} \cdot \boldsymbol{\lambda}_q. \tag{4.18}$$

Here $\mathbf{\Omega}$ is a square *doubly stochastic* matrix [24], given by

$$\mathbf{\Omega} = \begin{bmatrix} |v_{1,1}|^2 & |v_{2,1}|^2 & \cdots & |v_{M,1}|^2 \\ |v_{1,2}|^2 & |v_{2,2}|^2 & \cdots & |v_{M,2}|^2 \\ \vdots & \vdots & \vdots & \vdots \\ |v_{1,M}|^2 & |v_{2,M}|^2 & \cdots & |v_{M,M}|^2 \end{bmatrix}. \tag{4.19}$$

It has been shown in [62] that under these conditions (4.18) defines a *convex polytope* in the first quadrant of the real M-dimensional vector space. This is shown in Fig.4.7. The corners of that polytope are given by the permutations of the vector $\boldsymbol{\lambda}_q$ and are denoted by p_i in Fig.4.7. Since $f(\cdot)$ is a concave function defined over a convex polytope its absolute minimum is reached at one of these corners [see Fig.4.7(right) for a simplified argument]. That is to say, the optimal matrix $\mathbf{V}$ is a *permutation matrix*. But from the form (4.17) of the objective function $f(\mathbf{a})$ we conclude that without loss of generality we can take $\mathbf{V} = \mathbf{I}_M$. Summarizing, we have shown the following.

Theorem 4.1. Optimal precoder/equalizer (method 1). Consider the system for digital communications shown in Fig.4.5. The optimal precoder/equalizer matrix $\mathbf{T}$ in the sense of minimizing the output noise power for the fixed transmitted power constrained as in (4.4) is given by $\mathbf{T} = \mathbf{U}_q \mathbf{\Lambda}_p \mathbf{U}_q^\dagger$. Unitary matrix

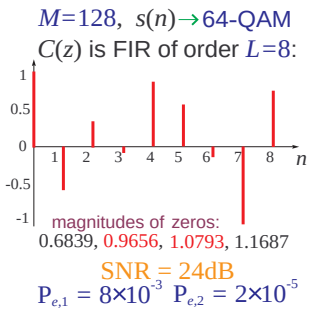

Figure 4.8: Summary of the parameters used: channel impulse response, zero magnitudes, SNR, probabilities of error.

$\mathbf{U}_q$ is obtained as in (4.8), given the definition of $\mathbf{Q}$ in (4.7). The diagonal elements of $\mathbf{\Lambda}_p$ are given by

$$\lambda_{p,i}^{(opt)} = \left(\frac{\sqrt{\lambda_{q,i}}}{\sum_{i=1}^{M} \sqrt{\lambda_{q,i}}} \right)^{-1/2}. \tag{4.20}$$

In other words, the optimal precoder $\mathbf{T}^{-1}$ determined in Theorem 4.1 simply performs the power allocation according to (4.20) but on a *modified* signal that is essentially projected into the equivalent noise subspace (operation defined by the unitary transform $\mathbf{U}_q$). As a special case, if the noise is white, $\mathbf{Q}$ in (4.7) becomes diagonal. Then $\mathbf{U}_q = \mathbf{I}$ and the precoder $\mathbf{T}^{-1}$ allocates the power to $\mathbf{s}(n)$ divided in M subbands according to the following allocation rule

$$\text{diag}\,[t_1, \quad t_2, \quad \cdots, \quad t_M] \stackrel{\triangle}{=} \mathbf{T}^{-1}, \quad \text{with} \quad t_i \propto \frac{1}{\sqrt{|C_M[i]|}}. \tag{4.21}$$

Interestingly, (4.21) is *opposite* in nature to the well-known water-filling allocation algorithm [27] which maximizes the channel throughput.

4.3.2 Experimental results

We now consider a simulation example designed to compare the equalization in the traditional cyclic prefix system (without $\mathbf{T}$) versus the modified system with optimal precoder for noise suppression. The parameters used in the experiment are summarized in Fig.4.8. The channel was real, of order 8, so there are four pairs of conjugate zeros, with magnitudes as in Fig.4.8. We see that four of these complex zeros are very close to the unit circle. As a consequence, several DFT coefficients of $C_M[n]$ are very low in magnitude, so that the frequency domain equalizer at those frequencies amplifies the noise severely. This resulted in very high probabilities of error at signal-to-noise ratios that are moderate to high, when the traditional cyclic prefix system is used. This can be seen in Fig.4.10. The quantity M was chosen to be 128, so that the FFT algorithm can be used. The input signal was drawn from the 64-QAM constellation. The signal-to-noise ratio used in the experiments was calculated at the input of the receiver (see Fig.4.5).

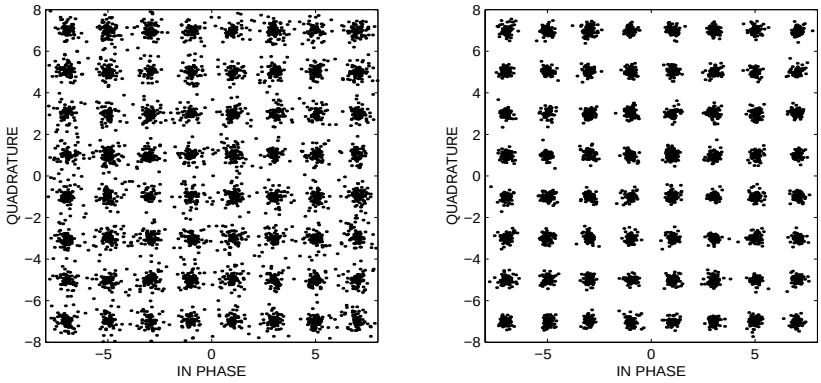

Figure 4.9: Equalization results using a modified system without (left), and with the optimal precoder/equalizer (right).

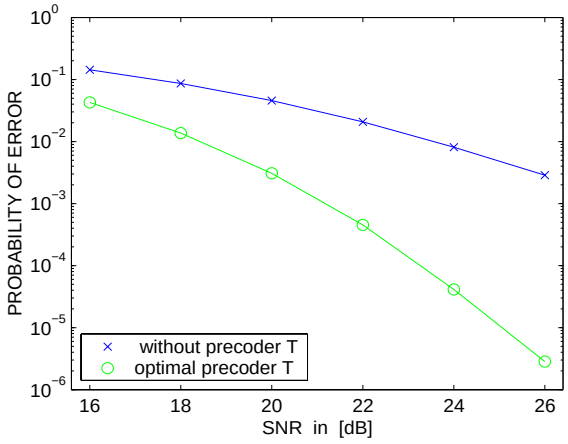

Figure 4.10: Probability of error vs. SNR: without precoder (dashed line) and with precoder (solid line).

In Fig.4.9 we show the scatter plots resulting from the channel equalization using the traditional system without precoding (left) and the modified system with optimal precoding (right). The plots are obtained at the signal-to-noise ratio of 24 dB. The average probability of error corresponding to the traditional system is slightly more than 8×10^{-3}, while the error probability in the system with precoder is less than 2×10^{-5}. In Fig.4.10 we show the average symbol error probability as a function of signal-to-noise ratio for the two systems (traditional and with pre- and post-processing). From this example we see that the improvement in performance resulting from optimal precoding can be significant (more than 6-8 dB).

4.4 Precoder design: alternative approach

In the following we consider an alternative approach to designing the optimal precoder/equalizer pair. It is different from the one presented in Section 4.3.1 in that the objective is to maximize SNR at the receiver (which is equivalent to minimizing the noise power) under the additional constraint that the noise variance

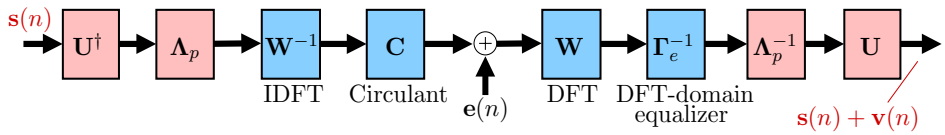

Figure 4.11: Cyclic prefix system with separated ISI cancellation and noise suppression. Second method.

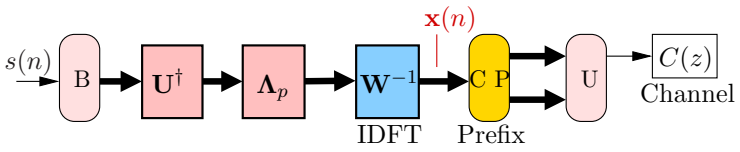

Figure 4.12: Channel input power constraint.

at the receiver should be *constant*, i.e., time-invariant. To see how this is achieved, consider the system in Fig.4.11. The basic cyclic prefix system from Section 4.2 is now preceded by two matrices: a unitary matrix $\mathbf{U}^\dagger$ and a diagonal matrix $\mathbf{\Lambda}_p$. The effect of these two matrices on the signal $\mathbf{s}(n)$ is neutralized by placing their inverses at the receiver; therefore the ISI-free condition is still satisfied.

Let us first study the purpose of a unitary matrix $\mathbf{U}$ at the receiver. If the noise $e(n)$ is wide-sense stationary (WSS) its autocorrelation matrix $\mathcal{R}_{ee}$ is Toeplitz in structure [61]. However, the autocorrelation of the noise component at the receiver, namely, $\mathbf{v}(n)$, is given by

$$\mathcal{R}_{vv} = \mathbf{U} \underbrace{\mathbf{\Lambda}_p^{-1}\mathbf{\Gamma}_c^{-1}\mathbf{W}\mathcal{R}_{ee}\mathbf{W}^\dagger\mathbf{\Gamma}_c^{-\dagger}\mathbf{\Lambda}_p^{-\dagger}}_{\mathbf{Z}}\mathbf{U}^\dagger. \tag{4.22}$$

In the absence of the correction matrix $\mathbf{U}$, we have $\mathcal{R}_{vv} = \mathbf{Z}$. Notice that $\mathbf{Z}$ is in general *not Toeplitz*. Indeed, even if the noise is white, the diagonal elements of $\mathbf{Z}$ are scaled by the channel magnitude responses and by the premultipliers in $\mathbf{\Lambda}_p$, so in general they are *not equal*. This implies that the unblocked noise $v(n)$ cannot be stationary, since its variance is a periodically time-varying signal. It is the purpose of $\mathbf{U}$ to compensate for this effect. Namely, given any positive definite $\mathbf{Z}$, there exists a unitary $\mathbf{U}$, such that $\mathbf{U}\mathbf{Z}\mathbf{U}^\dagger$ has *identical diagonal elements*. The algorithm for finding such $\mathbf{U}$ can be found in [35]. Returning to the special case of white noise, note that $\mathbf{Z}_{\text{wn}}$ is diagonal. Recalling the property of circulant matrices (4.2) we see that it suffices to take $\mathbf{U} = \mathbf{W}^{-1}$, since $\mathbf{U}\mathbf{Z}_{\text{wn}}\mathbf{U}^\dagger$ then becomes circulant and in particular its diagonal elements are equal, resulting in a constant variance of $v(n)$.

Having chosen $\mathbf{U}$, we proceed to find the optimal $\mathbf{\Lambda}_p$, which results in the maximum SNR for a fixed transmitted power. To determine the input power to the channel, we show the transmitter part in greater detail in Fig.4.12. If the cyclic block length M is assumed to be very large compared to the channel order L, we can make the approximation that the channel input power equals the power in signal $\mathbf{x}(n)$ (see Fig.4.12).

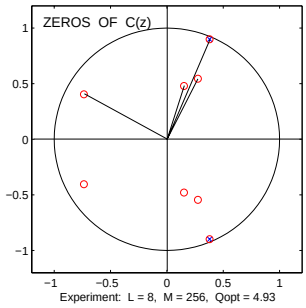

Figure 4.13: Summary of the parameters used: channel zero plot, M, improvement factor.

Therefore, recalling that $\mathcal{R}_{ss}$ is equal to a scaled identity, the channel input power becomes

$$P_{channel} \approx \frac{\sigma_s^2}{M}\mathrm{Tr}\{\mathbf{W}^{-1}\mathbf{\Lambda}_p\mathbf{\Lambda}_p^\dagger\mathbf{W}^{-\dagger}\} = \frac{\sigma_s^2}{M^2}\sum_{i=1}^{M}|p_i|^2, \tag{4.23}$$

where σ_s^2 is the signal variance and p_i are the diagonal elements of $\mathbf{\Lambda}_p$.

As for the SNR at the receiver, notice that the variance of the noise component $\mathbf{v}(n)$ can be written as

$$\sigma_v^2 = \frac{1}{M}\mathrm{Tr}\{\mathcal{R}_{vv}\} = \frac{1}{M}\mathrm{Tr}\{\mathbf{\Lambda}\mathbf{W}\mathcal{R}_{ee}\mathbf{W}^\dagger\} = \frac{1}{M}\sum_{i=1}^{M}\lambda_i d_i^2, \quad \text{where} \tag{4.24}$$

$$\mathbf{\Lambda} = \mathrm{diag}\,[\lambda_1,\ \ \lambda_2,\ \ \cdots,\ \ \lambda_M]\,,\ \ \lambda_i \triangleq \frac{1}{|C[i]p_i|^2},\ \ \text{and}\ \ d_i^2 = \left[\mathbf{W}\mathcal{R}_{ee}\mathbf{W}^\dagger\right]_{ii}. \tag{4.25}$$

Therefore, the constrained SNR maximization problem becomes

$$\max_{p_i}\left[\mathrm{SNR} = \frac{\sigma_s^2}{\frac{1}{M}\sum_{i=1}^{M} d_i^2/|C[i]p_i|^2}\right],\ \ \text{s.t.}\ \ \sum_{i=1}^{M}|p_i|^2 = M^2. \tag{4.26}$$

Using the method of Lagrange multipliers, the optimal power allocation coefficients are evaluated as

$$p_i = M\sqrt{|d_i/C[i]|}/\left(\sum_{k=1}^{M}|d_k/C[k]|\right)^{1/2}, \tag{4.27}$$

which is again inversely proportional to the square root of the channel magnitude response in the appropriate subband (see Fig.1.11). For a more detailed treatment of this optimization problem, with insightful discussion about the performance improvement resulting from the use of a precoder, the reader is referred to [68].

4.4.1 Experimental results

In computer simulations we compare the performance of two equalization methods: (a) plain channel inverse given by $1/C(z)$ and (b) method based on cyclic prefix with the optimal precoding as in Fig.4.11. The channel was of order 8 and all its zeros are inside the unit circle (channel zero plot is given in Fig.4.13).

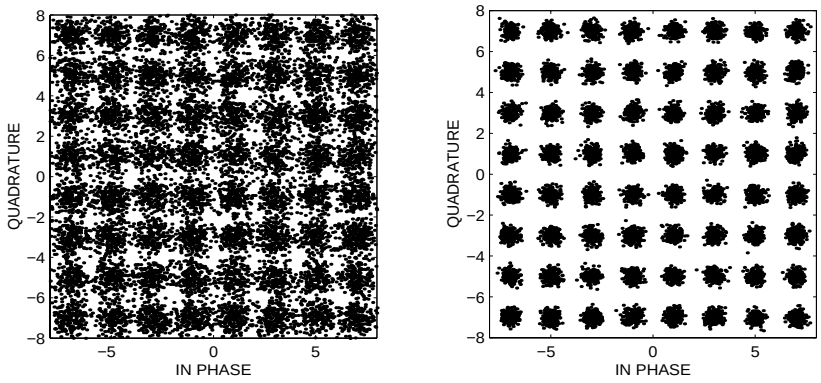

Figure 4.14: Equalization results using the channel inverse (left), and an optimal precoder/equalizer (right).

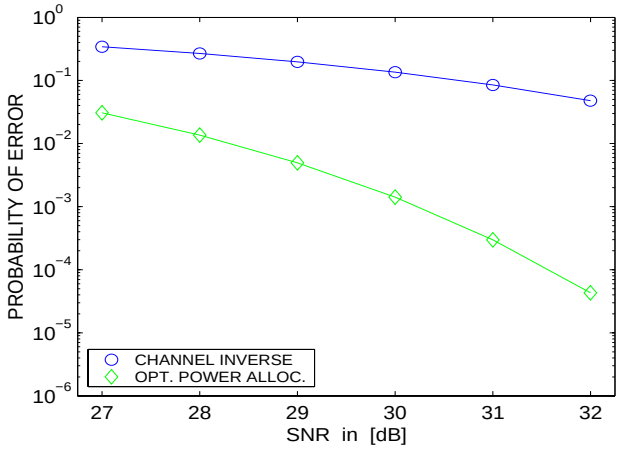

Figure 4.15: Probability of error vs. SNR using the two methods.

For this reason, the simple channel inverse is a stable equalizer and its performance should be comparable to that of a cyclic prefix system without precoding. However, a pair of conjugate zeros of $C(z)$ is very close to the unit circle (radius = 0.9755) and therefore the inverse $1/C(z)$ performs poorly in the presence of noise. The noise was assumed correlated with $\rho(k) = \sigma_e^2(0.3)^{|k|}$ and $M = 256$ was chosen. The scatter diagrams comparing the performance of the two equalizers (at SNR = 33 dB) are given in Fig.4.14 and the corresponding diagram relating the probabilities of error to the SNRs used is shown in Fig.4.15. In another experiment, we used p_i = const. for all i and compared the two performances as in Fig.4.14. The (non-optimized) cyclic prefix system and the channel inverse performed practically the same, indicating that nearly all the improvement comes as a result of optimizing p_i. However, note that the advantage of the cyclic prefix based method would be much more pronounced if $C(z)$ was not minimum phase.

4.5 Concluding remarks

We have considered cyclic prefix based systems with DFT matrices, commonly used in several equalization methods, such as the DFT-based DMT. Our approach was to treat the problem of noise suppression separately from the ISI cancellation and implement it in a separate module. With this in mind we have constructed two optimal constant (precoder, equalizer) pairs for noise reduction based on two sets of constraints. Both designs were constrained on the transmitted power and the requirement that there is no ISI in the absence of noise. In addition to that, the design procedure in Section 4.4 guarantees the constant SNR at the detection.

A more general precoder design would involve matrices with memory and/or substitute the restraint on the ISI-free solution by the minimum mean-squared error objective. A similar approach was taken in [91], although the authors there do not consider a cyclic prefix system, and unfortunately the solution in that case involves ideal (unrealizable) filtering. Another generalization of our approach would involve a *tall* instead of a square matrix precoder, and thus allow for some additional redundancy in the system. Moreover, a similar approach could be applied to modified DFT-based systems and generalized perfect DMT systems [30].

Finally, note that we referred to (4.20) and (4.27) as *power allocation strategies* that proved optimal in the two scenarios. However, a careful observation reveals that the actual task of the optimal precoder is simply to undo the effect of the equalizer part (for example, $\mathbf{T}$ in Section 4.3) on the signal. Consequently, it is the *equalizer*, i.e., the inverse of the precoder, that really affects the performance of the system. Thus it is not surprising that the water-filling *precoder* is not the optimal solution under these circumstances. Indeed, the optimal strategy is to allocate as much signal power in the frequency bands where the channel magnitude is *low*. This ensures that the noise amplification on the equalizer side is not severe in these regions, since large values of $1/|C_M[i]|$ in $\mathbf{\Gamma}_c^{-1}$ are compensated for by the small values of p_i^{-1} in $\mathbf{\Lambda}_p^{-1}$.

Chapter 5 Equalization with oversampling in multiuser communications

The area of multiuser communications has become increasingly important during the last decade as a result of a rapid expansion present in the wireless industry. Consequently, the ongoing research in many related fields, such as coding and information theory, communications, electromagnetics, etc., continues to attract attention. In this chapter we consider some important problems present in multiuser communications, however from the multirate signal processing perspective. Our focus is on the better understanding of these issues in terms of basic signal processing concepts. We then resort to standard multirate DSP techniques in solving these problems or proposing improvements to already existing solutions.

As opposed to single-user communication systems like the ones considered in the previous chapters, the performance of the new generation wireless systems is limited by *two* distinct effects: multiuser interference (**MUI**) and intersymbol interference (ISI). As a result, the receiver in multiuser systems first focuses on *extracting* the signal from a desired user out of a received combination of (interfering) signals. This process is called MUI cancellation or suppression. After that the aim is to mitigate the ISI effects present in the extracted signal and this is achieved by one of the numerous equalization techniques, some of which have been treated in the previous chapters.

The interference from other users (MUI) has traditionally been combated by orthogonal spreading codes at the transmitter [71]; however, this orthogonality is often destroyed after the transmitted signals have passed through the multipath channels. Furthermore, in the multichannel uplink scenario, exact multiuser equalization is possible only under certain conditions on the channel matrices [58]. The alternative approach is to suppress MUI statistically, however this is often less desirable.

In this chapter we concentrate on a recently developed method for MUI elimination called a mutually-orthogonal usercode-receiver (AMOUR), which has been introduced by Giannakis *et al.* [21], [86]. This approach aims at eliminating MUI deterministically and at the same time mitigating the undesired effects of multipath propagation for each user separately. One clear advantage of this over the previously known methods is that MUI elimination is achieved *irrespective of the channel nulls*. Moreover, ISI cancellation can be achieved using one of the previously known methods for *blind* channel equalization [21]. In summary, AMOUR can be used for deterministic MUI elimination and fading mitigation regardless of the (possibly unknown) multipath uplink channels.

In the following we consider an improvement of the basic AMOUR-CDMA system achieved by signal *oversampling* at the receiver. This equalizer structure can be considered as a *fractionally spaced equalizer* (FSE), similar to the ones treated in the previous chapters, and thus the name Fractionally Spaced AMOUR

(**FSAMOUR**). We consider two separate cases: integral and rational oversampling ratios. As mentioned previously in Chapters 2 and 3, the advantages of FSEs over the conventional symbol spaced equalizers (SSE) are lower sensitivity to the synchronization issues and freedom in the design of zero-forcing equalizers (ZFE). We will see that this freedom translates to better performance of FSAMOUR ZFEs.

An additional improvement of multiuser communication systems is achieved by exploiting the fact that zero-forcing channel equalizers in the multiuser setting are typically not unique. This *non-uniqueness* allows us to design ZFEs that also combat the noise at the receiver. While this observation is true in general for both AMOUR and FSAMOUR systems, shortly we will see that the improvement is more pronounced in the latter case. The content of this chapter is closely related to the material presented in [75].

5.1 Chapter outline

In Section 5.2 we provide an overview of AMOUR-CDMA systems. While the content of this section is mainly drawn from the original work by Giannakis *et al.* [20], [21], our approach to the system derivation is slightly different from the one usually encountered in literature and leads to notable simplifications, which prove useful in the derivation of FSEs in the subsequent sections. We should note that the multiuser system considered here assumes that all users are synchronized and they communicate at the same rate. In [86] this basic idea was extended to the case when different users communicate at different rates, and the synchronization issue was treated in [21]. In the remaining sections, we consider the possible improvements of the original AMOUR system obtained by oversampling the received signal, as well as the receiver optimization. The material in Sections 5.3 and 5.4 represents the original contribution of this chapter.

In Section 5.3 we design the FSAMOUR system with integral amount of oversampling. The system retains all the desired properties of conventional AMOUR and provides additional freedom in the design of ZF solutions, which corresponds to finding left inverses of tall matrices with excess rows. This freedom is further exploited and the corresponding improvement in performance over AMOUR systems is reported in the subsection with the experimental results.

In Section 5.4 we generalize the notion of FSAMOUR to the case of *fractional* oversampling at the receiver. If the amount of oversampling is given by $(M+1)/M$ for a large integer M the computational overhead in terms of the increased data rate at the receiver becomes negligible. Experimental results in Section 5.4.5 confirm that the improvements in the equalizer performance can be significant even if the oversampling is by just 6/5, i.e., only 20%.

5.2 AMOUR-CDMA systems

The structure in Fig.5.1 describes an AMOUR-CDMA system for M users, i.e., M transmitters and M potential receivers. The upper part of the figure shows the mth transmitter followed by the uplink channel corresponding to the mth user and the lower part shows the receiver tuned to the user m. The symbol

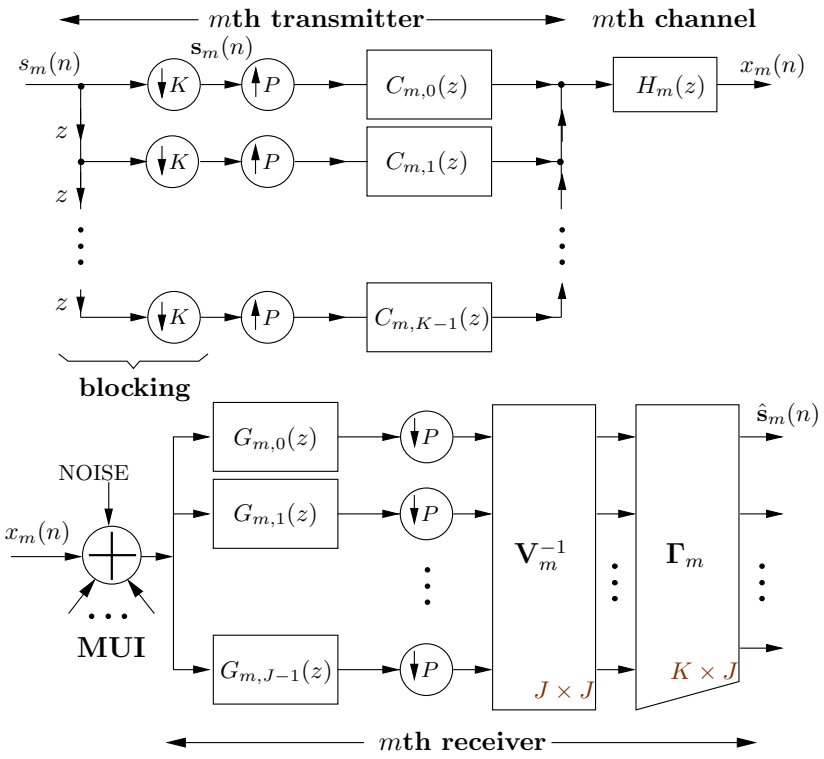

Figure 5.1: Discrete-time equivalent of a baseband AMOUR system.

stream $s_m(n)$ is first blocked into a vector signal $\mathbf{s}_m(n)$ of length K. This signal is upsampled by $P > K$ and passed through a synthesis filterbank $\{C_{m,k}(z)\}_{k=0}^{K-1}$. These filters are called the *spreading codes* for user m and are assumed to be FIR of length P. Moreover, the last L samples of each spreading code are set to zero, where L is the order of the channel $H_m(z)$. This constraint is introduced to eliminate the inter-block interference (IBI), a point that will be clear shortly.

A careful observation of Fig.5.1 reveals that each of the users introduces the *redundancy* in the amount of P/K. In other words, the symbol rate of $x_m(n)$ at the entrance to the mth receiver is by P/K higher than the rate of the information sequence $s_m(n)$. Based on the discussion in the introductory chapter, it should be clear that the redundancy introduced by the transmitters serves to facilitate the user separation and channel equalization at the receiver. The higher values of K tend to reduce the bandwidth expansion P/K. However, it will be explained shortly that for any fixed K there is the minimum required P (a function of K and the channel order L) for which user separation and perfect channel equalization is possible *regardless of the channel nulls*. We will also see that the bandwidth expansion tends to M when K tends to infinity. It is shown in [86] that a more general system where different users communicate at different information rates can be reduced to the single rate system. Therefore in the following we consider the case where K and P are fixed across different users.

The channels $H_m(z)$ are considered to be FIR of order $\leq L$ and are obtained by sampling the correspond-

ing physical continuous-time channels $h_m(n)$. For the purpose of MUI cancellation they can be considered unknown. As in the rest of the thesis, we assume that the channel state information (CSI) for the mth channel is available at the equalizer part of the mth receiver. If this is not the case, channel equalization can be done by incorporating some of the well-known *blind equalization* techniques [43], [34], [16], [18], etc. For a detailed treatment of blind AMOUR algorithms please refer to [21], [41].

At the mth receiver the signal from the user m, namely, $x_m(n)$ is corrupted by the interference from the other users and by the additive channel noise. The receiver is functionally divided into three parts: filterbank $\{G_{m,j}(z)\}_{j=0}^{J-1}$ for MUI cancellation, block $\mathbf{V}_m^{-1}$ which is supposed to eliminate the effects of $\{C_{m,k}(z)\}$ and $\{G_{m,j}(z)\}$ on the desired signal, and the equalizer $\mathbf{\Gamma}_m$ aimed at reducing the ISI introduced by the multipath channel $H_m(z)$. Much like the spreading codes, filters $G_{m,j}(z)$ are chosen to be FIR of length P. They are designed jointly with $\{C_{m,k}(z)\}$ so that the signals from the undesired users $\mu \neq m$ are filtered out regardless of their corresponding propagation channels. This design procedure will be described shortly. Notice that the length of the vector signal entering $\mathbf{V}_m^{-1}$ is J. We will see later that $J > K$ is required for the guaranteed recovery of $s_m(n)$ irrespective of the channel zeros. The vector signal at the entrance of $\mathbf{V}_m^{-1}$ depends only on the message from the desired user $s_m(n)$. However it is corrupted by the ISI effects introduced by the block for MUI elimination [namely, $\{C_{m,k}(z)\}$ and $\{G_{m,j}(z)\}$] and by the corresponding mth uplink channel $H_m(z)$. The square matrix $\mathbf{V}_m^{-1}$ neutralizes the effect of the block for MUI elimination and the rectangular matrix $\mathbf{\Gamma}_m$ depends only on the channel coefficients and is nothing but the blocked version of the equalizer for the corresponding channel.

In the following we design each of these building blocks by rewriting them in a matrix form. The banks of filters $\{C_{m,k}(z)\}$ and $\{G_{m,j}(z)\}$ can be represented in terms of the corresponding $P \times K$ and $J \times P$ polyphase matrices $\widehat{\mathbf{C}}_m$ and $\mathbf{G}_m$ respectively. The (j,i)th element of $\mathbf{G}_m$ is given by $g_{m,j}(i)$ and the (i,k)th element of $\widehat{\mathbf{C}}_m$ by $c_{m,k}(i)$. Note that the polyphase matrices $\widehat{\mathbf{C}}_m$ and $\mathbf{G}_m$ are *constant* due to the aforementioned length-P constraints on the filters.

The system from Fig.5.1 can now be redrawn as in Fig.5.2(a), where the receiver block is defined as $\mathcal{T}_m \stackrel{\triangle}{=} \mathbf{\Gamma}_m \mathbf{V}_m^{-1} \mathbf{G}_m$. The $P \times P$ block in Fig.5.2(a) consisting of the signal unblocking, filtering through the mth channel and blocking can be equivalently described as in Fig.5.2(b). Namely, it can be shown [61] that the corresponding $P \times P$ LTI system is given by the following matrix

$$\widehat{\mathbf{H}}_m = [\mathbf{H}_m \;\; \mathbf{X}(z)]. \tag{5.1}$$

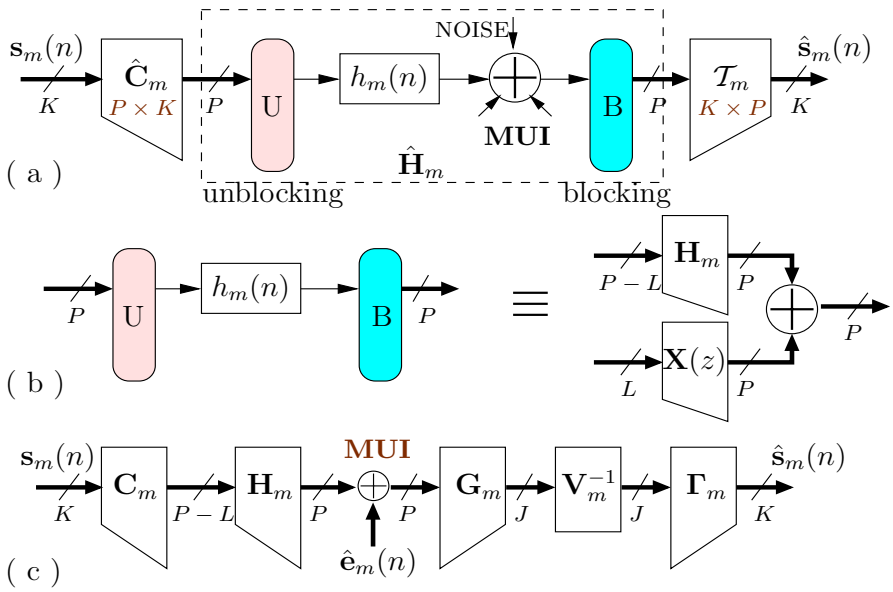

Figure 5.2: (a)-(c) Equivalent drawings of a symbol spaced AMOUR system.

Here we denote by $\mathbf{H}_m$ the $P \times P-L$ full banded lower triangular Toeplitz matrix

$$\mathbf{H}_m = \begin{bmatrix} h_m(0) & 0 & \cdots & 0 \\ \vdots & h_m(0) & & \vdots \\ h_m(L) & \vdots & \ddots & 0 \\ 0 & h_m(L) & & 0 \\ \vdots & \vdots & \ddots & \vdots \\ 0 & 0 & \cdots & h_m(L) \end{bmatrix}, \tag{5.2}$$

and $\mathbf{X}(z)$ is the $P \times L$ block that introduces the IBI. Since the last L samples of the spreading codes $\{C_{m,k}(z)\}$ are chosen to be zero, $\widehat{\mathbf{C}}_m$ is of the form $\widehat{\mathbf{C}}_m = [\mathbf{C}_m^T \;\; \mathbf{0}^T]^T$ with the $L \times K$ zero-block positioned appropriately to eliminate the IBI block $\mathbf{X}(z)$, namely, we have

$$\widehat{\mathbf{H}}_m \widehat{\mathbf{C}}_m = [\mathbf{H}_m \;\; \mathbf{X}(z)] \cdot \begin{bmatrix} \mathbf{C}_m \\ \mathbf{0} \end{bmatrix} = \mathbf{H}_m \mathbf{C}_m.$$

Therefore the IBI-free equivalent scheme is shown in Fig.5.2(c), with the noise vector signal $\widehat{\mathbf{e}}_m(n)$ obtained by blocking the noise from Fig.5.2(a). Next we use the fact that full banded Toeplitz matrices are diagonalizable by Vandermonde matrices. This is a generalization of the result used in Chapter 4 that provides the

diagonalization of circulant matrices using DFT matrices [c.f. (4.2)]. Let us choose

$$\mathbf{G}_m = \begin{bmatrix} 1 & \rho_{m,0}^{-1} & \cdots & \rho_{m,0}^{-P+1} \\ 1 & \rho_{m,1}^{-1} & \cdots & \rho_{m,1}^{-P+1} \\ \vdots & \vdots & & \vdots \\ 1 & \rho_{m,J-1}^{-1} & \cdots & \rho_{m,J-1}^{-P+1} \end{bmatrix}, \quad \text{for} \quad \rho_{m,j} \in \mathbb{C}, \tag{5.3}$$

denote by $\mathbf{\Theta}_m$ the first $P-L$ columns of $\mathbf{G}_m$ and define the diagonal matrix

$$\mathcal{H}_m(\boldsymbol{\rho}_m) \stackrel{\triangle}{=} \text{diag}[H_m(\rho_{m,0}), H_m(\rho_{m,1}), \cdots, H_m(\rho_{m,J-1})], \tag{5.4}$$

with the argument defined as $\boldsymbol{\rho}_m \stackrel{\triangle}{=} [\rho_{m,0} \;\; \rho_{m,1} \;\; \cdots \;\; \rho_{m,J-1}]$. For any $J \in \mathbb{N}$ and an arbitrary set of complex numbers $\{\rho_{m,j}\}_{j=0}^{J-1}$ the following holds

$$\mathbf{G}_m \mathbf{H}_m = \mathcal{H}_m(\boldsymbol{\rho}_m) \mathbf{\Theta}_m. \tag{5.5}$$

The choice of $\{\rho_{m,j}\}_{j=0}^{J-1}$ (which are also called *signature points*) is such that $\mathbf{G}_m$ eliminates MUI as explained next. It will become apparent that the signature points need to be distinct.

Consider the interference from user $\mu \neq m$. From Fig.5.2(c) it follows that the interfering signal $\mathbf{s}_\mu(n)$ passes through the concatenation of matrices

$$\mathbf{G}_m \mathbf{H}_\mu \mathbf{C}_\mu = \mathcal{H}_\mu(\boldsymbol{\rho}_m) \mathbf{\Theta}_m \mathbf{C}_\mu = \mathcal{H}_\mu(\boldsymbol{\rho}_m) \mathcal{C}_\mu(\boldsymbol{\rho}_m), \quad \text{where} \tag{5.6}$$

$$\mathcal{C}_\mu(\boldsymbol{\rho}_m) = \begin{bmatrix} C_{\mu,0}(\rho_{m,0}) & C_{\mu,1}(\rho_{m,0}) & \cdots & C_{\mu,K-1}(\rho_{m,0}) \\ C_{\mu,0}(\rho_{m,1}) & C_{\mu,1}(\rho_{m,1}) & \cdots & C_{\mu,K-1}(\rho_{m,1}) \\ \vdots & \vdots & & \vdots \\ C_{\mu,0}(\rho_{m,J-1}) & C_{\mu,1}(\rho_{m,J-1}) & \cdots & C_{\mu,K-1}(\rho_{m,J-1}) \end{bmatrix}. \tag{5.7}$$

The first equality in (5.6) is a consequence of (5.5). From (5.6) we see that in order to eliminate MUI *regardless of the channels* it suffices to choose $\{\rho_{m,j}\}_{m,j=0}^{M-1,J-1}$ such that

$$C_{\mu,k}(\rho_{m,j}) = 0, \quad \forall m \neq \mu, \quad \forall k \in [0, K-1], \quad \forall j \in [0, J-1]. \tag{5.8}$$

Equations (5.8) define $(M-1)J$ zeros of the polynomials $C_{m,k}(z)$. In addition to this, let $C_{m,k}(z)$ be such that

$$C_{m,k}(\rho_{m,j}) = A_m \rho_{m,j}^{-k}, \tag{5.9}$$

where the multipliers A_m introduce a simple power control for different users. At this point the total number of constraints for each of the spreading polynomials is equal to MJ. Recalling that the last L samples

of spreading codes are fixed to be zero, the minimum spreading code length is given by $P = MJ + L$. Substituting (5.9) in (5.6) for $\mu = m$ and recalling (5.5) we have

$$\mathbf{G}_m\mathbf{H}_m\mathbf{C}_m = A_m \underbrace{\begin{bmatrix} 1 & \rho_{m,0}^{-1} & \cdots & \rho_{m,0}^{-J+1} \\ 1 & \rho_{m,1}^{-1} & \cdots & \rho_{m,1}^{-J+1} \\ \vdots & \vdots & & \vdots \\ 1 & \rho_{m,J-1}^{-1} & \cdots & \rho_{m,J-1}^{-J+1} \end{bmatrix}}_{\mathbf{V}_m} \bar{\mathbf{H}}_m, \tag{5.10}$$

where $\bar{\mathbf{H}}_m$ is the $J \times K$ north-west submatrix of $\mathbf{H}_m$.

The details on the construction of spreading codes under these conditions are provided in [20]. The signature points are often chosen to be uniformly spaced around the unit circle [20]

$$\rho_{m,l} = e^{j\frac{2\pi(m+lM)}{MJ}}, \quad 0 \le l \le J-1, \tag{5.11}$$

since this leads to FFT based AMOUR implementations having low complexity.

In order to perform the channel equalization after MUI has been eliminated we need to invert the matrix product in (5.10), which in turn requires sufficient rank of the product in question. From (5.6) with $\mu = m$ we conclude that (5.10) can be further written as a product of a diagonal matrix $\mathcal{H}_m(\boldsymbol{\rho}_m)$ and a $J \times K$ Vandermonde matrix $\mathcal{C}_\mu(\boldsymbol{\rho}_m)$. This product needs to be invertible *regardless of the channel nulls* and we note that $\mathcal{C}_\mu(\boldsymbol{\rho}_m)$ is invertible as long as $\{\rho_{m,j}\}$ are distinct. Now we consider the worst case scenario where all the L zeros of $H_m(z)$ occur at the signature points $\rho_{m,j}$. In this case the rank of $\mathcal{H}_m(\boldsymbol{\rho}_m)$ drops to $J - L$ and thus the sufficient condition for the invertibility of (5.10) is $J = K + L$. In summary, the minimal system parameters are given by

$$J = K, \quad \text{(known CSI)}, \quad J = K + L, \quad \text{(unknown CSI)} \quad \text{and} \quad P = MJ + L.$$

In the limit when K tends to infinity the bandwidth expansion becomes

$$\text{BW expansion} = \frac{P}{K} = \begin{cases} [MK + L]/K & \text{for known CSI} \\ [M(K + L) + L]/K & \text{unknown CSI} \end{cases} \overset{K\to\infty}{\longrightarrow} M.$$

From Fig.5.2(c) it readily follows that (ignoring the noise)

$$\widehat{\mathbf{s}}_m(n) = A_m\boldsymbol{\Gamma}_m\mathbf{V}_m^{-1}\mathbf{V}_m\bar{\mathbf{H}}_m\mathbf{s}_m(n) = A_m\boldsymbol{\Gamma}_m\bar{\mathbf{H}}_m\mathbf{s}_m(n). \tag{5.12}$$

As noted in the previous chapters, when we considered equalizer design, $\boldsymbol{\Gamma}_m$ can be chosen to eliminate the ISI in the absence of noise, which leads to a zero-forcing equalizer (ZFE). Further, it can be chosen to minimize the expected error at the detector with noise taken into account, and this corresponds to the minimum mean-

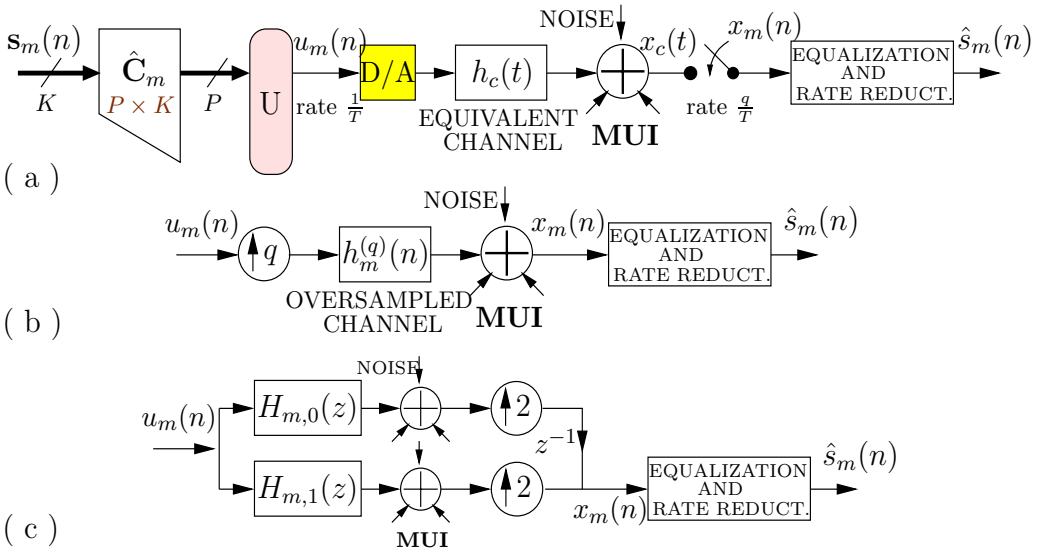

Figure 5.3: (a) Continuous-time model for an AMOUR system with integral oversampling. (b) Discrete-time equivalent drawing. (c) Polyphase representation for $q = 2$.

squared error (MMSE) solution. For more details, reader is referred to [20], [21]. In the following we consider the improvement of this conventional AMOUR system obtained by sampling the received continuous-time signal more densely than at the symbol-rate given by the transmitters.

5.3 AMOUR with integral oversampling

As demonstrated in Chapters 2 and 3, fractionally spaced equalizers typically show an improvement in performance at the expense of more computations per unit time required at the receiver. In this section we study the case when the received continuous-time signal is sampled q times faster than at the transmission rate, where q is assumed to be an integer greater than one. This roughly corresponds to some of the material presented in Chapter 2. However, the task here is complicated by the constraints on MUI elimination. Our goal is to introduce the benefits of FSEs in the ISI suppression, without violating the conditions for perfect MUI cancellation irrespective of the uplink channels. As will be clear shortly, this objective is achieved through the use of the fractionally-sampled AMOUR (FSAMOUR) system, introduced in the following.

In order to develop the discrete-time equivalent structure for an AMOUR system with integral oversampling at the receiver, we consider the continuous-time AMOUR system with an FSE shown in Fig.5.3(a). Let T be defined as the symbol spacing at the output of the transmitter [signal $u_m(n)$ in Fig.5.3(a)]. Working backwards we conclude that the rate of the blocked signal $\mathbf{s}_m(n)$ is P times lower, i.e., $1/PT$. Since $\mathbf{s}_m(n)$ is obtained by parsing the information sequence $s_m(n)$ into blocks of length K as shown in Fig.5.2(a), we conclude that the corresponding data rate of $s_m(n)$ at the transmitter is K/PT.

Each of the transmitted discrete signals $u_m(n)$ is first converted into analog signals and passed through the

corresponding *equivalent channel* denoted by $h_c(t)$. After going through the channel, the signal is corrupted by the additive noise and interference from other users. The received waveform $x_c(t)$ is sampled at q times the rate at the output of the transmitter [see Fig.5.3(a)]. The sequence $x_m(n)$ with rate q/T enters the fractionally spaced equalizer which operates at the correspondingly higher rate. Before entering the decision device at the detector, the signal rate needs to be reduced back to K/PT, so that it corresponds to that of $s_m(n)$.

Deriving the discrete-time equivalent for the system in Fig.5.3(a) closely follows the corresponding discussion in Chapter 2. In the absence of noise and MUI we have

$$x_m(n) = x_c(n\frac{T}{q}) = \sum_{k=-\infty}^{\infty} u_m(k) h_c(n\frac{T}{q} - kT). \tag{5.13}$$

Defining the discrete time sequence $h_m^{(q)}(n) \stackrel{\triangle}{=} h_c(nT/q)$, which is nothing but the waveform $h_c(t)$ sampled q times more densely than at integers, we have

$$x_m(n) = \sum_{k=-\infty}^{\infty} u_m(k) h_m^{(q)}(n - kq). \tag{5.14}$$

This is shown in Fig.5.3(b), where the noise and MUI which were continuous functions of time in Fig.5.3(a) now need to be modified (by appropriate sampling). Once again, note that Fig.5.3(b) only corresponds to the *equivalent structure*; receiver oversampling obviously does not result in any bandwidth expansion, since the physical structure is still given in Fig.5.3(a). Our goal in this section is to design the block in Fig.5.3(b) labeled 'equalization and rate reduction.' In the following we introduce one possible solution that preserves the MUI cancellation property as it was described in Section 5.2 yet provides additional flexibility when it comes to the ISI elimination part. For simplicity in what follows we assume $q = 2$; however, it is easy to show that a similar design procedure follows through for any integer q.

Oversampling by $q = 2$. First we redraw the structure from Fig.5.3(b) as shown in Fig.5.3(c). Here $H_{m,0}(z)$ and $H_{m,1}(z)$ are the Type 1 polyphase components [61] of the oversampled filter $H_m^{(2)}(z)$. In other words

$$H_m^{(2)}(z) = H_{m,0}(z^2) + z^{-1} H_{m,1}(z^2). \tag{5.15}$$

In Fig.5.3(c) we also moved the additive noise and the interference past the delay and upsamplers by splitting it into appropriate polyphase components in a fashion similar to (5.15). Before we proceed with the design of the fractionally spaced AMOUR receiver, we recall that the construction of the spreading codes $\{C_{m,k}(z)\}$ and the receive filters $\{G_{m,j}(z)\}$ in Section 5.2 ensured the elimination of MUI regardless of the propagation channels as long as their orders are bounded by L. Returning to Fig.5.3(c) in view of (5.15) we notice that $H_{m,0}(z)$ is nothing but the original integer-sampled channel $H_m(z)$. Also, each of the subchannels $H_{m,i}(z)$ can have the order at most equal to the order of $H_m(z)$, i.e., the maximum order of $H_{m,i}(z)$ is L. Moreover,

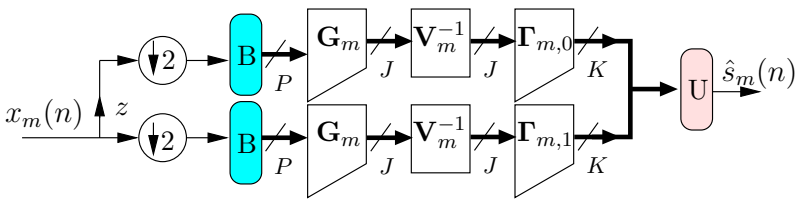

Figure 5.4: Proposed form of the equalizer with rate reduction.

each of the q polyphase components of MUI drawn in Fig.5.3(c) is obtained by passing the interfering signals $u_\mu(n)$ through the corresponding channel polyphase components $H_{\mu,i}(z)$. From the discussion in Section 5.2 we know how to eliminate each of these MUI components separately. Therefore, our approach in the equalizer design will be to keep these polyphase channels *separate*, perform the MUI cancellation in each of them and combine the results to obtain the MUI-free signal received from user m. This is achieved by the structure shown in Fig.5.4.

The received oversampled signal is first divided into the Type 2 polyphase components (a total of q polyphase components for oversampling by q). This operation assures that in each of the equalizer branches the symbol rate is equal to $1/T$. At the same time, each branch contains only one polyphase component of the desired signal and MUI from Fig.5.3(c). These polyphase components are next passed through a system that resembles the conventional AMOUR receiver structure from Fig.5.2(a). Notice one difference: while the matrices $\mathbf{G}_m$ and $\mathbf{V}_m^{-1}$ are kept the same as before, the matrices for ISI mitigation $\mathbf{\Gamma}_{m,i}$ are different in each branch and their outputs are combined, forming the information signal estimate $\widehat{s}_m(n)$. Careful observation confirms that the output symbol rate is equal to K/PT, precisely as desired.

In order to further investigate the properties of the proposed solution, we show the complete FSAMOUR system in terms of the equivalent matrix building blocks in Fig.5.5(a). The effect of the oversampling followed by the receiver structure with q branches is equivalent to receiving q copies of each transmitted signal, but after going through different multipath fading channels $H_{m,i}(z)$. This *temporal diversity* in the received signal is obviously beneficial for the equalization process as will be demonstrated in Section 5.3.1. As mentioned previously, MUI elimination in AMOUR systems does not depend on the uplink channels as long as their order is upper-bounded by L, and that is why the proposed FSAMOUR system eliminates MUI in each branch of Fig.5.5(a). Notice that the length conditions on P and J for MUI elimination remain the same as in Section 5.2.

Repeating the matrix manipulations similar to those demonstrated in Section 5.2, but this time in each branch separately, we conclude that the equivalent FSAMOUR system is shown in Fig.5.5(b). Lower triangular Toeplitz matrices $\bar{\mathbf{H}}_{m,i}$ here correspond to different polyphase components of the oversampled channel. Noise vectors $\mathbf{e}_i(n)$ are obtained by appropriately blocking and filtering the noise from Fig.5.5(a). As in [20], [21] the equalizer $\mathbf{\Gamma}_m = [\mathbf{\Gamma}_{m,0} \quad \mathbf{\Gamma}_{m,1}]$ can be constructed as a RAKE, zero-forcing or MMSE

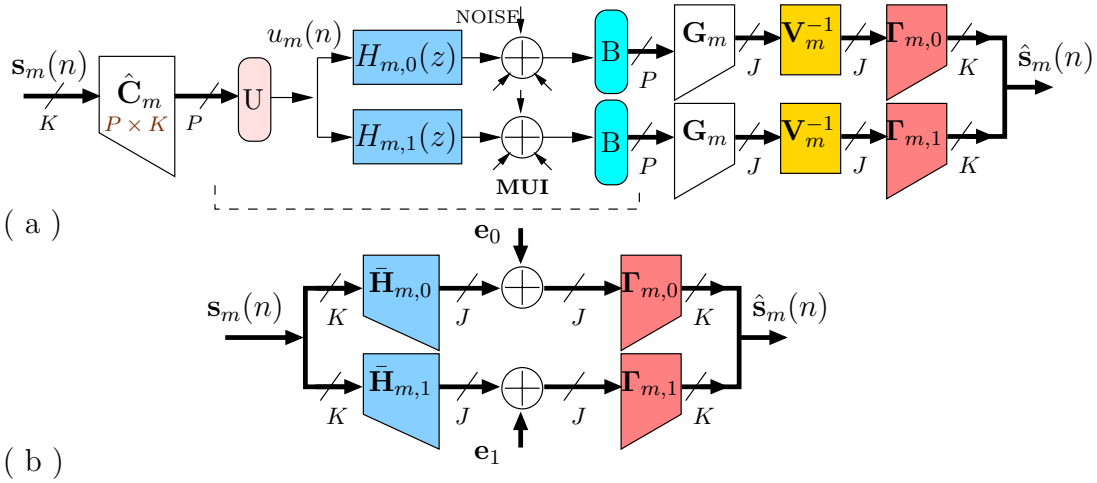

Figure 5.5: (a) A possible overall structure for the FSAMOUR system. (b) Simplified equivalent structure for ISI suppression.

receiver corresponding to the transmitter $\bar{\mathbf{H}}_m = [\bar{\mathbf{H}}_{m,0}^T \;\; \bar{\mathbf{H}}_{m,1}^T]^T$:

$$\begin{aligned}
\mathbf{\Gamma}_m^{(\text{rake})} &= \bar{\mathbf{H}}_m^\dagger, \\
\mathbf{\Gamma}_m^{(\text{zfe})} &= \left(\bar{\mathbf{H}}_m^\dagger \bar{\mathbf{H}}_m\right)^{-1} \bar{\mathbf{H}}_m^\dagger \quad \text{(pseudo-inverse)}, \\
\mathbf{\Gamma}_m^{(\text{mmse})} &= \mathcal{R}_{\mathbf{ss}} \bar{\mathbf{H}}_m^\dagger \left(\mathcal{R}_{\mathbf{ee}} + \bar{\mathbf{H}}_m \mathcal{R}_{\mathbf{ss}} \bar{\mathbf{H}}_m^\dagger\right)^{-1},
\end{aligned} \tag{5.16}$$

where $\mathcal{R}_{\mathbf{ss}}$ and $\mathcal{R}_{\mathbf{ee}}$ represent the autocorrelation matrices of the signal $\mathbf{s}_m(n)$ and noise $\mathbf{e}(n) \triangleq [\mathbf{e}_0^T(n) \;\; \mathbf{e}_1^T(n)]^T$ processes respectively. See Fig.5.5(b).

The improvement in performance over the conventional AMOUR system comes as a result of having more degrees of freedom in the construction of equalizers, namely, $qJ - K$ more rows than columns in FSAMOUR compared to $J - K$ in AMOUR. Another way to appreciate this additional freedom in the ZFE design is as follows. In AMOUR systems the construction of ZFEs amounts to finding $\mathbf{\Gamma}_m$ as in (5.12) such that $\mathbf{\Gamma}_m \widehat{\mathbf{H}}_m = \mathbf{I}_K$, in other words $\mathbf{\Gamma}_m$ is a *left inverse* of $\widehat{\mathbf{H}}_m$. On the other hand, referring to Fig.5.5(b) we conclude that the ZFEs in the FSAMOUR systems need to satisfy

$$\mathbf{\Gamma}_{m,0} \widehat{\mathbf{H}}_{m,0} + \mathbf{\Gamma}_{m,1} \widehat{\mathbf{H}}_{m,1} = \mathbf{I}_K$$

thus providing more possibilities for the design of $\mathbf{\Gamma}_{m,i}$. In addition to all this, the performance of the *zero-forcing* solutions can be further improved by noticing that left inverses of $\bar{\mathbf{H}}_m$ are not unique. This observation is closely related to similar claims from Chapters 2 and 3. Even though here the matrix under consideration is constant, the design procedure for the best ZFE in a given FSAMOUR system with the oversampling factor q is very similar in nature to the procedure in Section 2.4.2, for instance. This is why in the next subsection we focus on discussing the consequences and deriving the special forms of the result.

5.3.1 Optimal FSAMOUR ZFE

Consider the equivalent FSAMOUR system given in Fig.5.6(a). It corresponds to the system shown in Fig.5.5(b) with one difference, namely, the block-equalizer is allowed to have memory. In the following we consider the zero-forcing equalization, and therefore $\mathbf{\Gamma}_m(z)$ is designed to be a left inverse of $\bar{\mathbf{H}}_m$. Under the conditions on P and J described in Section 5.2 this inverse exists. Moreover, the fact that $\bar{\mathbf{H}}_m$ is tall implies that this inverse is not unique. Our goal is to find the left inverse $\mathbf{\Gamma}_m(z)$ as in Fig.5.6(a) of a given order that will minimize the noise power at the output, i.e., minimize the power of $\widehat{\mathbf{s}}_m(n)$ given that $\mathbf{s}_m(n) = 0$.

Using the *singular value decomposition* (SVD) of $\bar{\mathbf{H}}_m$, we have [24]

$$\bar{\mathbf{H}}_m = \mathbf{U}_m \cdot \begin{bmatrix} \mathbf{\Sigma}_m \\ \mathbf{0} \end{bmatrix} \cdot \mathbf{V}_m, \tag{5.17}$$

where $\mathbf{U}_m$ and $\mathbf{V}_m$ are $qJ \times qJ$ and $K \times K$ unitary matrices, respectively, and $\mathbf{\Sigma}_m$ is a $K \times K$ diagonal matrix of singular values. Since we assumed $\bar{\mathbf{H}}_m$ has rank K it follows that $\mathbf{\Sigma}_m$ is invertible. It can be seen from (5.17) that the most general form of a left inverse of $\bar{\mathbf{H}}_m$ is given by

$$\mathbf{\Gamma}_m(z) = \mathbf{V}_m^\dagger \begin{bmatrix} \mathbf{\Sigma}_m^{-1} & \mathbf{A}_m(z) \end{bmatrix} \mathbf{U}_m^\dagger, \tag{5.18}$$

where $\mathbf{A}_m(z)$ is an *arbitrary* $K \times (qJ - K)$ polynomial matrix. This matrix of free parameters makes it possible for constant matrices to have polynomial inverses. Defining the matrices $\mathbf{D}_0$, $\mathbf{D}_1$ and $\mathbf{B}_m(z)$ as

$$\begin{bmatrix} \mathbf{D}_0 \\ \mathbf{D}_1 \end{bmatrix} \stackrel{\triangle}{=} \mathbf{U}_m^\dagger, \quad \text{and} \quad \mathbf{B}_m(z) \stackrel{\triangle}{=} \mathbf{V}_m^\dagger \cdot \mathbf{A}_m(z), \tag{5.19}$$

Fig.5.6(a) can be presented as in Fig.5.6(b). Since there is a one to one correspondence (5.19) between the matrices $\mathbf{A}_m(z)$ and $\mathbf{B}_m(z)$, the design objective becomes that of finding the $\mathbf{B}_m(z)$ of a fixed order $N_b - 1$, given by its impulse response

$$\mathbf{B}_m(z) = \sum_{n=0}^{N_b-1} \mathbf{B}_{m,n} z^{-n}, \tag{5.20}$$

that minimizes the noise power $E\{\widehat{\mathbf{e}}_m^\dagger \widehat{\mathbf{e}}_m\}/K$ at the output of Fig.5.6(b). Similar as before, the optimal $\mathbf{B}_m(z)$ in this context is nothing but a *linear estimator* of a vector random process $-\mathbf{u}(n)$ given $\mathbf{v}(n)$. The solution is given by

$$[\mathbf{B}_{m,0} \;\; \mathbf{B}_{m,1} \;\; \cdots \;\; \mathbf{B}_{m,N_b-1}] \stackrel{\triangle}{=} \mathcal{B} = -E\{\mathbf{u}(n)\mathcal{V}^\dagger(n)\} \cdot \mathcal{R}_{\mathcal{V}\mathcal{V}}^{-1}, \tag{5.21}$$

where $\mathcal{V}(n) \stackrel{\triangle}{=} [\mathbf{v}^T(n) \;\; \mathbf{v}^T(n-1) \;\; \cdots \;\; \mathbf{v}^T(n - N_B + 1)]^T$ and $\mathcal{R}_{\mathcal{V}\mathcal{V}}$ is its autocorrelation matrix. Next we rewrite the solution (5.21) in terms of the input noise statistics, namely, its $qJ \times qJ$ cross-correlation matrices

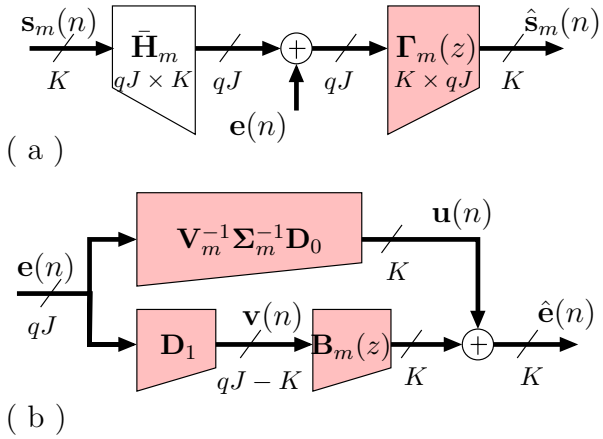

Figure 5.6: (a) Equivalent FSAMOUR system. (b) ZFE structure with noise input.

$\mathcal{R}_{\mathbf{ee}}(k) \triangleq E\{\mathbf{e}_m(n)\mathbf{e}_m^\dagger(n-k)\}$. First note that

$$\mathcal{R}_{\mathcal{VV}} = \begin{bmatrix} \mathbf{D}_1\mathcal{R}_{\mathbf{ee}}(0)\mathbf{D}_1^\dagger & \mathbf{D}_1\mathcal{R}_{\mathbf{ee}}(1)\mathbf{D}_1^\dagger & \cdots & \mathbf{D}_1\mathcal{R}_{\mathbf{ee}}(N_b-1)\mathbf{D}_1^\dagger \\ \mathbf{D}_1\mathcal{R}_{\mathbf{ee}}(1)\mathbf{D}_1^\dagger & \mathbf{D}_1\mathcal{R}_{\mathbf{ee}}(0)\mathbf{D}_1^\dagger & \cdots & \mathbf{D}_1\mathcal{R}_{\mathbf{ee}}(N_b-2)\mathbf{D}_1^\dagger \\ \vdots & \vdots & \ddots & \vdots \\ \mathbf{D}_1\mathcal{R}_{\mathbf{ee}}(N_b-1)\mathbf{D}_1^\dagger & \mathbf{D}_1\mathcal{R}_{\mathbf{ee}}(N_b-2)\mathbf{D}_1^\dagger & \cdots & \mathbf{D}_1\mathcal{R}_{\mathbf{ee}}(0)\mathbf{D}_1^\dagger \end{bmatrix}. \tag{5.22}$$

Similarly, we can rewrite

$$E\{\mathbf{u}(n)\mathcal{V}^\dagger(n)\} = \mathbf{V}_m^\dagger \cdot \mathbf{\Sigma}_m^{-1} \cdot \mathbf{D}_0 \cdot \left[\mathcal{R}_{\mathbf{ee}}(0)\mathbf{D}_1^\dagger \;\; \mathcal{R}_{\mathbf{ee}}(1)\mathbf{D}_1^\dagger \;\; \cdots \;\; \mathcal{R}_{\mathbf{ee}}(N_b-1)\mathbf{D}_1^\dagger\right]. \tag{5.23}$$

For sufficiently large input block size qJ it is often safe to assume that the noise is uncorrelated across different blocks; in other words $\mathcal{R}_{\mathbf{ee}}(k) = \mathbf{0}$ for $k \neq 0$. In this important special case the optimal $\mathbf{B}_m(z)$ is a constant, namely

$$\mathbf{B}_m(z) = \mathbf{B}_{m,0} = -\mathbf{V}_m^\dagger \mathbf{\Sigma}_m^{-1}\mathbf{D}_0\mathcal{R}_{\mathbf{ee}}(0)\mathbf{D}_1^\dagger \left(\mathbf{D}_1\mathcal{R}_{\mathbf{ee}}(0)\mathbf{D}_1^\dagger\right)^{-1}. \tag{5.24}$$

From (5.24) and Fig.5.6 we get the optimal form of a ZFE

$$\mathbf{\Gamma}_m^{(\text{opt})} = \mathbf{V}_m^\dagger \mathbf{\Sigma}_m^{-1}\left[\mathbf{I}_K \;\; -\mathbf{D}_0\mathcal{R}_{\mathbf{ee}}(0)\mathbf{D}_1^\dagger\left(\mathbf{D}_1\mathcal{R}_{\mathbf{ee}}(0)\mathbf{D}_1^\dagger\right)^{-1}\right]\mathbf{U}_m^\dagger. \tag{5.25}$$

Another important special case occurs when the noise samples at the input of the receiver are i.i.d., i.e., when $\mathcal{R}_{\mathbf{ee}}(k) = \delta_k \cdot \sigma_e^2 \cdot \mathbf{I}$. Note that in this case $\mathbf{D}_0\mathcal{R}_{\mathbf{ee}}(0)\mathbf{D}_1^\dagger = \mathbf{0}$, so that

$$\mathbf{\Gamma}_m^{(\text{white noise})} = \mathbf{V}_m^\dagger\left[\mathbf{\Sigma}_m^{-1} \;\; \mathbf{0}\right]\mathbf{U}_m^\dagger. \tag{5.26}$$

At this point we would like to make a distinction between the optimal ZFEs in AMOUR and FSAMOUR

systems. From the derivations presented in this subsection it is evident that the optimal ZFEs can be constructed in a traditional AMOUR system of [20], [21] and it is to be expected that this solution would perform better than the ordinary ZFE based on the matrix pseudo-inverse similar to (5.16). However, in the following we show that if the channel noise in Fig.5.3(a) is i.i.d. then any optimization of ZFEs in AMOUR systems will not improve their performance. This is not true for fractionally spaced AMOUR systems, since the noise samples in vectors $\mathbf{e}_0(n)$ and $\mathbf{e}_1(n)$ in Fig.5.6(b) need not have the same variances although they remain independent. This is due to the fact that $\mathbf{e}_0(n)$ and $\mathbf{e}_1(n)$ are obtained by passing the channel noise through the filters corresponding to *different* polyphase components of the channel. Consequently, in the FSAMOUR case, the noise autocorrelation matrix $\mathcal{R}_{\mathbf{ee}}(0)$ appearing in (5.25) in *not* given by a scaled identity matrix and (5.26) *does not* correspond to the optimal solution. Now let us compare the optimal AMOUR ZFE for white noise (5.26) to the corresponding zero-forcing solution given in (5.16). The result is summarized as follows.

Proposition 1. Pseudo-inverse is the optimal AMOUR ZF SSE if the noise is white.

Proof. Starting from the traditional ZFE $\mathbf{\Gamma}_m^{(\mathrm{zfe})}$ we have

$$\begin{aligned}\mathbf{\Gamma}_m^{(\mathrm{zfe})} = \left(\bar{\mathbf{H}}_m^\dagger \bar{\mathbf{H}}_m\right)^{-1} \bar{\mathbf{H}}_m^\dagger &= \left(\mathbf{V}_m^\dagger \begin{bmatrix}\mathbf{\Sigma}_m^\dagger & \mathbf{0}\end{bmatrix} \mathbf{U}_m^\dagger \mathbf{U}_m \begin{bmatrix}\mathbf{\Sigma}_m \\ \mathbf{0}\end{bmatrix} \mathbf{V}_m\right)^{-1} \mathbf{V}_m^\dagger \begin{bmatrix}\mathbf{\Sigma}_m^\dagger & \mathbf{0}\end{bmatrix} \mathbf{U}_m^\dagger \\ &= \mathbf{V}_m^\dagger \begin{bmatrix}\mathbf{\Sigma}_m^{-1} & \mathbf{0}\end{bmatrix} \mathbf{U}_m^\dagger = \mathbf{\Gamma}_m^{(\text{white noise})}. \end{aligned} \tag{5.27}$$

Therefore, a simple (Moore-Penrose) pseudo-inverse becomes the optimal ZFE in AMOUR systems with the white channel noise; in other words there is nothing to be gained by using the optimal solution. In contrast to this, using the optimal ZFEs in FSAMOUR systems leads to significant improvements in performance over the simple pseudo-inverses as is demonstrated next. Also, notice that $\mathbf{\Gamma}_m^{(\mathrm{mmse})}$ becomes practically equivalent to $\mathbf{\Gamma}_m^{(\mathrm{zfe})}$ in the high SNR environments. When SNR is high, $\mathbf{\Gamma}_m^{(\mathrm{mmse})}$ in (5.16) behaves as $\bar{\mathbf{H}}_m^\dagger \left(\bar{\mathbf{H}}_m \bar{\mathbf{H}}_m^\dagger\right)^{-1}$, where the 'inverse' actually stands for a pseudo-inverse. Therefore, we have $\mathbf{\Gamma}_m^{(\mathrm{mmse})} \approx \mathbf{\Gamma}_m^{(\mathrm{zfe})}$.

5.3.2 Performance evaluation

In this subsection we compare the performance of the conventional (SSE) AMOUR described in Section 5.2 and the FSAMOUR system from Section 5.3 with oversampling ratio $q = 2$. System parameters were given by $K = 12$, $M = 4$, while J and P are chosen to be the minimum for the guaranteed existence of ZFEs as explained in Section 5.2. The simulation results are averaged over *thirty* independently chosen real random channels of order $L = 4$. The half-integer sampled channel impulse responses $h_m^{(2)}(n)$ were also chosen randomly, under the constraint that they coincide with AMOUR channels at integers. In other words $h_m^{(2)}(2n) = h_m(n)$. The channel noise was taken to be AWGN. The signal-to-noise ratio (SNR) was measured after sampling at the entrance of the receiver [point $x_m(n)$ in Fig.5.3(a)]. Notice that SNR does not depend on the oversampling ratio q as long as the signal and the noise are stationary. The performance curves are

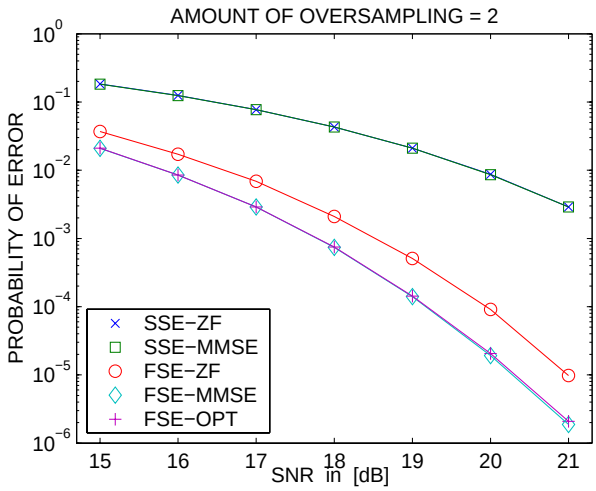

Figure 5.7: Probability of error as a function of SNR in AMOUR and FSAMOUR systems.

shown in Fig.5.7. The acronyms 'SSE' and 'FSE' represent AMOUR and FSAMOUR systems, while the suffices 'ZF,' 'MMSE' and 'OPT' correspond to zero-forcing, minimum mean-squared error and optimal ZFE solutions respectively. There are several important observations that can be made from these results:

- The overall performance of AMOUR systems is significantly improved by signal oversampling at the receiver.

- The performance of ZFEs in FSAMOUR systems can be further improved by about 0.7 dB if we use the optimal equalizers, exploiting the redundancy in ZFE design as described in Section 5.3.1. This is due to the fact that the optimal solution is given by (5.25) rather than (5.26). As explained previously, the same does not hold for AMOUR systems.

- The performance of the optimal ZFEs in FSAMOUR systems is almost identical to the performance of the corresponding MMSE equalizer. Thus there is practically no loss in performance as a result of using the optimal ZFE given by (5.25) instead of the MMSE equalizer (5.16). The *advantages* of using a ZFE become evident by comparing the expressions (5.25) and (5.16). As was elaborated in Chapter 3, as opposed to MMSE equalizers, ZFE solutions require no knowledge of the signal statistics $\mathcal{R}_{\mathbf{ss}}$ and if the noise is white and stationary, the solution $\mathbf{\Gamma}_m^{(\mathrm{opt})}$ is independent of the noise variance.

- Since a simple pseudo-inverse happens to be the optimal ZFE in AMOUR systems with no oversampling, its performance is also almost identical to that of the MMSE equalizer.

In the next section we introduce the modification of the idea of the integral oversampling of the received signal to a more general case when the amount of oversampling is a rational number.

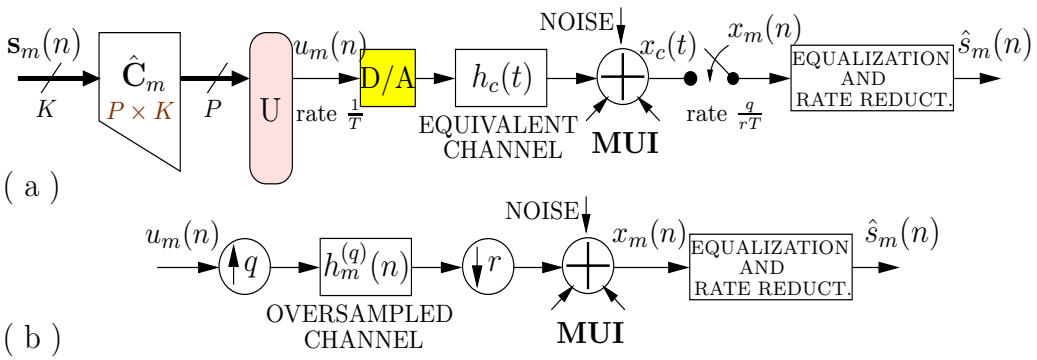

Figure 5.8: (a) Continuous-time model for an AMOUR system with fractional oversampling ratio q/r. (b) Discrete-time equivalent drawing.

5.4 AMOUR with fractional oversampling

While FSAMOUR systems with integral oversampling can lead to significant improvements in performance compared to traditional AMOUR systems, the notion of oversampling the received CDMA signal might be less popular due to very high data rates of the transmitted CDMA signals. According to the scenario of integral oversampling the data rates at the receiver are at least twice as high as the rates at the transmitter, which makes them prohibitively high for most sophisticated equalization techniques. In this section we explore the consequences of sampling the continuous-time received signal $x_c(t)$ in Fig.5.3(a) at a rate that is higher than the symbol rate $1/T$ by a fractional amount. To be more precise, suppose the amount of oversampling is q/r, where q and r are coprime integers satisfying $q > r$. If $q = r + 1$ for high values of r the data rate at the receiver becomes almost identical to the one at the transmitter which is rather advantageous from the implementational point of view. As explained in Chapter 3, the case when q and r share a common divisor can easily be reduced to the case of coprime factors. This said, it appears that the discussion from the previous section is redundant since it simply corresponds to fractional oversampling with $r = 1$. However, it is instructive to consider the integer case separately since it is easier to analyze, and provides some important insights.

Consider Fig.5.3(a) and suppose $x_c(t)$ has been sampled at rate q/r. This situation is shown in Fig.5.8(a). Performing the analysis very similar to the one in Section 5.3, we can easily show that in this case we have

$$x_m(n) = \sum_{k=-\infty}^{\infty} u_m(k) h_m^{(q)}(nr - kq). \tag{5.28}$$

This is shown in Fig.5.8(b), with appropriate modification of the noise from Fig.5.8(a) and with $h_m^{(q)}(n)$ denoting $h_c(nT/q)$, just as it did in the case of integer oversampling.

Now we are ready for the problem of multiuser communications with the rational oversampling ratio of q/r. The analysis of the fractionally oversampled FSAMOUR systems will turn out to be somewhat similar

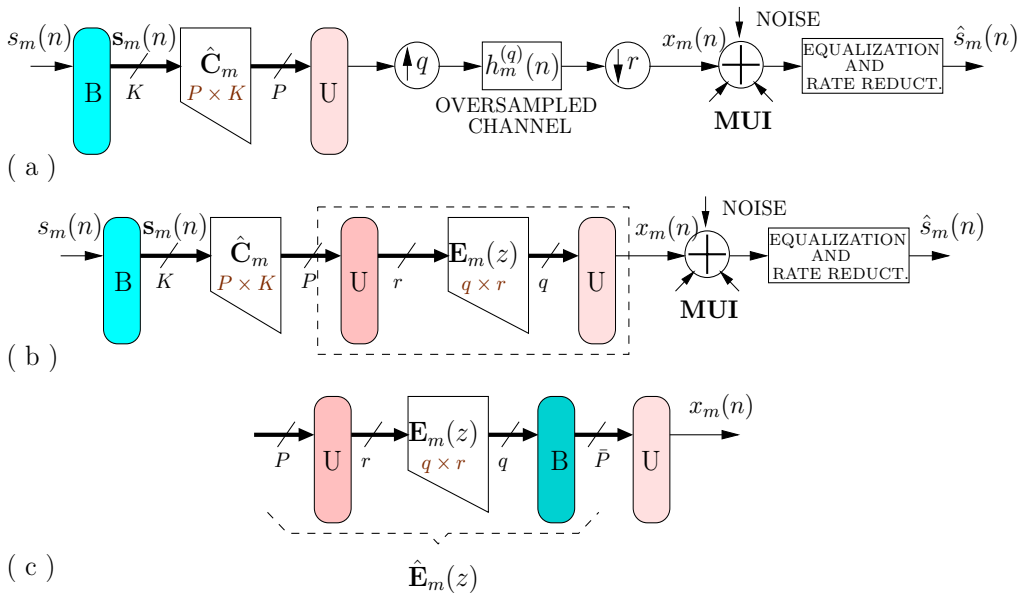

Figure 5.9: (a) Discrete-time model for the FSAMOUR system with the oversampling ratio q/r. (b) Equivalent drawing. (c) Redrawing a block from (b).

to the discussion in Section 5.2 and in order to make the presentation more accessible we have grouped the most important steps into separate subsections. One noticeable difference with respect to the material from Section 5.2 is that in this section we will mostly deal with larger, block matrices. This comes as a consequence of a result on fractionally sampled channel responses, presented in Chapter 3.

5.4.1 Writing the fractionally sampled channel as a block convolution

Combining the elements from Figs. 5.8(a) and 5.8(b), we conclude that the discrete-time equivalent scheme of the FSAMOUR system with the oversampling ratio q/r is shown in Fig.5.9(a). One of the results from Chapter 3 states that the operation of filtering by $H_m^{(q)}(z)$ surrounded by an expander and a decimator as it appears in Fig.5.9(a) is equivalent to blocking the signal, passing it through a $q \times r$ matrix transfer function $\mathbf{E}_m(z)$ and then unblocking it. This equivalent structure is employed in Fig.5.9(b). The unblocking element of darker shade represents the 'incomplete' unblocking, i.e., it converts a sequence of blocks of length P into a higher rate sequence of blocks of length r. In other words, it can be thought of as the *unblocking* of a length-P vector sequence into a scalar sequence, followed by the *blocking* of the obtained scalar signal into a length-r vector signal. Here for simplicity we assumed r divides P, however this condition is unnecessary for the above definition to hold and we return to this point later.

The relation between the filter $H_m^{(q)}(z)$ and the corresponding matrix $\mathbf{E}_m(z)$ is rather complicated and is

introduced in the following. First, let us write $H_m^{(q)}(z)$ in terms of its Type 2 q-fold polyphase components

$$H_m^{(q)}(z) = \sum_{k=0}^{q-1} H_{m,k}(z^q) z^k. \tag{5.29}$$

Next, recall from the Euclid's algorithm for integers that since q and r are mutually coprime, there exist $Q, R \in \mathbb{Z}$ such that

$$qQ + rR = 1. \tag{5.30}$$

Let us define the filters $P_{m,k}(z)$ and their Type 1 r-fold polyphase components $E_{k,l}(z)$ as

$$P_{m,k}(z) \stackrel{\triangle}{=} z^{kQ} H_{m,k}(z) = \sum_{l=0}^{r-1} E_{k,l}(z^r) z^{-l}, \quad \text{for} \;\; 0 \le k \le q-1. \tag{5.31}$$

We have shown in Chapter 3 that the equivalent matrix transfer function $\mathbf{E}_m(z)$ is given by

$$\mathbf{E}_m(z) = \begin{bmatrix} E_{0,0}(z) & E_{0,1}(z) & \cdots & E_{0,r-1}(z) \\ E_{1,0}(z) & E_{1,1}(z) & \cdots & E_{1,r-1}(z) \\ \vdots & \vdots & & \vdots \\ E_{q-1,0}(z) & E_{q-1,1}(z) & \cdots & E_{q-1,r-1}(z) \end{bmatrix}. \tag{5.32}$$

Now consider the block surrounded by a dashed line in Fig.5.9(b). This can trivially be redrawn as in Fig.5.9(c). The denoted $\bar{P} \times P$ transfer function $\widehat{\mathbf{E}}_m(z)$ is a block pseudo-circulant

$$\widehat{\mathbf{E}}_m(z) = \begin{bmatrix} \mathbf{E}_0 & \mathbf{0} & \cdots & \mathbf{0} & z^{-1}\mathbf{E}_N & z^{-1}\mathbf{E}_{N-1} & \cdots & z^{-1}\mathbf{E}_1 \\ \mathbf{E}_1 & \mathbf{E}_0 & \cdots & \mathbf{0} & \mathbf{0} & z^{-1}\mathbf{E}_N & \cdots & z^{-1}\mathbf{E}_2 \\ \vdots & \vdots & \ddots & \vdots & \vdots & \vdots & \ddots & \vdots \\ \mathbf{E}_N & \mathbf{E}_{N-1} & \cdots & \mathbf{E}_0 & \mathbf{0} & \mathbf{0} & \cdots & \mathbf{0} \\ \mathbf{0} & \mathbf{E}_N & \cdots & \mathbf{E}_1 & \mathbf{E}_0 & \mathbf{0} & \cdots & \mathbf{0} \\ \vdots & \vdots & \ddots & \vdots & \vdots & \vdots & & \vdots \\ \mathbf{0} & \mathbf{0} & \cdots & \mathbf{E}_N & \mathbf{E}_{N-1} & \mathbf{E}_{N-2} & \cdots & \mathbf{E}_0 \end{bmatrix}. \tag{5.33}$$

The $q \times r$ blocks $\mathbf{E}_n$, for $0 \le n \le N$ in (5.33) represent the impulse response of $\mathbf{E}_m(z)$, while N is the order of the matrix polynomial and it depends on the choice of r and on the maximum channel order L. This issue will be revisited shortly. It is implicitly assumed in (5.33) that q divides $\bar{P}$. For arbitrary values of r and q we can write

$$\bar{P} = q \cdot n_q + e_q \;\; \text{and} \;\; P = r \cdot n_r + e_r, \tag{5.34}$$

where $n_q, e_q, n_r, e_r \in \mathbb{N}$ and $e_q < q$, $e_r < r$. Equation (5.33) obviously corresponds to $e_q = e_r = 0$, i.e., when r divides P and q divides $\bar{P}$. For general values of r and q, the block pseudo-circulant $\widehat{\mathbf{E}}_m(z)$ from (5.33) gets

transformed by inserting e_r additional columns of zeros in each block-row and by adding e_q additional rows at the bottom. In the following we will assume $e_q = e_r = 0$ since this leads to essentially no loss of generality. Furthermore, we will assume that $n_q = n_r$, or equivalently that $\bar{P} = qn_r$, which is a valid assumption since $\bar{P}$ is a free design parameter.

5.4.2 Eliminating IBI

Next we would like to eliminate the memory dependence in (5.33) which is responsible for inter-block interference (IBI). It is apparent from Fig.5.9 that this can be achieved by choosing $\widehat{\mathbf{C}}_m$ such that its last rN rows are zero. This effectively means that the transmitter is inserting a redundancy of rN symbols after each block of length $P - rN$. Let us denote by $\bar{\mathbf{E}}_m$ the $\bar{P} \times (P - Nr)$ constant matrix obtained as a result of premultiplying $\widehat{\mathbf{C}}_m$ by $\widehat{\mathbf{E}}_m(z)$. Next, we note that the *blocked* version of the equality (5.5) holds true as well. In other words, $\bar{\mathbf{E}}_m$ can be block-diagonalized using block-Vandermonde matrices. Namely, let us choose

$$\mathbf{G}_m = \begin{bmatrix} \mathbf{I}_q & \rho_{m,0}^{-1}\mathbf{I}_q & \cdots & \rho_{m,0}^{-n_q+1}\mathbf{I}_q \\ \mathbf{I}_q & \rho_{m,1}^{-1}\mathbf{I}_q & \cdots & \rho_{m,1}^{-n_q+1}\mathbf{I}_q \\ \vdots & \vdots & & \vdots \\ \mathbf{I}_q & \rho_{m,J-1}^{-1}\mathbf{I}_q & \cdots & \rho_{m,J-1}^{-n_q+1}\mathbf{I}_q \end{bmatrix}, \quad \text{for} \quad \rho_{m,j} \in \mathbb{C}, \tag{5.35}$$

denote by $\mathbf{\Theta}_m$ the following $Jr \times (P - Nr)$ matrix, recalling that $n_r = n_q$

$$\mathbf{\Theta}_m = \begin{bmatrix} \mathbf{I}_r & \rho_{m,0}^{-1}\mathbf{I}_r & \cdots & \rho_{m,0}^{-(n_r-N-1)}\mathbf{I}_r \\ \mathbf{I}_r & \rho_{m,1}^{-1}\mathbf{I}_r & \cdots & \rho_{m,1}^{-(n_r-N-1)}\mathbf{I}_r \\ \vdots & \vdots & & \vdots \\ \mathbf{I}_r & \rho_{m,J-1}^{-1}\mathbf{I}_r & \cdots & \rho_{m,J-1}^{-(n_r-N-1)}\mathbf{I}_r \end{bmatrix}, \tag{5.36}$$

and define the $qJ \times rJ$ block-diagonal matrix

$$\mathcal{E}_m(\boldsymbol{\rho}_m) \stackrel{\triangle}{=} \text{diag}[\mathbf{E}_m(\rho_{m,0}), \mathbf{E}_m(\rho_{m,1}), \cdots, \mathbf{E}_m(\rho_{m,J-1})]. \tag{5.37}$$

Then for any $J \in \mathbb{N}$ and any set of distinct complex numbers $\{\rho_{m,j}\}_{j=0}^{J-1}$ the following holds

$$\mathbf{G}_m \bar{\mathbf{E}}_m = \mathcal{E}_m(\boldsymbol{\rho}_m)\mathbf{\Theta}_m. \tag{5.38}$$

Notice that we used the symbols $\mathbf{G}_m$ and $\mathbf{\Theta}_m$ to represent different matrices from the ones in Section 5.2. This is done for notational simplicity since no confusion is anticipated.

Once we have established the connection with the traditional AMOUR systems, we follow the steps similar to those in Section 5.2 in order to get conditions for MUI cancellation and channel equalization regardless of the channels $h_m(n)$. Given the analogy between the equations (5.38) and (5.5) we conjecture

that the block at the receiver in Fig.5.9 responsible for MUI elimination should be given by $\mathbf{G}_m$ as in (5.35). In the following we first clarify this point and then proceed to state the result on the existence of channel ZFEs.

5.4.3 MUI cancellation

The interference at the mth receiver coming from the user $\mu \neq m$ is proportional to the output of the concatenation of matrices $\mathbf{G}_m\bar{\mathbf{E}}_\mu\mathbf{C}_\mu$, where $\mathbf{C}_\mu$ is the nonzero part of the spreading code matrix $\widehat{\mathbf{C}}_\mu$ and is exactly the same as the one used in (5.6). Using (5.38) we see that the MUI term is proportional to

$$\mathbf{G}_m\bar{\mathbf{E}}_\mu\mathbf{C}_\mu = \mathcal{E}_\mu(\boldsymbol{\rho}_m)\boldsymbol{\Theta}_m\mathbf{C}_\mu = \mathcal{E}_\mu(\boldsymbol{\rho}_m)\mathcal{C}_\mu(\boldsymbol{\rho}_m), \quad \text{with} \tag{5.39}$$

$$\mathcal{C}_\mu(\boldsymbol{\rho}_m) \triangleq \begin{bmatrix} \mathbf{C}_\mu(\rho_{m,0}) \\ \mathbf{C}_\mu(\rho_{m,1}) \\ \vdots \\ \mathbf{C}_\mu(\rho_{m,J-1}) \end{bmatrix}, \quad \text{and} \quad \mathbf{C}_\mu(\gamma) \triangleq \begin{bmatrix} C_{\mu,0}^{(0)}(\gamma) & C_{\mu,1}^{(0)}(\gamma) & \cdots & C_{\mu,K-1}^{(0)}(\gamma) \\ C_{\mu,0}^{(1)}(\gamma) & C_{\mu,1}^{(1)}(\gamma) & \cdots & C_{\mu,K-1}^{(1)}(\gamma) \\ \vdots & \vdots & & \vdots \\ C_{\mu,0}^{(r-1)}(\gamma) & C_{\mu,1}^{(r-1)}(\gamma) & \cdots & C_{\mu,K-1}^{(r-1)}(\gamma) \end{bmatrix}. \tag{5.40}$$

The entries $C_{\mu,k}^{(l)}(\gamma)$, for $0 \leq k \leq K-1$, $0 \leq l \leq r-1$ in (5.40) represent the lth Type 1 polyphase components of the kth spreading code used by user μ, evaluated at $z = \gamma$. In other words, the kth spreading code in Fig.5.1(a) can be written as

$$C_{m,k}(z) = \sum_{l=0}^{r-1} C_{m,k}^{(l)}(z^r)z^{-l}.$$

It follows from (5.39)-(5.40) that MUI elimination can be achieved by choosing $\{\rho_{m,j}\}_{m,j=0}^{M-1,J-1}$ such that

$$C_{\mu,k}^{(l)}(\rho_{m,j}) = 0, \quad \forall m \neq \mu, \quad \forall k \in [0, K-1], \quad \forall j \in [0, J-1], \quad \forall l \in [0, r-1]. \tag{5.41}$$

Equations (5.41) define $(M-1)J$ zeros for *each* of the r polyphase components of $C_{m,k}(z)$. In addition to this, we will choose the nonzero values similarly as in Section 5.2 such that the channel equalization becomes easier. To this end, let us choose

$$C_{m,k}^{(l)}(\rho_{m,j}) = A_m \cdot \delta(l-\beta) \cdot \rho_{m,j}^{-\alpha}, \tag{5.42}$$

for integers α and β with $\beta < r$ chosen such that $k = \alpha r + \beta$. This brings the total number of constraints in each of the spreading code polynomials to MJr. Recalling that the last Nr samples of spreading codes are fixed to be zero, the minimum spreading code length is given by $P = (MJ + N)r$.

5.4.4 Channel equalization

The last step in the receiver design is to eliminate the ISI present in the MUI-free signal. For an arbitrary choice of integers K and r with $r < K$, we can write

$$K = r \cdot \alpha_r + \beta_r, \tag{5.43}$$

with $\alpha_r, \beta_r \in \mathbb{N}$ and $\beta_r < r$. Let us first assume that K was chosen such that $\beta_r = 0$ in (5.43). Substituting (5.42) in (5.40) for $\mu = m$, we have

$$\mathbf{C}_m(\rho_{m,j}) = A_m \begin{bmatrix} \mathbf{I}_r & \rho_{m,j}^{-1}\mathbf{I}_r & \cdots & \rho_{m,j}^{-(\alpha_r-1)}\mathbf{I}_r \end{bmatrix}, \tag{5.44}$$

which further leads to

$$\mathbf{G}_m\bar{\mathbf{E}}_\mu\mathbf{C}_\mu = A_m \cdot \mathcal{E}_\mu(\boldsymbol{\rho}_m) \cdot \begin{bmatrix} \mathbf{I}_r & \rho_{m,0}^{-1}\mathbf{I}_r & \cdots & \rho_{m,0}^{-(\alpha_r-1)}\mathbf{I}_r \\ \mathbf{I}_r & \rho_{m,1}^{-1}\mathbf{I}_r & \cdots & \rho_{m,1}^{-(\alpha_r-1)}\mathbf{I}_r \\ \vdots & \vdots & & \vdots \\ \mathbf{I}_r & \rho_{m,J-1}^{-1}\mathbf{I}_r & \cdots & \rho_{m,J-1}^{-(\alpha_r-1)}\mathbf{I}_r \end{bmatrix}. \tag{5.45}$$

Recalling the relationship (5.38) we finally have that

$$\mathbf{G}_m\bar{\mathbf{E}}_m\mathbf{C}_m = A_m \cdot \underbrace{\begin{bmatrix} \mathbf{I}_q & \rho_{m,0}^{-1}\mathbf{I}_q & \cdots & \rho_{m,0}^{-(\alpha_r+N-1)}\mathbf{I}_q \\ \mathbf{I}_q & \rho_{m,1}^{-1}\mathbf{I}_q & \cdots & \rho_{m,1}^{-(\alpha_r+N-1)}\mathbf{I}_q \\ \vdots & \vdots & & \vdots \\ \mathbf{I}_q & \rho_{m,J-1}^{-1}\mathbf{I}_q & \cdots & \rho_{m,J-1}^{-(\alpha_r+N-1)}\mathbf{I}_q \end{bmatrix}}_{\mathbb{V}_m} \cdot \mathbb{E}_m, \tag{5.46}$$

where $\mathbb{E}_m$ is the $(\alpha_r + N)q \times K$ north-west submatrix of $\bar{\mathbf{E}}_m$. If $\beta_r > 0$ in (5.43) that simply leads to adding the first β_r columns of the next logical block to the right end in (5.44), consequently augmenting the matrices $\mathbb{V}_m$ and $\mathbb{E}_m$ in (5.46).

The channel equalization which follows the MUI cancellation amounts to finding a *left* inverse of the matrix product $\mathbb{V}_m \cdot \mathbb{E}_m$ appearing on the right-hand side of (5.46). The first matrix in this product is block-Vandermonde and it is invertible if $J \geq \alpha_r + N$ and if $\{\rho_{m,j}\}_{j=0}^{J-1}$ are distinct (the latter was assured previously). Therefore we get the value for one of the parameters

$$J = \alpha_r + N. \tag{5.47}$$

Notice that since $q > r$, from (5.47) and (5.43) it automatically follows that $\mathbb{V}_m \cdot \mathbb{E}_m$ is a tall matrix, thus it *could* have a left inverse. However, these conditions are not sufficient. Another condition that needs to be

satisfied is the following

$$\text{rank}\{\mathbf{G}_m\bar{\mathbf{E}}_m\mathbf{C}_m\} = K \quad \Rightarrow \quad \text{rank}\{\mathcal{E}_m(\boldsymbol{\rho}_m)\} = K. \tag{5.48}$$

In other words, in order for the channel $h_m(n)$ to be equalizable using ZFEs after oversampling the received signal by q/r and MUI cancellation, we can allow for the rank of $\mathcal{E}_m(\boldsymbol{\rho}_m)$ in (5.37) to drop by the maximum amount of r, regardless of the choice of signature points $\{\rho_{m,j}\}$. Obviously, *this cannot be guaranteed regardless of the channel and other system parameters* simply because the matrix polynomial $\mathbf{E}_m(z)$ could happen to be rank-deficient for all values of z. At best we can only hope to establish the conditions under which the rank equality (5.48) stays satisfied regardless of the choice of signature points. This is different from the conventional AMOUR and integral FSAMOUR methods described in Sections 5.2 and 5.3, where we had two conditions on system parameters for guaranteed channel equalizability depending on whether the channel was known ($J \geq K$) or unknown ($J \geq K + L$). Here we *cannot* guarantee equalizability even for the known CSI, if the channel leads to rank-deficient $\mathbf{E}_m(z)$. Luckily, this occurs with zero probability. If this is not the case, the channel can be equalized under the same restrictions on the parameters regardless of the specific channel in question. The following theorem establishes the result, under one extra assumption on the decimation ratio r.

Theorem 5.1. Consider the FSAMOUR communication system given by its discrete-time equivalent in Fig.5.9(a). Let the maximum order of all the channels $\{h_m(n)\}_{m=0}^{M-1}$ be L. Let us choose the integers $r \geq L+1$ and $q > r$ such that the irreducible ratio q/r closely approximates the desired amount of oversampling at the receiver. Next, choose an arbitrary $\alpha_r \geq r$ and take the following values of the parameters:

$$K = r \cdot \alpha_r, \quad J = \alpha_r + 1, \quad P = (MJ+1)r, \quad \bar{P} = (MJ+1)q. \tag{5.49}$$

1. Multiuser interference (MUI) can be eliminated by blocking the received signal into the blocks of length $\bar{P}$ and passing it through the matrix $\mathbf{G}_m$ as introduced in (5.35) with $n_q = MJ + 1$, as long as the spreading codes $\{c_{m,k}(n)\}_{k=0}^{K-1}$ are chosen according to (5.41) and (5.42).

2. Under the above conditions, the channel can either be equalized for an arbitrary choice of the signature points $\{\rho_{m,j}\}$ or it cannot be equalized regardless of this choice. More precisely, let $\mathbf{E}_m(z)$ be the polyphase matrix corresponding to $h_m(n)$ as derived in (5.29)-(5.32). Under the above conditions there are two possible scenarios:
   - $\max\limits_{z\in\mathbb{C}} \text{rank}\{\mathbf{E}_m(z)\} = r$. In this case the system is ZFE-equalizable regardless of $\{\rho_{m,j}\}$.
   - $\max\limits_{z\in\mathbb{C}} \text{rank}\{\mathbf{E}_m(z)\} < r$. In this case there is no choice of $\{\rho_{m,j}\}$ that can make the system ZFE-equalizable.

Comment. The condition $r \geq L+1$ introduced in the statement of the theorem might seem restrictive at first. However, in most cases it is of special interest to minimize the amount of oversampling at the receiver and try to optimize the performance under those conditions. This amounts to keeping q roughly equal to, yet slightly larger than r and choosing r large enough so that the ratio q/r approaches unity. In such cases

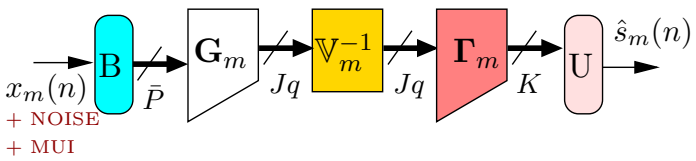

Figure 5.10: Proposed structure of the FSAMOUR receiver in systems with fractional oversampling

r happens to be greater than $L+1$ by design. The condition $\alpha_r \geq r$ is not necessary for the existence of ZFEs. It only ensures the absence of ZFEs if the rank condition on $\mathbf{E}_m(z)$ is not satisfied.

Proof. The only result that needs proof in the first part of the theorem is that the order of $\mathbf{E}_m(z)$ is $N=1$ whenever $r \geq L+1$. If $N=1$, all the parameters in (5.49) are consistent with the values used so far in Section 5.4. Then the first claim follows directly from the discussion preceding the theorem. In order to prove that $N=1$ we use the following lemma whose proof can be found in the appendix.

Lemma 5.1. Under the conditions of Theorem 5.1, $\mathbf{E}_m(z)$ can be written as

$$\mathbf{E}_m(z) = \mathbf{U}_m \cdot \mathbf{D}_m(z) \cdot \begin{bmatrix} \overset{r}{\mathbf{E}_{m,0}(z)} \\ \mathbf{E}_{m,1}(z) \end{bmatrix}_{q-r}^{r}, \tag{5.50}$$

where $\mathbf{E}_{m,0}(z)$ and $\mathbf{E}_{m,1}(z)$ are polynomial matrices of order $N=1$, $\mathbf{U}_m$ is a unitary matrix and $\mathbf{D}_m(z)$ is a diagonal matrix with advance operators z^i on the diagonals.

Having established Lemma 5.1, the first part of the theorem follows readily since $\mathbf{U}_m \cdot \mathbf{D}_m(z)$ can be equalized effortlessly and thus the order of $\mathbf{E}_m(z)$ is indeed $N=1$ for all practical purposes.

For the second part of Theorem 5.1, we use Lemma 5.2 which is also proved in the appendix.

Lemma 5.2. The difference between the maximum and the minimum achievable rank of $\mathcal{E}_m(\boldsymbol{\rho}_m)$ given by (5.37) is *upper bounded* by $r-1$.

From the proof of Lemma 5.2 it follows that we can distinguish between two cases:

- If the normal rank of $\mathbf{E}_m(z)$ is r, then the minimum rank of $\mathcal{E}_m(\boldsymbol{\rho}_m)$ over all choices of signature points is lower bounded by $rJ-r+1 = K+1$ and therefore ZFE is achieved by finding a left inverse of the product in (5.46).
- If the normal rank of $\mathbf{E}_m(z)$ is less than r, then the maximum rank of $\mathcal{E}_m(\boldsymbol{\rho}_m)$ is given by

$$\max_{\boldsymbol{\rho}_{m,j}} \operatorname{rank}\{\mathcal{E}_m(\boldsymbol{\rho}_m)\} \leq (r-1)J = (r-1)(\alpha_r+1) = K + (r-\alpha_r-1) < K.$$

Therefore, regardless of the signature points, ZFE does not exist.

This concludes the proof of Theorem 5.1. $\triangledown\triangledown\triangledown$

To summarize, in this section we established the algorithm for multiuser communications based on AMOUR systems with fractional amount of oversampling at the receiver. The proposed form of the receiver (block labeled 'equalization and rate reduction' in Fig.5.9) is shown in Fig.5.10. As was the case with

the simple AMOUR systems, the receiver is divided into three parts, namely, $\mathbf{G}_m$, $\mathbb{V}_m^{-1}$ and $\mathbf{\Gamma}_m$. The first block $\mathbf{G}_m$ is supposed to eliminate MUI at the receiver. Second block $\mathbb{V}_m^{-1}$ represents the inverse of $\mathbb{V}_m$ defined in (5.46) and essentially neutralizes the effect of $\widehat{\mathbf{C}}_m$ and $\mathbf{G}_m$ on the MUI-free signal. Finally, $\mathbf{\Gamma}_m$ is the block that aims at equalizing the channel which is now embodied in the tall matrix $\mathbb{V}_m$ [see (5.46)].

Note that even though the notations may be similar as in Section 5.2, the building blocks in Fig.5.10 are quite different from the corresponding ones in AMOUR systems. The construction of $\mathbf{G}_m$ is described in (5.35) with the signature points chosen in accordance with the spreading code constraints (5.41)-(5.42). The channel equalizer $\mathbf{\Gamma}_m$ can be chosen according to one of the several design criteria described in (5.16). Instead of $\bar{\mathbf{H}}_m$ in (5.16) we should use the corresponding matrix $\mathbb{E}_m$. In addition to these three conventional solutions, we can choose the *optimal zero-forcing equalizer* as the one described in Section 5.3.1. The details of the construction of this solution are omitted since they are analogous to the derivations in Section 5.3.1.

The conditions for the existence of any ZFE $\mathbf{\Gamma}_m^{(\mathrm{zfe})}$ are described in the previous theorem. Under the same conditions there will exist the optimal ZFE $\mathbf{\Gamma}_m^{(\mathrm{opt})}$ as well. The event that the normal rank of $\mathbf{E}_m(z)$ is less than r occurs with zero probability and thus for all practical purposes we can assume the channel is equalizable regardless of the choice of signature points. Again, for the reasons of computational benefits, signature points can be chosen to be uniformly distributed on the unit circle [see (5.11)]. In the following we demonstrate the advantages of the FSAMOUR systems with fractional oversampling over the conventional AMOUR systems.

5.4.5 Performance evaluation

In this section we present the simulation results comparing the performance of the conventional AMOUR system to the FSAMOUR system with a fractional oversampling ratio. The simulation results are averaged over *thirty* independently chosen real random channels of order $L = 4$. The q-times oversampled channel impulse responses $h_m^{(q)}(n)$ were also chosen randomly, under the constraint that they coincide with AMOUR channels at integers. In other words $h_m^{(q)}(qn) = h_m(n)$. The channel noise was taken to be *colored* in order to demonstrate the difference of using optimal ZFEs to conventional ZFEs. Noise was modeled as an auto-regressive process of first order [54], i.e., AR(1) process with the correlation given by $\rho(k) = \sigma_e^2(0.8)^{|k|}$. The SNR was measured at the receiver as explained in Section 5.3.2. The amount of oversampling at the receiver was chosen to be $q/r = 6/5$, and the parameter $\alpha_r = 6$. The other parameters were chosen as in (5.49). Notice that the advantage of this system over the one described in Section 5.3 is in the lower data rate at the receiver. Namely, for each 5 symbols of the input data stream $s_m(n)$ the receiver in Fig.5.3 needs to deal with 10 symbols, while the receiver in Fig.5.9 deals with only 6. This represents not only the reduction in complexity of the receiver, but also minimizes the additional on-chip RF noise resulting from fast-operating integrated circuits.

The performance curves are shown in Fig.5.11. The acronyms 'SSE' and 'FSE' represent the AMOUR system with no oversampling and the FSAMOUR system with the oversampling ratio 6/5, while the suffices

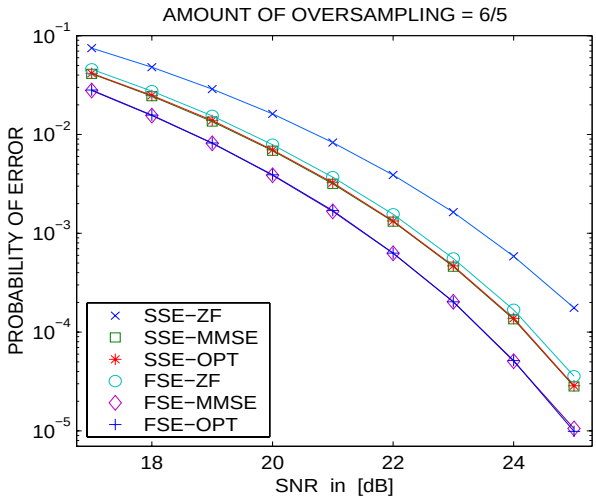

Figure 5.11: Probability of error as a function of SNR in AMOUR and FSAMOUR systems with oversampling ratio 6/5.

'ZF,' 'MMSE' and 'OPT' correspond to the zero-forcing, minimum mean-squared error and optimal ZFE solutions, respectively. The optimal ZFEs are based on optimal matrix inverses as explained in Section 5.3.1. Comparing these performances we conclude:

- When the noise is colored, the optimal ZFE in both AMOUR and FSAMOUR systems perform significantly better than the conventional ZFE. This comes in contrast to some of the results in Section 5.3.2 where we presented the results with the white noise at the receiver.

- The optimal ZFEs in both systems on Fig.5.11 perform almost identically to the MMSE solutions. As explained in Section 5.3.2 the complexity of $\mathbf{\Gamma}_m^{(\mathrm{opt})}$ is reduced comparing to that of $\mathbf{\Gamma}_m^{(\mathrm{mmse})}$ and so is the required knowledge of the signal and the noise statistics.

- The FSAMOUR system with the oversampling ratio 6/5 performs better than the corresponding AMOUR system with no oversampling. The price to be paid is in the data rate and the complexity at the receiver. As expected, the FSAMOUR system with the oversampling ratio 6/5 is still outperformed by the FSAMOUR system with the oversampling ratio $q = 2$ (this can be assessed by comparing Fig.5.11 and Fig.5.7).

5.5 Concluding remarks

In this final chapter we have considered some of the problems facing the designers of modern wireless communication systems. The recent development of a mutually-orthogonal usercode-receiver (AMOUR) for asynchronous or quasi-synchronous CDMA systems [20], [21] represents a novel approach in dealing with one of these problems, namely, multiuser interference. The main advantage over some of the other methods

lies in the fact that both the suppression of multiuser interference (MUI) and inter-symbol interference (ISI) within a single user can be achieved *regardless* of the multipath channels. For this reason it is very easy to extend the AMOUR method to the case where these channels are unknown [21]. In this chapter we have introduced a modification of the traditional AMOUR system in that the received continuous-time signal is oversampled by an integral or a rational amount. This idea leads to the concept of Fractionally Spaced AMOUR (FSAMOUR) receivers that have been derived for both integral and rational amounts of oversampling. Their performance has been compared to the corresponding performance of the conventional method and significant improvements are observed. An important point often overlooked in the design of *zero-forcing* channel equalizers is that often they are not unique. This common theme propagated through Chapters 2 and 3 as well. In the FSAMOUR setting we have exploited this flexibility in the receiver design and further improved the performance of multiuser communication systems.

5.6 Appendix

Proof of Lemma 5.1. Without loss of generality we only consider $r = L+1$, since the proof for $r > L+1$ follows essentially the same lines. The polyphase components $H_{m,k}(z)$ of the q-fold oversampled channel $H^{(q)}(z)$ defined in (5.29) can be thought of as FIR filters of order L (or less). As a special case, note that $H_{m,0}(z) = H_m(z)$. Next, consider the auxiliary filters $P_{m,k}(z)$ as in (5.31). From (5.30) it follows not only that q and r are coprime, but at the same time that Q and r are coprime as well. For this reason the numbers

$$l_k \stackrel{\triangle}{=} [kQ \mod r]$$

are distinct for each $0 \leq k \leq r-1$. As a consequence, the first r filters

$$P_{m,k}(z) = z^{kQ} H_{m,k}(z), \quad 0 \leq k \leq r-1$$

of length $L+1$ are delayed by the amounts that are all different relative to the start of blocks of length r. This combined with the fact that $r = L+1$ leads us to conclude that the entries of $\mathbf{E}_m(z)$, namely, $E_{k,l}(z)$ defined in (5.32) are all given by

$$E_{k,l}(z) = \widetilde{e}_{k,l} \cdot z^{n_{k,l}}. \tag{5.51}$$

Here $\widetilde{e}_{k,l}$ are constants, $n_{k,l} \geq 0$, $n_{k,l+1} \geq n_{k,l}$ and $n_{k,r-1} \leq n_{k,0} + 1$. Moreover, the index within the kth row of $\mathbf{E}_m(z)$ where the exponent $n_{k,l}$ increases by one *is different* for each of the first r rows and all the polyphase components $E_{k,l}(z)$ for $k = 0$ are constant. It follows that indeed $\mathbf{E}_m(z)$ can be written as (5.50), with $\mathbf{U}_m$ denoting the unitary matrix corresponding to row permutations and $\mathbf{D}_m(z)$ given by

$$\mathbf{D}_m(z) = \mathrm{diag}\,[z^{m_0} \quad z^{m_1} \quad \cdots \quad z^{m_{q-1}}], \quad m_k \in \mathbb{N}$$

whose purpose is to pull out any common delay elements from each row of $\mathbf{E}_m(z)$. $\triangledown\triangledown\triangledown$

Proof of Lemma 5.2. Consider (5.50). Depending on $\mathbf{U}_m$, $\mathbf{E}_{m,0}(z)$ can be chosen to be of the form

$$\mathbf{E}_{m,0}(z) = \begin{bmatrix} e_{0,0} & e_{0,1} & e_{0,2} & \cdots & e_{0,r-1} \\ e_{1,0} & z \cdot e_{1,1} & z \cdot e_{1,2} & \cdots & z \cdot e_{1,r-1} \\ e_{2,0} & e_{2,1} & z \cdot e_{2,2} & \cdots & z \cdot e_{2,r-1} \\ \vdots & \vdots & \vdots & \ddots & \vdots \\ e_{r-1,0} & e_{r-1,1} & e_{r-1,2} & \cdots & z \cdot e_{r-1,r-1} \end{bmatrix}. \tag{5.52}$$

From (5.52) it follows that

$$\text{ord}\{\det[\mathbf{E}_{m,0}(z)]\} \leq r-1. \tag{5.53}$$

Therefore, (5.52) can be rewritten using the Smith-McMillan form for the FIR case [61]

$$\mathbf{E}_{m,0}(z) = \widehat{\mathbf{U}}_0(z)\mathbf{\Lambda}_0(z)\widehat{\mathbf{V}}_0(z), \tag{5.54}$$

where $\widehat{\mathbf{U}}_0(z)$ and $\widehat{\mathbf{V}}_0(z)$ are unimodular and $\mathbf{\Lambda}_0(z)$ is diagonal with polynomials $\lambda_i(z)$ on the diagonal for $0 \leq i \leq r-1$. From (5.53) it follows that

$$\sum_{i=0}^{r-1} \text{ord}\{\lambda_i(z)\} \leq r-1. \tag{5.55}$$

Note that some of the diagonal polynomials $\lambda_i(z)$ can be identically equal to zero, and that will result in $\text{rank}\{\mathbf{E}_{m,0}(\gamma)\} < r$ regardless of γ. However, if this is not the case it follows from (5.55) that by varying z the rank of $\mathbf{E}_{m,0}(z)$ can drop by at most $r-1$. This concludes the proof. $\triangledown\triangledown\triangledown$

Chapter 6 Conclusion

In this thesis, we have made an extensive study of multirate systems, especially those that are used in modern communications. Our focus in the first part of the thesis was on communication systems with finer signal sampling at the receiver. These considerations have led naturally to the introduction of an important property of linear systems employed in multirate systems, namely, the biorthogonal partner property. We have developed a comprehensive theory of the vector (or MIMO) biorthogonal partners as well as the fractional biorthogonal partners. Many important results on the existence, uniqueness and parameterization of biorthogonal partners have been derived, and several diverse applications of biorthogonal partners have been closely examined. The special attention was placed on the applications in digital communications.

In the second part of the thesis we have considered another group of multirate structures appearing in communication systems, better known as (filter bank) precoders. The goal of these systems is to introduce the redundancy in the transmitted message, but in a controlled fashion so as to further facilitate the design of the receiver. We have determined the optimal precoders in general systems with cyclic prefix-based redundancy. We have also considered the multiaccess communication systems where the redundancy is meant to help separate the users and neutralize the effects of their multipath propagations in the unknown or time-varying channel environments. Our contribution was to help further understand such systems, design the optimal equalizers and increase the design flexibility at the cost of an increased receiver complexity.

After this ample treatment, several theoretical and practical issues remain unanswered. It remains to be seen if the paradigm of MIMO biorthogonal partners can be successfully extended to the case when the expansion and decimation ratios in different channels are not equal. This theoretical problem might have a practical significance in the communication systems with different users or array sensors communicating at different rates and with different priorities. Also, the single-dimensional definition of biorthogonal partners can be nontrivially extended to multiple dimensions. These considerations could, for example, lead to improvements in some image processing algorithms that are inherently nonseparable. We can also ask the question of the theoretical bounds on the improvement in performance of the flexible zero-forcing channel equalizers if their order can be infinite. Yet another extension of the problems treated here would result in new multirate concepts, such as 'joint MIMO biorthogonal partners.' Namely, suppose that instead of two we now have a concatenation of three possibly rectangular matrix transfer functions. The question is: given the middle transfer function, how to characterize the class of possible solutions for the surrounding MIMO systems that guarantees the Nyquist properties of their combination. The solution to this problem would lead to joint transmitter and receiver optimization in MIMO communication systems.

On the practical side, it would be interesting to consider more realistic multiuser systems than the ones treated here. Some of the practical issues that should be taken into account are: (a) the transmitted power

limitations across different users; (b) the sensitivity of the equalization algorithms to the channel order estimates and the channel state information; (c) alternative sampling strategies at the receiver in a more realistic case of nonuniform transmission rates for different users, and user synchronization issues; (d) design of the multiaccess receivers with computational limitations: constraints on the number of operations per unit time and/or receivers with limited precision operations. Indeed, even though present algorithms for multiuser and multirate transmission systems go a long way in facilitating reliable communications, in many aspects the research in this area is still at the beginning.

Bibliography

[1] A. N. Akansu, P. Duhamel, X. Lin, and M. de Courville, "Orthogonal transmultiplexers in communication: A review," *IEEE Trans. Sig. Proc.,* vol. 46, no. 4, pp. 979–995, April 1998.

[2] N. Al-Dhahir and J. M. Cioffi, "Efficiently computed reduced-parameter input-aided MMSE equalizers for ML detection: A unified approach," *IEEE Trans. Info. Theory*, vol. 42(5), pp. 903–915, May 1996.

[3] A. Aldroubi, "Oblique projections in atomic spaces," *Proc. Amer. Math. Soc.*, vol. 124, pp. 2051–2060, 1996.

[4] A. Aldroubi and M. Unser, "Oblique projections in discrete signal subspaces of ℓ_2 and the wavelet transform," in *Proc. SPIE*, vol. 2303, *Wavelet applications in signal and image processing, II*, pp. 36–45, San Diego, CA, 1994.

[5] J. A. C. Bingham, "Multicarrier modulation for data transmission: an idea whose time has come," *IEEE Comm. Magazine*, pp. 5–14, May 1990.

[6] C. de Boor, *A Practical Guide to Splines*. New York: Springer-Verlag 1978.

[7] G. Cherubini, E. Eleftheriou, S. Olcer, and J. M. Cioffi, "Filter bank modulation techniques for very high speed digital subscriber lines," *IEEE Comm. Mag.,* pp. 98–104, May 2000.

[8] P.S. Chow, J.C. Tu, and J.M. Cioffi, "A discrete multitone transreceiver system for HDSL applications," *IEEE J. Sel. Areas Comm.,* vol. 9, no. 6, pp. 895–908, Aug. 1991.

[9] P. S. Chow, J. C. Tu and J. M. Cioffi, "Performance evaluation of a multichannel transceiver system for ADSL and VHDSL services," *IEEE J. Select. Areas Comm.*, vol. 9, pp. 909–919, Aug. 1991.

[10] T. M. Cover and J. A. Thomas, *Elements of Information Theory.* John Wiley & Sons, Inc., 1991.

[11] Z. Ding and L. Qiu, "Blind MIMO channel identifiability from second order statistics," in *Proc. Conf. on Decision and Control*, Sydney, Australia, Dec. 2000.

[12] G. C. Donovan, J. S. Geronimo and D. P. Hardin, "Orthogonal polynomials and the construction of piecewise polynomial smooth wavelets," *SIAM J. Math. Anal.*, vol. 30 (5), pp. 1029–1056, 1999.

[13] N. J. Fliege, *Multirate Digital Signal Processing.* Chichester: John Wiley and Sons, 1994.

[14] G. D. Forney, Jr., "Convolutional codes I: Algebraic structure," *IEEE Trans. Information Theory*, vol. 16(6), pp. 720–738, Nov. 1970.

[15] J. S. Geronimo, D. P. Hardin and P. R. Massopust, "Fractal functions and wavelet expansions based on several scaling functions," *J. Approx. Theory*, vol. 78, pp. 373–401, 1994.

[16] I. Ghauri and D. T. M. Slock, "Blind maximum SINR receiver for the DS-CDMA downlink," in *Proc. ICASSP*, Istanbul, Turkey, June 2000.

[17] G. B. Giannakis, "Filter banks for blind channel identification and equalization," *IEEE Signal Processing Letters*, vol. 4(6), pp. 184–187, June 1997.

[18] G. B. Giannakis, Y. Hua, P. Stoica and L. Tong (Eds), *Signal Processing Advances in Wireless and Mobile Communications—Volume I, Trends in Channel Estimation and Equalization*. Prentice-Hall, September 2000.

[19] G. B. Giannakis, Y. Hua, P. Stoica and L. Tong (Eds), *Signal Processing Advances in Wireless and Mobile Communications—Volume II, Trends in Single- and Multi-User Systems*. Prentice-Hall, September 2000.

[20] G. B. Giannakis, Z. Wang, A. Scaglione, S. Barbarossa, "AMOUR—generalized multicarrier CDMA irrespective of multipath," in *Proc. Globecom*, Brasil, Dec. 1999.

[21] G. B. Giannakis, Z. Wang, A. Scaglione, S. Barbarossa, "AMOUR—generalized multi-carrier transceivers for blind CDMA regardless of multipath," *IEEE Trans. Comm.*, vol. 48(12), pp. 2064–76, Dec. 2000.

[22] R. M. Gray, "On the asymptotic eigenvalue distribution of Toeplitz matrices," *IEEE Trans. Inform. Theory,* vol. IT-18, no. 6, pp. 725–730, Nov. 1972.

[23] S. Haykin, *Adaptive Filter Theory*. Prentice Hall, Inc., Upper Saddle River, N.J., 1996.

[24] R. A. Horn and C. R. Johnson, *Matrix Analysis.* Cambridge University Press, 1985.

[25] H. S. Hou and H. C. Andrews, "Cubic splines for image interpolation and digital filtering," *IEEE Trans. Acoust., Speech, Signal Processing*, vol. ASSP-26, pp. 508–517, 1978.

[26] T. Kailath, *Linear Systems*. Prentice Hall, Inc., Englewood Cliffs, N.J., 1980.

[27] I. Kalet, "The multitone channel," *IEEE Trans. Communications*, vol. 37(2), pp. 119–124, Feb. 1989.

[28] J. Kovačević and M. Vetterli, "Perfect reconstruction filter banks with rational sampling factors," *IEEE Trans. Signal Processing*, vol. 41(6), pp. 2047–2066, June 1993.

[29] J. Lebrun and M. Vetterli, "Balanced multiwavelets theory and design," *IEEE Trans. Signal Processing*, vol. 46 (4), pp. 1119–1125, Apr. 1998.

[30] Y.-P. Lin and S.-M. Phoong, "Perfect discrete multitone modulation with optimal transceivers," *IEEE Trans. Signal Proc.*, vol. 48(6), pp. 1702–1711, June 2000.

[31] S. Mallat, *A Wavelet Tour of Signal Processing.* Academic Press, 1998.

[32] H. S. Malvar and D. H. Staelin, "Optimal pre- and postfilters for multichannel signal processing," *IEEE Trans. Acoust., Speech and Signal Process.*, vol. 36 (2), pp. 287–289, Feb. 1988.

[33] P. J. W. Melsa, R. C. Younce, C. E. Rohrs, "Impulse response shortening for descrite multitone receivers," *IEEE Trans. Communications*, vol 44(12), pp. 1662–1672, Dec. 1996.

[34] E. Moulines, P. Duhamel, J. Cardoso, and S. Mayrargue, "Subspace methods for the blind identification of multichannel FIR filters," *IEEE Trans. Signal Processing*, vol. 43(2), pp. 516–525, Feb. 1995.

[35] C. T. Mullis and R. A. Roberts, "Synthesis of minimum roundoff noise fixed point digital filters," *IEEE Trans. Circuits and Systems*, pp. 551–562, Sep. 1976.

[36] K. Nayebi, T. P. Barnwell, III and M. J. T. Smith, "The design of perfect reconstruction nonuniform band filter banks," *Proc. ICASSP*, Toronto, Canada, May 1991.

[37] A. Papoulis, *Signal Analysis*. McGraw Hill, 1977.

[38] H. V. Poor and G. W. Wornell (Eds), *Wireless Communications: Signal Processing Perspectives*. Prentice-Hall, 1998.

[39] J. G. Proakis, *Digital Communications*. McGraw Hill, 1995.

[40] C. B. Ribeiro, M. L. R. de Campos and P. S. R. Diniz, "FIR equalizers with minimum redundancy," *Proc. ICASSP*, Orlando, FL, May 2002.

[41] A. Scaglione and G. B. Giannakis, "Design of user codes in QS-CDMA systems for MUI elimination in unknown multipath," *IEEE Comm. Letters*, vol. 3(2), pp. 25–27, Feb. 1999.

[42] A. Scaglione, G. B. Giannakis and S. Barbarossa, "Redundant filter bank precoders and equalizers Part I: Unification and optimal design," *IEEE Trans. Signal Proc.*, vol. 47 (7), pp. 1988–2006, July 1999.

[43] A. Scaglione, G. B. Giannakis and S. Barbarossa, "Redundant filterbank precoders and equalizers part II: Blind channel estimation, synchronization and direct equalization," *IEEE Trans. Signal Processing*, vol. 47(7), pp. 2007–22, July 1999.

[44] I. J. Schoenberg, *Cardinal Spline Interpolation*. SIAM, 1973.

[45] I. W. Selesnick, "Interpolating multiwavelet bases and the sampling theorem," *IEEE Trans. Signal Processing*, vol. 47 (6), pp. 1615–1621, June 1999.

[46] I. W. Selesnick, "Multiwavelet bases with extra approximation properties," *IEEE Trans. Signal Processing*, vol. 46 (11), pp. 1898–2908, Nov. 1998.

[47] D. T. M. Slock, "Blind fractionally-spaced equalization, perfect-reconstruction filter banks and multichannel linear prediction," in *Proc. ICASSP*, Adelaide, Australia, Apr. 1994.

[48] D. T. M. Slock, "Blind joint equalization of multiple synchronous mobile users using oversampling and/or multiple antennas," in *Proc. 28th Asilomar Conference on Signals, Systems and Computers*, Pacific Grove, CA, Oct. 1994.

[49] T. Starr, J. M. Cioffi, and P. J. Silverman, *Understanding Digital Subscriber Line Technology.* Prentice-Hall, NJ, 1999.

[50] G. Strang and T. Nguyen, *Wavelets and Filter Banks.* Wellesley-Cambridge Press, 1996.

[51] G. Strang and V. Strela, "Short wavelets and matrix dilation equation," *IEEE Trans. Signal Processing*, vol. 43 (1), pp. 108–115, Jan. 1995.

[52] V. Strela, P. N. Heller, G. Strang, P. Topiwala, and C. Heil "The application of multiwavelet filterbanks to image processing," *IEEE Trans. Image Processing*, vol. 8(4), Apr. 1999.

[53] G. L. Stuber, *Principles of Mobile Communication.* Kluwer Academic Publishers, 1996.

[54] C. W. Therrien, *Discrete Random Signals and Statistical Signal Processing.* Prentice-Hall, Englewood Cliffs, NJ, 1992.

[55] A. Tkacenko and P. P. Vaidyanathan, "On the least squares signal approximation model for overdecimated rational nonuniform filter banks and applications," in *Proc. ICASSP*, Hong-Kong, Apr. 2003.

[56] L. Tong, G. Xu and T. Kailath, "A new approach to blind identification and equalization of multipath channels," in *Proc. 25th Asilomar Conference on Signals, Systems and Computers*, Pacific Grove, CA, Nov. 1991.

[57] J. R. Treichler, I. Fijalkow and C. R. Johnson, Jr., "Fractionally spaced equalizers: how long should they really be?," *IEEE Signal Processing Magazine*, pp. 65–81, May 1996.

[58] M. K. Tsatsanis, "Inverse filtering criteria for CDMA systems," *IEEE Trans. Signal Processing*, vol. 45(1), pp. 102–112, Jan. 1997.

[59] M. Unser, A. Aldroubi, and M. Eden, "B-spline signal processing: Part I—Theory," *IEEE Trans. Signal Processing*, vol. 41(2), pp. 821–833, Feb. 1993.

[60] M. Unser, A. Aldroubi, and M. Eden, "B-spline signal processing: Part II—Efficient design and applications," *IEEE Trans. Signal Processing*, vol. 41(2), pp. 834–848, Feb. 1993.

[61] P. P. Vaidyanathan, *Multirate Systems and Filter Banks.* Englewood Cliffs, NJ: Prentice-Hall, 1993.

[62] P. P. Vaidyanathan and S. Akkarakaran, "A review of the theory and applications of optimal subband and transform coders," *Appl. and Computat. Harm. Anal.*, vol. 10, pp. 254–289, 2001.

[63] P. P. Vaidyanathan and T. Chen, "Role of anticausal inverses in multirate filterbanks—Part I: System-theoretic fundamentals," *IEEE Trans. Signal Proc.*, vol. 43(5), May 1995.

[64] P. P. Vaidyanathan, Y.-P. Lin, S. Akkarakaran, and S.-M. Phoong, "Discrete multitone modulation with principal component filter banks," *IEEE Trans. Inform. Theory*, vol. 49(10), pp. 1397–1412, Oct. 2002.

[65] P. P. Vaidyanathan and B. Vrcelj, "Biorthogonal partners and applications," *IEEE Trans. Signal Processing*, vol. 49(5), pp. 1013–1027, May 2001.

[66] P. P. Vaidyanathan and B. Vrcelj, "Fast and robust blind-equalization based on cyclic prefix," in *Proc. IEEE Int. Conf. on Comm.*, New York, Apr–May 2002.

[67] P. P. Vaidyanathan and B. Vrcelj, "Filter banks for cyclic-prefixing the nonuniform DMT system," (invited paper) in *Proc. 36th Asilomar Conference on Signals, Systems and Computers*, Pacific Grove, CA, Nov. 2002.

[68] P. P. Vaidyanathan and B. Vrcelj, "On power allocation for generalized cyclic-prefix based channel equalizers," in *Proc. IEEE Int. Symp. on Circuits and Systems*, Scottsdale, AZ, May 2002.

[69] P. P. Vaidyanathan and B. Vrcelj, "On sampling theorems for non bandlimited signals," in *Proc. ICASSP*, Salt Lake City, Utah, May 2001.

[70] P. P. Vaidyanathan and B. Vrcelj, "Theory of fractionally spaced cyclic-prefix equalizers," in *Proc. ICASSP*, Orlando, FL, May 2002

[71] S. Verdú, *Multiuser Detection*. Cambridge Press, 1998.

[72] M. Vetterli and J. Kovačević, *Wavelets and Subband Coding.* Englewood Cliffs, NJ: Prentice-Hall, 1995.

[73] M. Vetterli and G. Strang, "Time-varying filter banks and multiwavelets," *Sixth Digital Signal Processing Workshop, IEEE*, pp. 223-226, 1994.

[74] B. Vrcelj and P. P. Vaidyanathan, "Efficient implementation of all-digital interpolation," *IEEE Trans. Image Processing*, vol. 10(11), pp. 1639–46, Nov. 2001.

[75] B. Vrcelj and P. P. Vaidyanathan, "Equalization with oversampling in multiuser CDMA systems," submitted to *IEEE Trans. Signal Processing.*

[76] B. Vrcelj and P. P. Vaidyanathan, "Fractional biorthogonal partners and application in signal interpolation," in *Proc. IEEE Int. Symp. on Circuits and Systems*, Scottsdale, AZ, May 2002.

[77] B. Vrcelj and P. P. Vaidyanathan, "Fractional biorthogonal partners in channel equalization and signal interpolation," *IEEE Trans. Signal Processing*, vol. 51(7), pp. 1928–1940, July 2003.

[78] B. Vrcelj and P. P. Vaidyanathan, "Fractional biorthogonal partners in fractionally spaced equalizers," in *Proc. ICASSP*, Orlando, FL, May 2002.

[79] B. Vrcelj and P. P. Vaidyanathan, "Least squares signal approximation using multirate systems: multichannel nonuniform case," in *Proc. 35th Asilomar Conference on Signals, Systems and Computers*, Pacific Grove, CA, Nov. 2001.

[80] B. Vrcelj and P. P. Vaidyanathan, "MIMO biorthogonal partners and applications," *IEEE Trans. Signal Processing*, vol. 50(3), pp. 528–42, Mar. 2002.

[81] B. Vrcelj and P. P. Vaidyanathan, "On the general form of FIR MIMO biorthogonal partners," (invited paper) in *Proc. 35th Asilomar Conference on Signals, Systems and Computers*, Pacific Grove, CA, Nov. 2001

[82] B. Vrcelj and P. P. Vaidyanathan, "Pre- and post-processing for optimal noise reduction in cyclic prefix based channel equalizers," in *Proc. IEEE Int. Conf. on Comm.*, New York, Apr-May 2002.

[83] B. Vrcelj and P. P. Vaidyanathan, "Results on vector biorthogonal partners," in *Proc. ICASSP*, Salt Lake City, Utah, May 2001.

[84] B. Vrcelj and P. P. Vaidyanathan, "The role of biorthogonal partners in sampling theory for non bandlimited signals: a review," (invited paper) in *Proc. 36th Asilomar Conference on Signals, Systems and Computers*, Pacific Grove, CA, Nov. 2002.

[85] B. Vrcelj and P. P. Vaidyanathan, "Theory of MIMO biorthogonal partners and their application in channel equalization," in *Proc. IEEE Int. Conf. on Comm.*, Helsinki, Finland, June 2001.

[86] Z. Wang, G. B. Giannakis, "Block precoding for MUI/ISI-resilient generalized multicarrier CDMA with multirate capabilities," *IEEE Trans. Comm*, vol. 49(11), pp. 2016–27, Nov. 2001.

[87] J.-J. Werner, "The HDSL environment," *IEEE J. Sel. Areas Comm.,* vol. 9(6), pp. 785–800, Aug. 1991.

[88] X.-G. Xia, "A new prefilter design for discrete multiwavelet transform," *IEEE Trans. Signal Processing*, vol. 46(6), pp. 1558–1570, June 1998.

[89] X.-G. Xia, "New precoding for intersymbol interference cancellation using nonmaximally decimated multirate filterbanks with ideal FIR equalizers," *IEEE Trans. Signal Processing*, vol. 45(10), pp. 2431–2441, Oct. 1997.

[90] X.-G. Xia, J. S. Geronimo, D. P. Hardin and B. W. Suter, "Design of prefilters for discrete multiwavelet transforms," *IEEE Trans. Signal Processing*, vol. 44, pp. 25–35, Jan. 1996.

[91] J. Yang and S. Roy, "On joint transmitter and receiver optimization for multiple-input-multiple-output (MIMO) transmission systems," *IEEE Trans. Comm.*, vol. 42(12), pp. 3221–3231, Dec. 1994.

[92] `http://www.systems.caltech.edu/bojan`